Elastic and Related Transport Cross Sections for Collisions among Isotopomers of $H^+ + H$, $H^+ + H_2$, $H^+ + He$, $H + H$, and $H + H_2$

P.S. Krstić and D.R. Schultz
Physics Division, Oak Ridge National Laboratory, Oak Ridge, TN 37831-6372

Acknowledgement

This work has been supported by the U.S. Department of Energy, Office of Fusion Energy Sciences, at Oak Ridge National Laboratory which is managed by Lockheed Martin Energy Research Corp. under contract No. DE-AC05-96OR22464.

CONTENTS

Part A: Introduction and theory

CONTENTS (continued)

Part B: Ion-neutral collision systems

CONTENTS (continued)

Part C: Neutral-neutral collision systems

I.1 Introduction

The microscopic, atomic physics influencing bulk properties such as transport and charge balance in the edge and divertor plasmas of the new generation of reactors (such as ITER) has been recently of growing interest for plasma modeling and engineering of magnetically confined fusion devices [1, 2]. This interest arises because these regions might play crucial roles in the realization of useful energy production from controlled fusion. In particular, the edge plasma should suppress the inflow of deleterious impurities into the plasma core and the divertor is used to exhaust both heat and particles. These regions are characterized by relatively low plasma temperatures (10-500 eV in the former and 1-50 eV in the latter) with high densities (in comparison to the core), thus providing conditions for numerous interparticle collisions involving both atomic and molecular particles (i.e neutrals and ions). Owing to the low temperature, the increased densities of neutrals, and the relatively large elastic cross sections involving neutral particles at low energies in comparison to inelastic ones, elastic processes play the dominant role in neutral particle transport and overall momentum balance [2]. However, calculation and measurement of these processes have been overshadowed by the production of data for energy and charge exchanging inelastic processes.

Thus, the goal of the present work is to produce and tabulate elastic scattering data for the most abundant particles of the divertor and edge plasmas, data which almost without exception cannot be found in literature. The existing, published data typically cover only a limited collision energy and/or angular scattering range, and are not tabulated or fitted for use in plasma modeling codes. Previous work [3, 4], which sought to partially ameliorate this lack, provided limited comprehensive compilations based on classical [3] and semi-classical [4] approaches, and on literature surveys.

The particular species considered here include the fuel, hydrogen, in all isotopic atomic (H, D, T), ionic (H^+, D^+, T^+), and molecular (H_2, D_2, T_2, HD, HT, DT) forms, and helium, produced in fusion and exhausted through the divertor. For the fifty-one collision pairs which are isotopic variants of the prototypes $H^+ + H$, $H^+ + H_2$, $H^+ + He$, $H + H$, and $H + H_2$, we provide cross sections for center-of-mass (CM) collision energies in the range of 0.1-100 eV. This range extends somewhat beyond the typical divertor plasma temperatures to allow inclusion of data for energies towards the tails of the Maxwellian distributions. We note that to calculate the cross sections at the yet higher energies present in the tokamak edge plasmas would require different theoretical techniques that would treat the opening and interaction with inelastic channels.

Included in this work are both differential and total cross sections, generally computed for ten points per energy decade at $E_{CM} = 10^{0.1j-1}$ eV, j =0, 30. The exceptions to this are the data which involve molecules for $E_{CM} > 10$ eV, for which results are calculated at $E_{CM} = 10^{0.1j+1}$ eV, j=23, 27, 30, i.e. for the three energies in the last decade, $E_{CM} \approx$ 20, 50, and 100 eV. The differential cross sections are obtained for 768 values of the CM scattering angle $\theta_j = \frac{\pi}{2}(1 + x_j)$ radians, j=1, 768, where x_j is the j^{th} zero of the Legendre polynomial $P_{768}(x)$ in the interval [-1,1]. Thus θ_j constitute the set of abscissas for a Gauss-Legendre integration in the interval $[0, \pi]$, used in calculation of the integral cross sections. Concerning different isotopic forms of the constituents of a collision system, we have found that no scaling of differential elastic cross sections can be discovered in the range of energies considered, thus requiring isotope specific calculations for the fifty-one collision systems, resulting in more than 2800 differential cross sections and more than 200 integral cross sections. These were obtained using state of the art quantal calculations which were implemented so as to reach the highest practical accuracy.

Presentation of the data for each system follows approximately the same pattern:

(a) Elastic and transport integral cross sections (elastic scattering, momentum transfer, viscosity, and where appropriate spin exchange or charge transfer) tabulated at three points per energy decade,

(b) Fitting coefficients of the Chebyshev rational functions used as analytical approximants of the integral cross sections as functions of the CM collision energy,

(c) Graphical presentation of the integral cross sections at all energies and of the respective analytical fits,

(d) Fitting coefficients of the exponential Chebyshev rational functions, used as analytical approximants of the differential cross sections (elastic and when appropriate spin exchange or charge transfer) as functions of CM scattering angle and collision energy,

(e) Graphical presentation of the differential cross sections, three per energy decade, and the respective analytical fits.

To facilitate the use of the fitted data and to provide the original data to those users who would benefit by attempting other fits or interpolations of the cross sections, all data generated in this project are available through the WWW site of the Oak Ridge National Laboratory's Controlled Fusion Atomic Data Center (`www-cfadc.phy.ornl.gov`). Vibrational excitations (with quantum numbers $\nu \leq 9$) were included in the calculations of the elastic cross sections (scattering from the ground, $\nu = 0$, vibrational state) for the molecular targets due to the strength of these inelastic channels; however the relevant total and differential cross sections are neither fitted nor tabulated in the present volume but are available upon request.

I.2 Important note on usage and interpretation of the data

Considerable confusion in applications of elastic data has arisen due to the difference between the classical and quantum mechanical definitions of elastic scattering for very slow collisions involving identical nuclei such as in $H^+ + H$ or $H + H$. The specific cause of the confusion is the quantum mechanical indistinguishability of identical particles. This results in the inability to distinguish slow protons elastically scattered on H from the recoiling target protons produced by charge transfer or slow hydrogen atoms elastically scattered on H from the recoiling H target atom. This phenomenon is manifested through interference of the wavefunctions for the elastic and charge transfer channels or for elastically scattered and recoiled neutral atoms. At higher collision energies the overlap of the two channels vanishes, leading to pronounced peaks for forward (elastic) and backward (charge transfer or target recoil) scattering peaks in the differential cross sections. Thus the elastic cross section defined quantum mechanically tends, at higher collision energies, to the total differential scattering cross section (i.e. sum of classically distinguishable elastic scattering and charge transfer).

An immediate consequence of this definition is a significant increase of the momentum transfer cross section, because it depends dominantly on the magnitude of the elastic differential cross section at large (backward) scattering angles. Therefore, modeling of the particle transport should not further account for momentum transfer by the resonant charge transfer, because this is already contained in the quantum-mechanically defined "elastic" cross section.

With the increase of collision energy the overlap of the two processes vanishes and the classical limit of distinguishability of particles is reached. Thus one could calculate or measure the elastic cross section for the scattering of the projectile separately from the charge transfer from, or recoil of, the target. We show that this limit is reached for $E_{CM} > 1$ eV. However, to maintain a quantum-mechanically correct definition, consistent with conventions well established in the literature in the energy range considered here, we treat the identical nuclei in ion-atom and atom-atom scattering as indistinguishable, even at higher energies, when the "elastic" cross section transitions to the total scattering cross section, containing the non-overlapping sum of direct and recoil channels.

To separate these processes in the integral cross sections for $H^+ + H$ (in all its isotopic variations), one can subtract the charge transfer cross section from the "elastic" one, leading to the elastic cross section in the distinguishable particle sense, which is, of course, well defined only at higher collision energies. The "true elastic" differential cross sections may be approximated as the absolute value of the difference of the presented "elastic" and charge transfer differential cross sections. This can then be used to recalculate the integral quantities, such as momentum transfer and viscosity cross sections to obtain results that have the right classical limit. We will show elsewhere that the distinguishability of the particles introduced in such a way does not lead to more than 10% uncertainty in the integral cross sections for the hydrogenic systems at 0.1 eV. As far as charge transfer is concerned, the "spin exchange" cross sections defined in the low energy limit goes smoothly over to the proper charge transfer cross section in the classical limit of distinguishability. In the case of scattering of identical atoms (e.g. $H + H$), due to the full symmetry of the system, the division of the integral elastic cross section by two would lead to the correct classical limit, while the transport-relevant integral cross sections can be obtained from separation of the forward and backward recoil peaks in the differential cross sections.

I.3 Basic definitions

An extensive literature exists on both the basic definitions and various theoretical approaches (classical, semi-classical, quantum mechanical) to the computation of the elastic cross sections for collisions of both structureless and structured particles. As an excellent starting point, we refer the interested reader to the relevant chapters in the renowned textbooks on quantum mechanics and collision theory [5, 6, 7, 8, 9, 10]. Given here is a brief review of the basic terminology and formulas relevant for the quantum mechanical approach, to orient the reader for later more detailed descriptions of the methods employed. We employ atomic units (a.u.) throughout this discussion and throughout the tabulated results unless it is convenient or conventional to do otherwise, in which case the units are explicitly noted.

I.3.1 Defining the elastic cross section

The prototypical example for studying elastic heavy particle scattering is a collision of two structureless particles subject to a spherically symmetric interaction potential, $V(R)$, where R is the interparticle separation. If the z-axis of the system of spherical coordinates (R, θ, ϕ) is chosen in the direction $\vec{k}$ ($\vec{k}$ is the relative wavevector) of the incident particle, the problem possesses azimuthal symmetry. The wavefunction $\Psi(\vec{R})$ may be expanded in partial waves of angular momentum ℓ in terms of Legendre polynomials $P_\ell(\cos\theta)$, $\cos\theta = z/R$, as

$$\Psi(\vec{R}) = \sum_{\ell=0}^{\infty}(2\ell+1)i^\ell a_\ell \frac{u_\ell(R)}{kR} P_\ell(\cos\theta). \tag{1}$$

The function $u_\ell(R)$ satisfies the radial Schrödinger equation

$$\left[\frac{d}{dR^2} - \frac{\ell(\ell+1)}{R^2} - 2\mu V(R) + k^2\right] u_\ell(R) = 0 \tag{2}$$

where we define $\varepsilon = k^2/2\mu$ as the total CM energy of the system at $R \to \infty$, and where μ is the system reduced mass, with the boundary condition $u_\ell(0) = 0$ (such that $\Psi(R)$ stays finite at $R \to 0$). Concerning the boundary condition at $R \to \infty$, $u_\ell(R)$ is a superposition of the ℓ components of the incident wave $\exp(ikR)$ and the outgoing, scattered waves. Thus

$$u_\ell(R) = \frac{i^{\ell+1}}{2}(\exp(-ikR) - (-1)^\ell S_\ell \exp(ikR)), \quad kR \gg \ell \tag{3}$$

where S_ℓ is the diagonal element of the scattering matrix corresponding to the orbital angular momentum ℓ. This yields the asymptotic value of the the wavefunction

$$\Psi(R) = \exp(-ikR) + f(\theta)\frac{\exp(ikR)}{R}, \quad kR \gg \ell \tag{4}$$

where the scattering amplitude $f(\theta)$ of the scattered wave $\Psi_{sc} = \exp(ikR)/R$ is usually expressed in terms of S_ℓ as

$$f(\theta) = \frac{i}{2k}\sum_{\ell=0}^{\infty}(2\ell+1)(1-S_\ell)P_\ell(\cos\theta). \tag{5}$$

The scattering matrix element S_ℓ determines the scattering amplitude uniquely. In the present case of potential scattering it can be expressed in terms of the (real) phase shifts δ_ℓ as

$$S_\ell = \exp(2i\delta_\ell). \tag{6}$$

Since this is a periodic function of δ_ℓ the definition of the phase shifts is not unique. Applying the boundary condition that $\delta_\ell \to 0$ as $V(R)$ vanishes, the phase shifts can lie either in the interval $[0,\pi]$ or within $[-\pi/2,\pi/2]$. We choose the former interval.

The scattering is usually described by the differential cross section $d\sigma(\theta,\phi)/d\Omega$, defined as the ratio of the number of particles scattered per unit time into an element of solid angle $d\Omega = \sin\theta d\theta d\phi$, per unit solid angle, to the flux of incoming particles. Since $j_R dA$ particles pass through an element of surface area $dA = R^2 d\Omega$ per second, where the radial flux density j_R is given as

$$j_R = \frac{1}{2i\mu}[\Psi^*_{sc}\frac{\partial\Psi_{sc}}{\partial R} - \Psi_{sc}\frac{\partial\Psi^*_{sc}}{\partial R}] = \frac{k}{\mu R^2}\left|f(\theta)\right|^2 \tag{7}$$

and since the flux density of incoming particles is k/μ, it follows that

$$\frac{d\sigma(\theta,\phi)}{d\Omega} = \left|f(\theta)\right|^2. \tag{8}$$

The differential cross section is only a function of the scattering angle θ for the central potential $V(R)$. This is the case for all systems treated in this work. For convenience, we express all of the tabulated and graphically presented differential cross sections in this work in terms of the quantity $2\pi\sin\theta d\sigma(\theta)/d\Omega$.

These basic definitions of elastic scattering can be readily extended to collisions involving distinguishable particles with internal degrees of freedom, such as the ion-atom and atom-atom scattering considered below. Expanding, in this case, the wavefunction of the system

$$\Psi(\vec{r},\vec{R}) = \sum_{L,\kappa}\frac{F^{(L)}_\kappa(R)}{R}P_L(\cos\theta)\psi_\kappa(\vec{r},R) \tag{9}$$

in terms of the electronic eigenfunctions of the adiabatic quasimolecular Hamiltonian

$$\mathcal{H}(R)\psi_\kappa(\vec{r},R) = E_\kappa(R)\psi_\kappa(\vec{r},R), \tag{10}$$

where $\vec{r}$ is a set of internal (electronic) coordinates, and $E_\kappa(R)$ are the electronic eigenenergies that correspond to the set of quantum numbers κ. The equation for the nuclear radial functions $F_\kappa^{(L)}(R)$ in the center of the mass coordinates takes the form of a system of coupled equations [5]

$$\left(\frac{1}{2\mu}\frac{d^2}{dR^2} + \frac{L(L+1)}{2\mu R^2} + \frac{Z_1 Z_2}{R} + E_\kappa(R) - \varepsilon\right) F_\kappa^{(L)} = \sum_{\kappa'} W_{\kappa\kappa'}^{LL'}(R) F_{\kappa'}^{(L')} \tag{11}$$

where L is the angular quantum number of nuclear motion, and $W_{\kappa\kappa'}^{LL'}(R)$ are the matrix elements of the nonadiabatic coupling. The internuclear distance R is an external parameter, and both eigenfunctions and eigenenergies in this equation reduce to the atomic wavefunctions and to the energy levels of isolated atoms E_κ, respectively, when $R \to \infty$.

The asymptotic form of the radial wavefunctions defines the $S_\kappa^{(L)}$-matrix elements of the transition from the initial atomic state κ_0 to the final one, κ:

$$F_\kappa^{(L)}(R \to \infty) = (-1)^{L+1} \exp(-iK_{\kappa_0} R)\delta_{\kappa\kappa_0} + S_\kappa^{(L)} \exp(iK_\kappa R) \tag{12}$$

where $K_\kappa = \sqrt{2\mu(\varepsilon - E_\kappa)}$ and $\delta_{\alpha\beta}$ is the Kronecker symbol. This yields the amplitude and total cross sections for inelastic transitions and elastic scattering of the form

$$f_{\kappa\kappa_0}(\theta) = \frac{i}{2K_{\kappa_0}} \sum_{\ell=0}^{\infty} (2\ell+1)(\delta_{\kappa\kappa_0} - S_{\kappa\kappa_0}^{(L)}) P_\ell(\cos\theta) \tag{13}$$

$$\sigma_{\kappa\kappa_0} = \frac{\pi}{K_{\kappa_0}^2} \sum_{L=0}^{\infty} (2L+1) \left|\delta_{\kappa\kappa_0} - S_{\kappa\kappa_0}^{(L)}\right|^2. \tag{14}$$

Eq. (13) reduces to formula (5) in the case of potential scattering, where $S_{\kappa_0\kappa_0}^{(L)}$ is expressible in terms of the relevant phase shift only (Eq. (6)).

I.3.2 Defining the total and transport cross sections

The flux of particles scattered in all directions is the total (elastic) scattering cross section, defined as

$$\sigma_{el} = \int d\Omega \frac{d\sigma(\theta,\phi)}{d\Omega} = 2\pi \int_0^\pi d\theta \sin\theta \, |f(\theta)|^2 \tag{15}$$

which, in case of scattering of structureless particles yields

$$\sigma_{el} = \frac{4\pi}{k^2} \sum_{\ell=0}^{\infty} (2\ell+1) \sin^2\delta_\ell. \tag{16}$$

The first two moments of the total elastic cross section are also of interest for plasma modelers (see e.g. [11]). These are the momentum transfer (diffusion) cross section

$$\sigma_{mt} = \int d\Omega \frac{d\sigma(\theta,\phi)}{d\Omega}(1-\cos\theta) = 2\pi \int_0^\pi d\theta \sin\theta \,|f(\theta)|^2 (1-\cos\theta)$$
$$= \frac{4\pi}{k^2}\sum_{\ell=0}^{\infty}(\ell+1)\sin^2(\delta_{\ell+1}-\delta_\ell) \qquad (17)$$

and viscosity cross section

$$\sigma_{vi} = \int d\Omega \frac{d\sigma(\theta,\phi)}{d\Omega}\sin^2\theta = 2\pi \int_0^\pi d\theta \sin^3\theta \,|f(\theta)|^2$$
$$= \frac{4\pi}{k^2}\sum_{\ell=0}^{\infty}\frac{(\ell+1)(\ell+2)}{2\ell+3}\sin^2(\delta_{\ell+2}-\delta_\ell). \qquad (18)$$

The expressions in Eqs. (16-18) containing the sums over phase shifts are valid for potential scattering.

We have calculated both moments of the elastic cross section for all collision systems considered here. To see how they relate to transport, consider the elastic scattering of a particle labeled a from another particle. The linear momentum of particle a is simply μv_a. Hence, its change in momentum is $\mu v_a(1-\cos\theta_{CM})$ and σ_{mt} is a measure of the average momentum lost in such a collision. Since backscattering retards the diffusion of particles in a gas or plasma, this loss of forward momentum determines the rate of diffusion. One can also use σ_{mt} to define such quantities as momentum transfer mean free path, collision frequency, and fractional energy loss per collision. The viscosity cross section, in contrast, is inversely related to the heat conductivity and viscosity of the gas or plasma. That is, collisions resulting in scattering to CM angles near $\pi/2$ are more effective in inhibiting conductivity because they tend to equalize energy and thus lead to smaller viscosity and heat conduction. The weighting factor $\sin^2\theta$, which is maximum at $\theta=\pi/2$ and goes to zero for $\theta \longrightarrow 0$ or π, emphasizes just such events.

I.4 Asymmetric ion-atom collisions: H^+ + He

For elastic scattering of hydrogen ions from ground state He in the energy range considered here, the excitation energy of He is high enough that couplings between different electronic states in Eq. (11) may be neglected. This is manifested by a significantly larger (by several orders of magnitude) integral elastic cross section in comparison to those for the inelastic channels. This approximation reduces the system of coupled equations (11) to equation (2), just as for the scattering of structureless particles. Thus, this is the approach adopted here for ion-helium scattering and, therefore, use is made of Eq. (8), with Eq. (5) for the differential cross section, as well as Eqs. (15-18) for the integral cross sections. The methods of computation of the phase shifts δ_ℓ as well as of the potential $V(R)$, used in this work, will be discussed below (in sections I.6 and I.9 (1), respectively).

I.5 Scattering of indistinguishable particles

Identical collision partners (as in H($1s$) + H($1s$) scattering) or identical incident and scattered+reaction product particles (as in elastic + symmetric charge transfer in H^+ + H scattering) keep their "individuality" in classical mechanics, in spite of their physical identity. Classically speaking, each of the particles can be labeled as well as their individual paths distinguished.

However, in quantum mechanics, identical particles lose their individuality, as follows from the uncertainty principle. If we localize one of the particles at some point in space at some instant, there is no way to detect which of them has arrived at the point. At larger velocities, as the wavelength of the colliding particles becomes much smaller than the effective interaction region, the particles take on classical properties: We can distinguish (or "label") each of the particles by their energy. For example, the wavelength of a proton of 1 eV is about 0.1 a.u. Assuming that the interaction region for scattering from a hydrogen atom in the ground state is of the dimension of the atom (~1 a.u.), one could expect the classical distinguishability of elastically scattered particles for this or higher energies which we show later to be the case.

The formulas in the preceding section are valid for scattering of distinguishable particles. Such particles obey so-called Boltzmann statistics [5, 12]. If $\Psi(\vec{R}_1, \vec{R}_2)$ is the wavefunction of the system of two indistinguishable particles, then the wavefunction obtained from Ψ by merely interchanging the particles must be equivalent physically to Ψ, i.e. could differ from the former only by a phase (φ) factor,

$$\Psi(\vec{R}_2, \vec{R}_1) = \exp(i\varphi)\Psi(\vec{R}_1, \vec{R}_2). \tag{19}$$

Since this must remain valid under repeated interchange, the phase factor is necessarily ± 1. The physical properties of the particles determine whether the system is described by a symmetrical or antisymmetrical wavefunction. The former are said to satisfy Bose-Einstein statistics (bosons) while the latter satisfy Fermi-Dirac statistics (fermions). In particular, the statistics obeyed by the particles is related to their spins: particles with integer spin are bosons and those with half-integer spin are fermions. Thus the total wavefunction of a system of bosons is symmetric, while that for a system of fermions is antisymmetric. The latter is a consequence of the Pauli exclusion principle, defined for fermions.

For a system of identical particles of spin s, the symmetry of the total wavefunction is determined by the sign of $(-1)^{2s}$. The symmetry of the spatial wavefunction of the relative motion is uniquely determined by the symmetry of the spin functions under an interchange of the particles. For example, there are $(2s+1)^2$ different spin states for two spin-s particles, defining the total spin of the system and its z-component. The total spin S takes $2s+1$ values $S = 2s, 2s-1, ..., 1, 0$. Since the spin function χ and the total function $\Psi = \Phi(\vec{R}_1, \vec{R}_2)\chi(1,2)$, upon interchange of particles change as $\chi_s(1,2) = (-1)^{2s-S}\chi_s(2,1)$

and $\Psi(1,2) = (-1)^{2s}\Psi(2,1)$ respectively, the spatial wavefunction changes as $\Phi(\vec{R}_1, \vec{R}_2) = (-1)^S \Phi(\vec{R}_2, \vec{R}_1)$, i.e. its symmetry is defined by the parity of the total spin.

Thus, the spatial wavefunction of a system of two identical particles is symmetrical if the total spin is even (singlet, for example), and antisymmetrical when the total spin is odd (triplet). If the spin couplings are neglected, all spin states are degenerate. If s is half integer, there are $s(2s+1)$ states with even values of S and $(s+1)(2s+1)$ with odd S values. On the other hand, when s is an integer, there are $(s+1)(2s+1)$ even S states and $s(2s+1)$ odd ones. Complex particles, composed of an even number of fermions (like the deuteron) obey Bose statistics (having integer s), while those with an odd number of fermions (the proton and triton) are fermions (with half-integer s). These details need to be taken carefully into account in considering the low energy elastic scattering of symmetric ion-atom and atom-atom of hydrogen or hydrogen isotopes [5, 6, 12].

I.5.1 Scattering of identical particles with definite total spin

None of the collision systems considered in this work obey spin-zero or definite total spin statistics. The examples given in this section will, however, emphasize the need for attention to the definition of the cross section as it emerges from the symmetry properties of the relevant wavefunctions before they can be compared with reference data taken from the literature or used in plasma modeling. In addition, they provide the opportunity to present a number of definitions required to describe the collisions that are treated here.

In the scattering of spin-zero particles, the total (spatial) wavefunction must be symmetric. In the center of mass system the relative motion of the particles is defined by the vector $\vec{R} = \vec{R}_1 - \vec{R}_2$, and interchange of the particles means a change of the sign $\vec{R} \to -\vec{R}$, i.e. while R is unchanged the scattering angle θ changes into $\pi - \theta$. Obviously, the symmetric form (under particle interchange) of the asymptotic wavefunction is

$$\Psi(R) = A\left[\exp(ikz) + \exp(-ikz) + (f(\theta) + f(\pi-\theta))\frac{\exp(ikR)}{R}\right] \ , R \to \infty \qquad (20)$$

where A is a normalization factor. The first two terms of this equation define the initial motion of the two particles moving in the CM system toward each other. Taking A=1 the flux density of each of the colliding particles has a magnitude $v = \frac{k}{\mu}$, where v is their relative velocity. Due to quantum indistinguishability, there is no way to determine which particle is the incident one. The last term is the scattered wave in the direction θ. The detector at angle θ counts both particles scattered at angles θ and $\pi - \theta$. Thus the elastic scattering cross section when any one of the particles is deflected into the solid angle $d\Omega$, at angle θ is [7, 9, 10]

$$\frac{d\sigma_{sym}}{d\Omega} = |f(\theta) + f(\pi - \theta)|^2 \qquad (21)$$

where we use the subscript sym as a shorthand notation for "symmetric," referring to the symmetry of the spin-zero wavefunction. Each of the amplitudes f is defined by Eq. (5), which yields

$$\frac{d\sigma_{sym}}{d\Omega} = \frac{4}{k^2}\left|\sum_{\ell=even} \exp(i\delta_\ell)\sin\delta_\ell P_\ell(\cos\theta)\right|. \tag{22}$$

Restoring for the moment the distinguishability of particles, the differential cross section that either of the particles will be deflected by an angle θ is simply the incoherent sum of the cross sections that one particle will scatter through an angle θ and the other through $\pi - \theta$,

$$\frac{d\sigma_{\text{``}cl\text{''}}}{d\Omega} = |f(\theta)|^2 + |f(\pi-\theta)|^2 \tag{23}$$

where we denote this cross section with classically distinguishable particles by $\sigma_{\text{``}cl\text{''}}$, and using the definition of the amplitudes we have

$$\frac{d\sigma_{\text{``}cl\text{''}}}{d\Omega} = \frac{1}{k^2}\left\{\left|\sum_{\ell=0}^{\infty}\exp(i\delta_\ell)\sin\delta_\ell P_\ell(\cos\theta)\right|^2 + \left|\sum_{\ell=0}^{\infty}(-1)^\ell\exp(i\delta_\ell)\sin\delta_\ell P_\ell(\cos\theta)\right|^2\right\}. \tag{24}$$

The difference between the two expressions is caused by the exchange effect: the interference of the two amplitudes due to the correlation in the motion of the particles arising from the symmetry of the states under an interchange of particles. Note that $d\sigma/d\Omega(\theta=\pi/2) = 2d\sigma_{\text{``}cl\text{''}}/d\Omega(\theta=\pi/2)$. If one assumes Boltzmann statistics, therefore allowing a labeling of the incident particle, the differential cross section is

$$\frac{d\sigma_B}{d\Omega} = |f(\theta)|^2 \tag{25}$$

which is a factor of 4 smaller (at $\theta = \pi/2$) than the cross section in Eq. (21).

Straightforward generalization of this treatment of spin zero colliding particles results when non-zero spin colliding identical particles have a definite value of the total spin. If the total spin is even, then the formulas for the total wavefunction and the differential cross section, Eqs. (20-21), are directly applicable. On the other hand, when the total spin is odd (as in the triplet state), the spatial wavefunction is antisymmetric

$$\Psi(R) = A\left[\exp(ikz) - \exp(-ikz) + (f(\theta) - f(\pi-\theta))\frac{\exp(ikR)}{R}\right], R\to\infty \tag{26}$$

and the cross section that either of the particles scatters through angle θ is

$$\frac{d\sigma_{antisym}}{d\Omega} = |f(\theta) - f(\pi-\theta)|^2 \tag{27}$$

i.e.

$$\frac{d\sigma_{antisym}}{d\Omega} = \frac{4}{k^2}\left|\sum_{\ell=odd}\exp(i\delta_\ell)\sin\delta_\ell P_\ell(\cos\theta)\right|. \tag{28}$$

This cross section has a value of 0 at $\theta = \pi/2$, in obvious disagreement with $\sigma_{\text{“}cl\text{”}}$.

The total elastic cross sections calculated from Eqs. (21, 23, 27), upon integration over all solid angles is readily obtained to be

$$\sigma_{el,sym} = 4\frac{4\pi}{k^2}\sum_{\ell=even}(2\ell+1)\sin^2\delta_\ell \tag{29}$$

$$\sigma_{el,antisym} = 4\frac{4\pi}{k^2}\sum_{\ell=odd}(2\ell+1)\sin^2\delta_\ell \tag{30}$$

$$\sigma_{el,\text{“}cl\text{”}} = 2\frac{4\pi}{k^2}\sum_{\ell=0}^{\infty}(2\ell+1)\sin^2\delta_\ell \tag{31}$$

and the one calculated under the assumption of complete distinguishability of particles, $\sigma_{el,B}$, is equivalent to Eq. (16), which we repeat here for convenience

$$\sigma_{el,B} = \frac{4\pi}{k^2}\sum_{\ell=0}^{\infty}(2\ell+1)\sin^2\delta_\ell. \tag{32}$$

The higher momenta of the elastic cross section, defined in Eqs. (17-18) are also strongly influenced by the symmetry properties of the wavefunctions. Thus, for the symmetric case,

$$\sigma_{mt,sym} = 4\frac{2\pi}{k^2}\sum_{\ell,\ell'=even}\exp i(\delta_\ell-\delta_{\ell'})\sin\delta_\ell\sin\delta_{\ell'}\int_0^\pi d\theta\sin\theta(1-\cos\theta)P_\ell(\cos\theta)P_{\ell'}(\cos\theta). \tag{33}$$

Using the recurrence relation of Legendre polynomials [13]

$$xP_\ell(x) = \frac{\ell+1}{2\ell+1}P_{\ell+1}(x) + \frac{\ell}{2\ell+1}P_{\ell-1}(x) \tag{34}$$

it follows that

$$\begin{aligned}\int_0^\pi d\theta\sin\theta\cos\theta P_\ell(\cos\theta)P_{\ell'}(\cos\theta) &= \\ \frac{\ell+1}{2\ell+1}\int_{-1}^1 dxP_{\ell+1}(x)P_{\ell'}(x) &+ \frac{\ell}{2\ell+1}\int_{-1}^1 dxP_{\ell-1}(x)P_{\ell'}(x) = 0\end{aligned} \tag{35}$$

where zero is obtained using the orthogonality of the Legendre polynomials of differing index ℓ. Since both ℓ and ℓ' are even, we have $\ell \neq \ell' \pm 1$ always. This yields

$$\sigma_{mt,sym} = \sigma_{el,sym}. \tag{36}$$

Similarly,

$$\sigma_{mt,antisym} = \sigma_{el,antisym}. \tag{37}$$

For classical scattering of identical particles, one obtains from Eq. (24)

$$\sigma_{mt,\text{“}cl\text{”}} = 2\frac{4\pi}{k^2}\sum_{\ell=0}^{\infty}(\ell+1)\sin^2(\delta_{\ell+1}-\delta_\ell) = 2\sigma_{mt,B} \tag{38}$$

where $\sigma_{mt,B}$ for distinguishable particles is given by Eq. (17). The viscosity cross section, defined in Eq. (18) is obtained in the form

$$\sigma_{vi,sym,antisym} = 4\frac{4\pi}{k^2}\sum_{\ell=even,odd}^{\infty}\frac{(\ell+1)(\ell+2)}{2\ell+3}\sin^2(\delta_{\ell+2}-\delta_\ell) \tag{39}$$

while

$$\sigma_{vi,\text{“}cl\text{”}} = 2\sigma_{vi,B} \tag{40}$$

where $\sigma_{vi,B}$ is given in Eq. (18) for the case of distinguishable particles.

I.5.2 Scattering of identical particles with nonzero spin: H + H, D + D, T + T

Usually, neither projectile nor target particles are in a definite spin state, the situation being described as scattering of the unpolarized beam of particles of spin s on the unpolarized target. Under these conditions one must average over all possible total spin states, odd and even, assuming that each of the spin combinations has equal probability. When the total spin is odd the cross section is given by Eq. (27), and when it is even, by Eq. (21). It follows [12] that the cross section that either of the particles will be scattered through an angle θ is, when s is half-integer

$$\frac{d\sigma_{el}}{d\Omega} = \frac{s}{2s+1}\frac{d\sigma_{sym}}{d\Omega} + \frac{s+1}{2s+1}\frac{d\sigma_{antisym}}{d\Omega}, \tag{41}$$

and, when s is integer

$$\frac{d\sigma_{el}}{d\Omega} = \frac{s+1}{2s+1}\frac{d\sigma_{sym}}{d\Omega} + \frac{s}{2s+1}\frac{d\sigma_{antisym}}{d\Omega} \tag{42}$$

where $d\sigma_{sym,antisym}/d\Omega$ are given by Eqs. (21, 27).

These formulas are directly applicable to the symmetric scattering of hydrogen atoms (and its isotopes). The H($1s$) + H($1s$) system can evolve both along the (ground of H_2) singlet $X^1\sum_g^+$ and the triplet $b^3\sum_u^+$ states, which are degenerate for $R \to \infty$. In particular, two kinds of symmetries are involved in this problem: symmetry with respect to the electronic spins and symmetry with respect to nuclear spins. Thus, the proper symmetrization of the amplitudes with respect to both total electron spin (S_e) and total nuclear spin (S_N) yields scattering amplitudes of the form

$$f(\theta) + (-1)^{S_N+S_e} f(\pi - \theta). \tag{43}$$

Since the hydrogen nuclei are fermions of spin 1/2, we apply Eq. (41) for both singlet and triplet states. Only parity of the total spins matters and the indices s and a in the equation are interpreted as the parity of the S_N. Further, $S_e = 0$ corresponds to the singlet electronic curve and $S_e = 1$ to the triplet. Thus, we obtain for the (electronic) singlet case

$$\frac{d\sigma_{el,s}}{d\Omega} = \frac{1}{4}\left|f_s(\theta) + f_s(\pi - \theta)\right|^2 + \frac{3}{4}\left|f_s(\theta) - f_s(\pi - \theta)\right|^2 \tag{44}$$

and for the (electronic) triplet

$$\frac{d\sigma_{el,t}}{d\Omega} = \frac{1}{4}\left|f_t(\theta) - f_t(\pi - \theta)\right|^2 + \frac{3}{4}\left|f_t(\theta) + f_t(\pi - \theta)\right|^2. \tag{45}$$

Due to the electron spin statistics, the singlet and triplet contributions to the total elastic cross sections are weighted by factors 1/4 and 3/4, respectively, leading to the total differential elastic cross sections for scattering of two H(1s) atoms in the form

$$\frac{d\sigma_{el}}{d\Omega} = \frac{1}{4}\frac{d\sigma_{el,s}}{d\Omega} + \frac{3}{4}\frac{d\sigma_{el,t}}{d\Omega} \tag{46}$$

which can be expressed as [12]

$$\begin{aligned}\frac{d\sigma_{el}}{d\Omega} \;=\; & \frac{1}{8k^2}\{\left|\sum_{\ell=even}(2\ell+1)(\exp(i\delta_\ell^s)\sin\delta_\ell^s P_\ell(\cos\theta)\right|^2 + \\ & 9\left|\sum_{\ell=even}(2\ell+1)(\exp(i\delta_\ell^t)\sin\delta_\ell^t P_\ell(\cos\theta)\right|^2 + \\ & 3\left|\sum_{\ell=odd}(2\ell+1)(\exp(i\delta_\ell^s)\sin\delta_\ell^s P_\ell(\cos\theta)\right|^2 + \\ & 3\left|\sum_{\ell=even}(2\ell+1)(\exp(i\delta_\ell^t)\sin\delta_\ell^t P_\ell(\cos\theta)\right|^2\}. \end{aligned} \tag{47}$$

Among the most notable work in the literature, Jamieson *et al.* [14] introduce an additional factor of 1/2 in order to adjust the cross section to become identical to that derivable from Boltzmann statistics in the classical limit (at high collision energy). We adopt this convention here as well. Upon integration over the scattering angle, this yields for the total integral elastic cross section [12, 14]

$$\sigma_{el} = \frac{2\pi}{k^2}\left[\sum_{\ell=even}(2\ell+1)(\frac{1}{4}\sin^2\delta_\ell^s + \frac{9}{4}\sin^2\delta_\ell^t) + \sum_{\ell=odd}(2\ell+1)(\frac{3}{4}\sin^2\delta_\ell^s + \frac{3}{4}\sin^2\delta_\ell^t)\right]. \tag{48}$$

Since $d\sigma_{el}/d\Omega$ contains the symmetry effects, expressed through the separate sums over even and odd partial waves, the part of the integral containing $\cos\theta$ in the integrand of the momentum transfer, Eq. (17) vanishes as in the derivation of Eqs. (36-37), and thus

$$\sigma_{mt} = \sigma_{el}. \tag{49}$$

This differs substantially from the formula

$$\begin{aligned}\sigma_{mt,Jamieson} = \frac{2\pi}{k^2}[\sum_{\ell=even} (\ell+1)(\frac{1}{4}\sin^2\Delta_\ell^s + \frac{9}{4}\sin^2\Delta_\ell^t) + \\ \sum_{\ell=odd} (2\ell+1)(\frac{3}{4}\sin^2\Delta_\ell^s + \frac{3}{4}\sin^2\Delta_\ell^t)]\end{aligned} \tag{50}$$

with $\Delta_\ell^{s,t} = \delta_{\ell+1}^{s,t} - \delta_\ell^{s,t}$, obtained by Jamieson *et al.* [14], starting from the same differential cross section, Eqs. (46-47), but agrees with the definitions of Hirschfelder *et al.* [12], for Bose (nuclear) and Fermi (electronic) statistics applied to the scattering of identical particles. Similarly conflicting definitions are applied in obtaining the momentum transfer cross section by Allison *et al.* [15]. An alternative momentum transfer cross section may be considered for H + H scattering at higher energies if one assumes full distinguishability of the projectile and target nuclei (Boltzmann statistics), thus applying only electronic spin statistics. This yields

$$\sigma_{mt,B} = \frac{4\pi}{k^2}\sum_{\ell=0}^{\infty}(\ell+1)(\frac{1}{4}\sin^2\Delta_\ell^s + \frac{3}{4}\sin^2\Delta_\ell^t). \tag{51}$$

Finally, we obtain the viscosity cross section from Eqs. (18, 47), in full agreement with Jamieson *et al.* [14]

$$\sigma_{vi} = \frac{2\pi}{k^2}\left[\sum_{\ell=even}\frac{(\ell+1)(\ell+2)}{2\ell+1}(\frac{1}{4}\sin^2\Lambda_\ell^s + \frac{9}{4}\sin^2\Lambda_\ell^t) + \sum_{\ell=odd}(2\ell+1)(\frac{3}{4}\sin^2\Lambda_\ell^s + \frac{3}{4}\sin^2\Lambda_\ell^t)\right] \tag{52}$$

where $\Lambda_\ell^{s,t} = \delta_{\ell+2}^{s,t} - \delta_\ell^{s,t}$. For the cases H + H and T + T (the proton and triton are both fermions with $s = 1/2$), we have integrated the elastic differential cross section with the appropriate weights numerically to prove that we obtain the same results as those defined through the formulas given in Eqs. (48-49, 52).

In case of elastic scattering of deuterium on deuterium, the statistics of the nuclear spins changes Eq. (42), since the deuteron, having spin $s = 1$, is a boson, rather than a fermion. Of course, the statistics of the electron spins is the same as in the H + H and T + T cases. Thus, we have again

$$\frac{d\sigma_{el}}{d\Omega} = \frac{1}{4}\frac{d\sigma_{el,s}}{d\Omega} + \frac{3}{4}\frac{d\sigma_{el,t}}{d\Omega} \tag{53}$$

but with

$$\frac{d\sigma_{el,s}}{d\Omega} = \frac{2}{3}\left|f_s(\theta) + f_s(\pi-\theta)\right|^2 + \frac{1}{3}\left|f_s(\theta) - f_s(\pi-\theta)\right|^2 \tag{54}$$

$$\frac{d\sigma_{el,t}}{d\Omega} = \frac{2}{3}\left|f_t(\theta) - f_t(\pi-\theta)\right|^2 + \frac{1}{3}\left|f_t(\theta) + f_t(\pi-\theta)\right|^2 \tag{55}$$

which yields

$$\begin{aligned}\frac{d\sigma_{el}}{d\Omega} \quad &= \quad \frac{1}{6k^2}\{2\left|\sum_{\ell=even}(2\ell+1)(\exp(i\delta_\ell^s)\sin\delta_\ell^s P_\ell(\cos\theta)\right|^2 \\ &\quad +3\left|\sum_{\ell=even}(2\ell+1)(\exp(i\delta_\ell^t)\sin\delta_\ell^t P_\ell(\cos\theta)\right|^2 \\ &\quad +\left|\sum_{\ell=odd}(2\ell+1)(\exp(i\delta_\ell^s)\sin\delta_\ell^s P_\ell(\cos\theta)\right|^2 \\ &\quad +6\left|\sum_{\ell=odd}(2\ell+1)(\exp(i\delta_\ell^t)\sin\delta_\ell^t P_\ell(\cos\theta)\right|^2\}. \end{aligned} \tag{56}$$

The integral cross section is obtained by integration of Eq. (56) over θ, which gives

$$\sigma_{el} = \frac{2\pi}{k^2}\left[\sum_{\ell=even}(2\ell+1)(\frac{2}{3}\sin^2\delta_\ell^s + \sin^2\delta_\ell^t) + \sum_{\ell=odd}(2\ell+1)(\frac{1}{3}\sin^2\delta_\ell^s + 2\sin^2\delta_\ell^t)\right]. \tag{57}$$

The momentum transfer cross section is equal to the elastic one, as in cases of H + H and T + T. The viscosity cross section is readily obtained in the form

$$\sigma_{vi} = \frac{2\pi}{k^2}\left[\sum_{\ell=even}\frac{(\ell+1)(\ell+2)}{2\ell+1}(\frac{2}{3}\sin^2\Lambda_\ell^s + \sin^2\Lambda_\ell^t) + \sum_{\ell=odd}(2\ell+1)(\frac{1}{3}\sin^2\Lambda_\ell^s + 2\sin^2\Lambda_\ell^t)\right]. \tag{58}$$

Assuming distinguishability of nuclei, the Boltzmann-distribution momentum transfer cross section takes on the same form as in the H + H and T + T cases. Moreover, assuming the Boltzmann distribution of nuclei, all differential and integral cross sections take similar forms, irrespective of the type of nuclei.

For convenience, we summarize the formulas for differential and integral cross sections in Tables I and II. For the differential cross section we adopt the form

$$\frac{d\sigma_{el}}{d\Omega} = \frac{1}{k^2}\left[\alpha_s\Gamma_s^+ + \alpha_t\Gamma_t^+ + \beta_s\Gamma_s^- + \beta_t\Gamma_t^-\right] \tag{59}$$

where

$$\Gamma_{s,t}^{\pm} = \left|\sum_{\ell=\pm}(2\ell+1)(\exp(i\delta_\ell^{s,t})\sin\delta_\ell^{s,t}P_\ell(\cos\theta)\right|^2 \tag{60}$$

and $\ell = \pm$ means $\ell = even$ and $\ell = odd$, respectively.

System	α_s	α_t	β_s	β_t
H+H, T+T	$\frac{1}{4}$	$\frac{9}{4}$	$\frac{3}{4}$	$\frac{3}{4}$
D+D	$\frac{2}{3}$	1	$\frac{1}{3}$	2

Table I. Parameters for the formulas (Eqs. (59-60)) defining the elastic differential cross section $d\sigma_{el}/d\Omega$ for neutral-atom–neutral-atom scattering.

The following general formula for the integral cross sections summarizes Eqs. (48-58):

$$\sigma = \frac{2\pi}{k^2} \sum_{\ell=\pm} g(\ell)(\omega_1^{\pm} \sin^2 \eta_1 + \omega_2^{\pm} \sin^2 \eta_2). \tag{61}$$

Parameters specific to the various isotopic variants of the collision systems and for the various integral cross sections are given in Table II, including, in addition to the elastic and transport cross sections, the spin-exchange cross section. Spin exchange comes from scattering of a polarized beam of incident particles on an unpolarized target followed by the detection of spin-changed particles. Since no interactions of spins is present, the detected particles come from the recoiled target atoms. Except for the momentum transfer cross section, the coefficients agree with those given by Jamieson *et al.* [14]. The D + D case has not been considered explicitly in the literature previously.

				H + H, T + T				D + D			
Type	g	η_1	η_2	ω_1^+	ω_2^+	ω_1^-	ω_2^-	ω_1^+	ω_2^+	ω_1^-	ω_2^-
el	$2\ell+1$	δ_ℓ^s	δ_ℓ^t	$\frac{1}{4}$	$\frac{9}{4}$	$\frac{3}{4}$	$\frac{3}{4}$	$\frac{2}{3}$	1	$\frac{1}{3}$	2
mt	$2\ell+1$	δ_ℓ^s	δ_ℓ^t	$\frac{1}{4}$	$\frac{9}{4}$	$\frac{3}{4}$	$\frac{3}{4}$	$\frac{2}{3}$	1	$\frac{1}{3}$	2
mt, B	$\ell+1$	$\delta_{\ell+1}^s - \delta_\ell^s$	$\delta_{\ell+1}^t - \delta_\ell^t$	$\frac{1}{4}$	$\frac{3}{4}$	$\frac{1}{4}$	$\frac{3}{4}$	$\frac{1}{4}$	$\frac{3}{4}$	$\frac{1}{4}$	$\frac{3}{4}$
vi	$\frac{(\ell+1)(\ell+2)}{2\ell+3}$	$\delta_{\ell+2}^s - \delta_\ell^s$	$\delta_{\ell+2}^t - \delta_\ell^t$	$\frac{1}{4}$	$\frac{9}{4}$	$\frac{3}{4}$	$\frac{3}{4}$	$\frac{2}{3}$	1	$\frac{1}{3}$	2
se	$2\ell+1$	$\delta_\ell^s - \delta_\ell^t$	0	$\frac{3}{16}$	0	$\frac{3}{8}$	0	$\frac{3}{16}$	0	$\frac{3}{8}$	0

Table II. Parameters for the integral cross sections in neutral-atom–neutral-atom scattering given by Eq. (61). (Abbreviations are *el* for elastic, *mt* for momentum transfer, *mt, B* for momentum transfer formula based on Boltzmann statistics, *vi* for viscosity, and *se* for spin exchange).

I.5.3 Symmetric ion-atom scattering: H^+ + H, D^+ + D, T^+ + T

The symmetric ion-atom scattering considered here is not scattering of identical particles in the full sense of the phrase and thus requires a separate treatment. Rather, only the nuclei of the colliding partners are identical and the two possible outcomes of the non-energy changing collision are elastic scattering and symmetric charge exchange, in which case the products of the two processes are indistinguishable.

The prototypical example is $H^+ + H(1s)$, a two-center–one-electron system (see e.g. [7]). We label the two centers with the letters A and B. In the separated atom limit, the eigenfunctions of the system must approach a symmetrized combination of atomic orbitals,

$\phi_j(\vec{r}_B)$ centered on B and $\phi_j(\vec{r}_A)$ centered on A. Thus the lowest molecular orbitals of H_2^+ separate into two combinations

$$\begin{aligned}\psi_{1s\sigma_g}(\vec{r}, R \to \infty) &\to \frac{1}{\sqrt{2}}[\phi_{1s}(\vec{r}_B) + \phi_{1s}(\vec{r}_A)]\\ \psi_{2p\sigma_u}(\vec{r}, R \to \infty) &\to \frac{1}{\sqrt{2}}[\phi_{1s}(\vec{r}_B) - \phi_{1s}(\vec{r}_A)].\end{aligned} \tag{62}$$

The total Hamiltonian of the problem is $\mathcal{H} = -\frac{1}{2\mu}\nabla_R^2 + \mathcal{H}_e$ where ∇_R^2 is the nuclear kinetic energy operator and $\mathcal{H}_e$ is the electronic Hamiltonian. The total Hamiltonian commutes with the parity operator so that the coupled equations for the radial wavefunctions of the nuclear motion, $F_{g,u}^{(L)}(R)$ divide into separate sets of even and odd parity (ignoring electron translation factors). Thus, the radial functions $F_{g,u}^{(L)}(R)$ satisfy the uncoupled equations

$$\left[\frac{d^2}{dR^2} - \frac{L(L+1)}{R^2} - 2\mu E_{g,u}(R) + 2\mu E\right] F_{g,u}^{(L)}(R) = 0 \tag{63}$$

where $E_{g,u}(R)$ are the adiabatic potentials of the $1s\sigma_g$ and $2p\sigma_u$ states, respectively, commonly known by their symmetry as gerade (g) and ungerade (u) states. Elastic scattering takes place in each of the uncoupled channels and the total nuclear function has the asymptotic form

$$F_{g,u}(\vec{R}) \mid_{R\to\infty} \to \exp(i\vec{k}\cdot\vec{R}) + f_{g,u}(\theta)\frac{\exp(ikR)}{R} \tag{64}$$

where $f_{g,u}(\theta)$ are the scattering amplitudes for the scattering angle θ

$$f_{g,u}(\theta) = \frac{1}{2ik}\sum_{L=0}^{\infty}(2L+1)(\exp(i2\delta_\ell) - 1)P_L(\cos\theta). \tag{65}$$

Furthermore, the initial arrangement in which ion A is incident on the atom $(B + e^-)$ is described according to Eq. (62) by the radial functions $[F_g^{(L)}(R) + F_u^{(L)}(R)]/2$. The scattering amplitude in this channel representing (direct) elastic scattering is [7]

$$f_d(\theta) = \frac{f_g(\theta) + f_u(\theta)}{2}. \tag{66}$$

Similarly, the amplitude for finding the configuration $(A + e^-) + B$ after the same initial arrangement is obtained from the radial function $[F_g^{(L)}(R) - F_u^{(L)}(R)]/2$, and thus the (exchange) scattering amplitude for charge transfer is

$$f_{ex}(\theta) = \frac{f_g(\theta) - f_u(\theta)}{2}. \tag{67}$$

The total initial wavefunction of the system can be written as $\phi_{1s}(\vec{r}_B)\exp(ikz)$, while in the final state the electron is attached either to A or to B. So there are two possible scattered waves that could reach the detector, i.e. [16]

$$\Psi_B \mid_{R\to\infty} \to \phi_{1s}(\vec{r}_B)\exp(ikz) + f_d(\theta)\phi_{1s}(\vec{r}_B)\frac{\exp(ikR)}{R} + f_{ex}(\theta)\phi_{1s}(\vec{r}_A)\frac{\exp(ikR)}{R} \tag{68}$$

where the first scattered wave is the proton and the second one is the hydrogen atom. These formulas thus define the elastic (direct) and charge transfer (exchange) channels in the case of ion-atom scattering when the nuclei have the same charge, but are distinguishable by other means (as is the case for collisions of different isotopes of hydrogen). This will be considered in further detail in the following section. In the case of identical nuclei another possible arrangement follows if the electron is initially on center A. This situation is derived from Eq. (68) if z is changed to $-z$ in the incident wave. If the direction of the detector is unchanged this means also a change of θ to $\pi - \theta$ in the amplitudes. Thus

$$\Psi_A \mid_{R\to\infty} \to \phi_{1s}(\vec{r}_A)\exp(-ikz) + f_d(\pi-\theta)\phi_{1s}(\vec{r}_A)\frac{\exp(ikR)}{R} + f_{ex}(\pi-\theta)\phi_{1s}(\vec{r}_B)\frac{\exp(ikR)}{R} \tag{69}$$

where the first scattered wave is the hydrogen atom and the second one is the proton. Since the nuclei are fermions of spin 1/2 the total wavefunction is antisymmetric upon interchange of the (space+spin) coordinates of the two protons. Thus, the singlet and triplet total nuclear spin states are

$$\Psi^{s,t} = \frac{1}{\sqrt{2}}(\Psi_B \pm \Psi_A) \tag{70}$$

respectively, which yields

$$\begin{aligned}\Psi^{s,t} \mid_{R\to\infty} \to \frac{1}{\sqrt{2}} & \{\phi_{1s}(\vec{r}_B)\exp(ikz) \pm \phi_{1s}(\vec{r}_A)\exp(-ikz)\} + \\ & \frac{\exp(ikR)}{\sqrt{2}R}\phi_{1s}(\vec{r}_B)\{f_d(\theta) \pm f_{ex}(\pi-\theta)\} + \\ & \frac{\exp(ikR)}{\sqrt{2}R}\phi_{1s}(\vec{r}_A)\{f_{ex}(\theta) \pm f_d(\pi-\theta)\}\,.\end{aligned} \tag{71}$$

The first scattered wave in this expression represents a beam of protons reaching the detector and the second one a beam of hydrogen atoms in the same direction. The differential cross section for deflection of protons in the direction θ is the ratio between the number of protons per second A reaching the detector and the flux of A protons per unit area in the incident beam. Although the flux of protons is 1 in the incident beam, the flux of protons labeled A is 1/2. Therefore the singlet-triplet components (s,t) of the differential cross section for the scattering of a proton in the direction θ are

$$\frac{d\sigma_{el}^{s,t}}{d\Omega} = |f_d(\theta) \pm f_{ex}(\pi-\theta)|^2\,. \tag{72}$$

Similarly, one can define the charge transfer cross section corresponding to the detection of hydrogen atoms in the direction θ for 1/2 the flux of the protons A in the incident beam, which yields

$$\frac{d\sigma_{ct}^{s,t}}{d\Omega} = \left| f_{ex}(\theta) \pm f_d(\pi - \theta) \right|^2 . \tag{73}$$

We consider the scattering of unpolarized protons by an unpolarized hydrogen atom target by a polarization insensitive detector. Taking into account the spin statistics of the two identical fermions, one obtains [7, 16, 17], therefore,

$$\frac{d\sigma_{el}}{d\Omega} = \frac{3}{4} \left| f_d(\theta) - f_{ex}(\pi - \theta) \right|^2 + \frac{1}{4} \left| f_d(\theta) + f_{ex}(\pi - \theta) \right|^2 . \tag{74}$$

Thus, this is the elastic cross section we calculate for the case of ion-atom scattering involving indistinguishable nuclei.

One can similarly define the flux of hydrogen atoms in the direction θ for an initially unpolarized incident proton beam. This would contain both recoiled hydrogen atoms and those formed by charge transfer, just as the elastic cross section contains both protons from the projectile beam and from the target. Thus we need somehow to distinguish the hydrogens produced by charge transfer from those elastically scattered. For that purpose we use the nuclear spin for labeling. If the incident flux of protons is polarized (for example of spin 1/2), and we are able experimentally to measure the spin of the protons reaching detector, the protons of the spin $-1/2$ are certainly formed in the unpolarized hydrogen target. Thus one defines the cross section for charge transfer between the proton and hydrogen atom of different nuclear spins, i.e. spin exchange. Since we are now able to distinguish the nuclei of the projectile and of the target by their spin, this is the heteronuclear-like collision, and as in Eq. (67) the spin exchange cross section is defined by [7, 16, 17]

$$\frac{d\sigma_{se}}{d\Omega} = \frac{1}{4} \left| f_g(\pi - \theta) - f_u(\pi - \theta) \right|^2 = \left| f_{ex}(\pi - \theta) \right|^2 \tag{75}$$

where the factor $\pi - \theta$ comes from the fact that the detected flux is of the recoiled target protons. *This is the spin exchange cross section that we calculate for ion-atom collisions with indistinguishable nuclei.* Note that the flux of the hydrogen atoms formed from the incident proton beam by charge transfer would be defined as $\left| f_{ex}(\theta) \right|^2$.

At relatively high collision energies $f_{g,u}(\theta)$ are sharply peaked in a narrow cone about $\theta = 0$. As a consequence, the overlap of $f_{g,u}(\theta)$ and $f_{g,u}(\pi - \theta)$ is minimal for small θ, i.e. these do not interfere. Then Eq. (74) can be written in the classical limit as

$$\frac{d\sigma_{el}}{d\Omega} \approx \left| f_d(\theta) \right|^2 + \left| f_{ex}(\pi - \theta) \right|^2 \tag{76}$$

which is the total differential cross section for detecting protons at an angle θ both by scattering of the beam of protons on the target of H atoms and by capturing electrons from the target atoms, assuming we have a means of distinguishing the scattered and charge transfer fluxes (for example by spin, or by energy). In that case, the charge transfer flux is in a small cone around $\theta = \pi$, while the elastic flux peaked around $\theta = 0$.

In this classical limit of distinguishable protons, one can define separately "pure" elastic and charge transfer cross sections as $|f_d(\theta)|^2$ and $|f_{ex}(\theta)|^2$, respectively. The latter one represents the flux of H atoms formed through electron capture to the impacting beam of protons. The corresponding flux of protons $|f_{ex}(\pi - \theta)|^2$, formed by charge transfer in the H target (producing the same integral cross section) would be deflected to angles near $\pi - \theta$. The spin-exchange cross section thus tends to the charge transfer cross section in the classical limit of distinguishability of nuclei, while the elastic cross section in Eq. (74) under the same circumstances leads to the "total" differential cross section. The energy at which this condition of distinguishability holds is well established (see e.g. [18]) and we find that it occurs for $E_{CM} >\sim 1$ eV. At lower energies the interference between the elastic and charge transfer channels brings an error into the calculation of the elastic cross section if this separation is done, the size of which we will discuss below.

Next, we consider the pertinent elastic and transport formulas by evaluating Eqs. (73-74). Thus, using Eqs. (65-67) in Eq. (74) one obtains

$$\frac{d\sigma_{el}}{d\Omega} = \frac{1}{4k^2}\left[\left|\gamma_g^+\right|^2 + 3\left|\gamma_u^+\right|^2 + \left|\gamma_u^-\right|^2 + 3\left|\gamma_g^-\right|^2 + 2\mathrm{Re}\{\gamma_g^{+*}\gamma_u^- + 3\gamma_g^{-*}\gamma_u^+\}\right] \tag{77}$$

where

$$\gamma_{g,u}^{\pm} = \sum_{\ell=\pm}(2\ell+1)\exp(i\delta_\ell^{g,u})\sin\delta_\ell^{g,u}P_\ell(\cos\theta) \tag{78}$$

and $\ell = \pm$ denotes summation over even (upper sign) and odd (lower sign) ℓ. For spin exchange we find

$$\frac{d\sigma_{se}}{d\Omega} = \frac{1}{k^2}\left|\sum_{\ell=0}^{\infty}(2\ell+1)\exp(i(\delta_\ell^g + \delta_\ell^u))\sin(\delta_\ell^g - \delta_\ell^u)P_\ell(\cos\theta)\right|^2. \tag{79}$$

The integral elastic cross section, its transport moments, and the spin exchange cross section are obtained from Eqs. (77-78):

$$\sigma_{el} = \frac{4\pi}{k^2}\left[\sum_{\ell=even}(2\ell+1)(\frac{1}{4}\sin^2\delta_\ell^g + \frac{3}{4}\sin^2\delta_\ell^u) + \sum_{\ell=odd}(2\ell+1)(\frac{3}{4}\sin^2\delta_\ell^g + \frac{1}{4}\sin^2\delta_\ell^u)\right] \tag{80}$$

$$\sigma_{mt} = \frac{4\pi}{k^2}\left[\sum_{\ell=even}(\ell+1)(\frac{1}{4}\sin^2\Delta_\ell^{gu} + \frac{3}{4}\sin^2\Delta_\ell^{ug}) + \sum_{\ell=odd}(\ell+1)(\frac{3}{4}\sin^2\Delta_\ell^{gu} + \frac{1}{4}\sin^2\Delta_\ell^{ug})\right] \tag{81}$$

$$\sigma_{vi} = \frac{4\pi}{k^2}[\sum_{\ell=even}\frac{(\ell+1)(\ell+2)}{2\ell+3}(\frac{1}{4}\sin^2\Lambda_\ell^g + \frac{3}{4}\sin^2\Lambda_\ell^u) +$$

$$\sum_{\ell=odd} \frac{(\ell+1)(\ell+2)}{2\ell+3}(\frac{3}{4}\sin^2\Lambda_\ell^g + \frac{1}{4}\sin^2\Lambda_\ell^u)] \tag{82}$$

$$\sigma_{se} = \frac{4\pi}{k^2}\sum_{\ell=0}^{\infty}(2\ell+1)\sin^2(\delta_\ell^g - \delta_\ell^u) \tag{83}$$

where $\Delta_\ell^{gu} = \delta_\ell^g - \delta_{\ell+1}^u, \Delta_\ell^{ug} = \delta_\ell^u - \delta_{\ell+1}^g$ and $\Lambda_\ell^{g,u} = \delta_{\ell+2}^{g,u} - \delta_\ell^{g,u}$. As in the case of scattering of atoms, described in the previous section, the formulas derived are applicable for both H^+ + H and T^+ + T collisions, since both the proton and the triton are fermions of spin $s = 1/2$. The scattering of the deuteron on deuterium must be treated separately since deuterons are bosons of spin $s = 1$, thus obeying different spin statistics. Applying similar details of derivation as in case of scattering of two deuterium atoms we obtain

$$\frac{d\sigma_{el}}{d\Omega} = \frac{1}{3k^2}\left[2\left|\gamma_g^+\right|^2 + \left|\gamma_u^+\right|^2 + 2\left|\gamma_u^-\right|^2 + \left|\gamma_g^-\right|^2 + 2\mathrm{Re}\{2\gamma_\mathrm{g}^{+*}\gamma_\mathrm{u}^- + \gamma_\mathrm{g}^{-*}\gamma_\mathrm{u}^+\}\right] \tag{84}$$

$$\sigma_{el} = \frac{4\pi}{k^2}\left[\sum_{\ell=even}(2\ell+1)(\frac{2}{3}\sin^2\delta_\ell^g + \frac{1}{3}\sin^2\delta_\ell^u) + \sum_{\ell=odd}(2\ell+1)(\frac{1}{3}\sin^2\delta_\ell^g + \frac{2}{3}\sin^2\delta_\ell^u)\right] \tag{85}$$

$$\sigma_{mt} = \frac{4\pi}{k^2}\left[\sum_{\ell=even}(\ell+1)(\frac{2}{3}\sin^2\Delta_\ell^{gu} + \frac{1}{3}\sin^2\Delta_\ell^{ug}) + \sum_{\ell=odd}(\ell+1)(\frac{1}{3}\sin^2\Delta_\ell^{gu} + \frac{2}{3}\sin^2\Delta_\ell^{ug})\right] \tag{86}$$

$$\begin{aligned}\sigma_{vi} \quad = \quad & \frac{4\pi}{k^2}[\sum_{\ell=even}\frac{(\ell+1)(\ell+2)}{2\ell+3}(\frac{2}{3}\sin^2\Lambda_\ell^g + \frac{1}{3}\sin^2\Lambda_\ell^u) + \\ & \sum_{\ell=odd}\frac{(\ell+1)(\ell+2)}{2\ell+3}(\frac{1}{3}\sin^2\Lambda_\ell^g + \frac{2}{3}\sin^2\Lambda_\ell^u)].\end{aligned} \tag{87}$$

These formulas are used in our calculations and, as in the case of neutral-atom–neutral atom scattering, can be conveniently summarized in the form of Eq. (61) the appropriate parameters of which are given in Table III. (We note that the spin-exchange cross section, being defined by invoking a polarized beam of particles, does not change its forms with choice of nuclei.)

				H^+ + H, T^+ + T				D^+ + D			
Type	g	η_1	η_2	ω_1^+	ω_2^+	ω_1^-	ω_2^-	ω_1^+	ω_2^+	ω_1^-	ω_2^-
el	$2\ell+1$	δ_ℓ^g	δ_ℓ^u	$\frac{1}{2}$	$\frac{3}{2}$	$\frac{3}{2}$	$\frac{1}{2}$	$\frac{4}{3}$	$\frac{2}{3}$	$\frac{2}{3}$	$\frac{4}{3}$
mt	$\ell+1$	$\delta_\ell^g - \delta_{\ell+1}^u$	$\delta_\ell^u - \delta_{\ell+1}^u$	$\frac{1}{2}$	$\frac{3}{2}$	$\frac{3}{2}$	$\frac{1}{2}$	$\frac{4}{3}$	$\frac{2}{3}$	$\frac{2}{3}$	$\frac{4}{3}$
vi	$\frac{(\ell+1)(\ell+2)}{2\ell+3}$	$\delta_{\ell+2}^g - \delta_\ell^g$	$\delta_{\ell+2}^u - \delta_\ell^u$	$\frac{1}{2}$	$\frac{3}{2}$	$\frac{3}{2}$	$\frac{1}{2}$	$\frac{4}{3}$	$\frac{2}{3}$	$\frac{2}{3}$	$\frac{4}{3}$
se	$2\ \ell+1$	$\delta_\ell^g - \delta_\ell^u$	$\delta_\ell^g - \delta_\ell^u$	2	2	2	2	2	2	2	2

Table III. Parameters for the integral cross sections in symmetric ion-atom scattering given by Eq. (61).

I.5.4 Isotopic effects: $D^+ + H$, $T^+ + H$, $T^+ + D$

Next we discuss the isotopic effects present in hydrogen-ion–hydrogen-atom elastic and charge transfer scattering, for the example of a deuteron colliding with hydrogen. The binding energy of D($1s$) is greater than that of H($1s$) by 0.0037 eV (this comes from the difference in the reduced masses of the $H^+ + e^-$ and $D^+ + e^-$ systems). This implies that the reaction $H^+ + D \rightarrow H + D^+$ has a threshold at a laboratory frame energy of $E_{LAB}^{threshold} = \frac{3}{2} \cdot 0.0037$ eV $= 0.0056$ eV and the corresponding cross section becomes much smaller than for the reaction $D^+ + H \rightarrow D + H^+$ as the collision energy decreases towards this value. In this case, the projectile can be distinguished in mass from the target nucleus and thus the cross section differs from the one which involves identical nuclei (like $H^+ +$ H).

The difference in masses of D^+ and H^+ not only influences the threshold energy, it also has an effect on the molecular potentials and the mechanism through which states are mixed. Technically, the center of mass for the DH^+ system is shifted from the mid-point of the internuclear distance, and the strict gerade-ungerade symmetry is lost. This is easily seen if the asymmetry in mass of the nuclei is converted to an asymmetry of the nuclear charges by introducing special coordinates [19]. Thus, in the new coordinates the one-electron system consisting of two nuclei, A and B, of masses M_A and M_B and of equal charges Z is transformed into a system of identical masses M^* and different charges Z_A and Z_B, with an "electron" of mass m^*, where

$$M^* = \frac{1}{1 - \sqrt{\mu_A \mu_B}}, Z_A = \sqrt{\mu_A} Z, Z_B = \sqrt{\mu_B} Z, m^* = \frac{1}{\mu_A \mu_B} \tag{88}$$

and

$$\mu_A = \frac{M_A}{M_A + 1}, \mu_B = \frac{M_B}{M_B + 1} \tag{89}$$

with all masses are expressed in atomic units.

The effective degree of departure from the symmetry is defined by the small parameter $\delta = 1/M_A - 1/M_B$ ($\approx 1.4 \cdot 10^{-4}$ for the HD^+ system). In these new coordinates, since we now have a system with asymmetrical charges, the two lowest adiabatic states, $1s\sigma$ and $2p\sigma$, lose their asymptotic degeneracy. Thus, for H^+ + D($1s$) collisions, the system initially evolves along the lower potential and charge transfer is a consequence of radial coupling with the higher potential of H($1s$) + D^+, accounting also for the threshold for the reaction. On the other hand, for D^+ + H($1s$) collisions, the system evolves along the higher curve initially, and being exothermic the charge transfer reaction is possible at any arbitrarily low energy. Strictly speaking, the problem should be treated within the two-state coupled-channel molecular orbital formalism, especially at energies close to the threshold. Such treatment was undertaken by Hunter and Kuriyan [20], who also tabulated the radial coupling matrix elements for the two lowest states of the HD^+ system.

Once the amplitudes for charge transfer and elastic scattering are calculated in that way, the cross section is found by the standard methods for distinguishable particles, outlined above.

However, due to the smallness of the parameter δ, one may approach the problem using a perturbative treatment [21]. This relies on the energy asymmetry parameter

$$\Delta\varepsilon = \Delta Z(1 + \frac{\Delta Z}{2}) \tag{90}$$

where ΔZ is the asymmetry in charges, defined as follows from Eq. (88)

$$\Delta Z = (\sqrt{\mu_A} - \sqrt{\mu_B})Z \tag{91}$$

and $Z = 1$ for the three systems of present interest. If the collision energy is large enough, for example $E_{CM} > 10\Delta\varepsilon$, the charge asymmetry can be neglected and the system behaves as a symmetric one. The two lowest potentials correspond to the gerade $V_{1s\sigma}$ and ungerade $V_{2p\sigma}$ states. As the energy decreases, the asymmetry effects become more important, and the effective potentials become

$$V_{\mp} = \frac{V_{1s\sigma} + V_{2p\sigma}}{2} \mp \frac{\sqrt{(V_{2p\sigma} - V_{1s\sigma})^2 + \Delta\varepsilon^2}}{2} \pm \frac{\Delta\varepsilon}{2}. \tag{92}$$

Obviously, when $\Delta\varepsilon \to 0$ then $V_- \to V_{1s\sigma}$ and $V_+ \to V_{2p\sigma}$. In first order perturbation theory, only the energies are perturbed and so scattering in the $V_\pm$ potentials interfere as in the symmetric case, but now with distinguishable particles (as in the classical limit). There is no need of recourse to the spin-exchange cross section and we can readily define the charge transfer cross section for all collision energies. The elastic cross section is clearly defined as well. The principal variation arises from the fact that the final and initial momenta are now slightly different because of the asymptotic difference in the binding energies. This was taken into account in calculating the cross sections at the lowest energies considered. As demonstrated in Figure 1, the perturbation theory approach is tested by a comparison of the present fully quantal results with those of Hunter and Kuriyan [20]. In the energy range above 0.1 eV, no significant difference between the two sets of integral cross sections is found.

Once the phase shifts are found for the gerade and ungerade states, we use the distinguishability of the nuclei (in mass) to obtain the elastic scattering and charge transfer amplitudes (see Eqs. (65-67) and the discussion below these equations), i.e.

$$f_{el}(\theta) = \frac{f_g(\theta) + f_u(\theta)}{2} \tag{93}$$

$$f_{ct}(\theta) = f_{ex}(\theta) = \frac{f_g(\theta) - f_u(\theta)}{2}. \tag{94}$$

These yield the elastic and charge transfer cross sections in the form

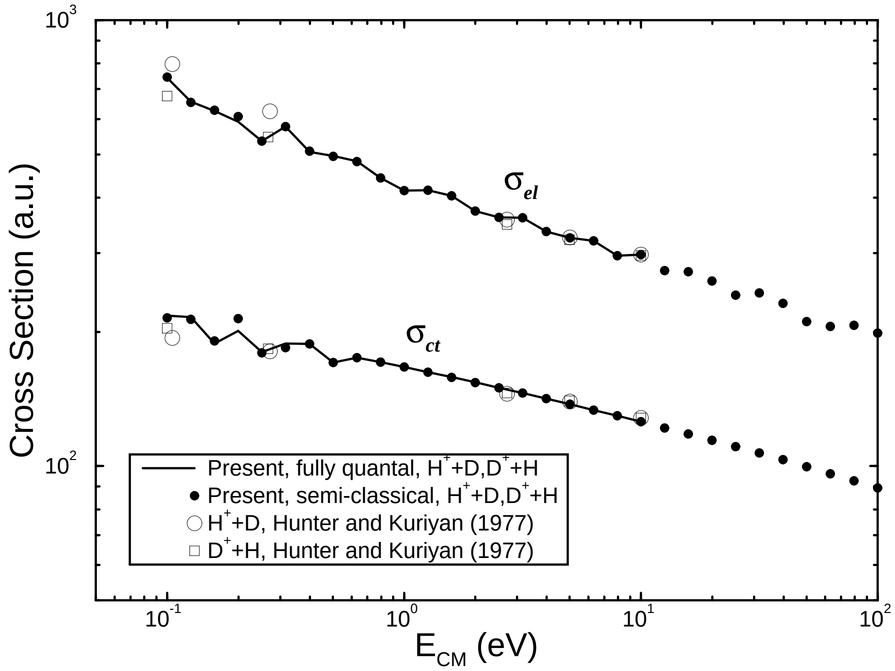

Figure 1: Comparison of the present fully quantal and semi-classical results with those of Hunter and Kuriyan [20]

$$\frac{d\sigma_{el}}{d\Omega} = \frac{1}{4k^2}\left|\sum_{\ell=0}^{\infty}(2\ell+1)(\exp(i\delta_\ell^g)\sin\delta_\ell^g + \exp(i\delta_\ell^u)\sin\delta_\ell^u)P_\ell(\cos\theta)\right|^2 \tag{95}$$

$$\frac{d\sigma_{ct}}{d\Omega} = \frac{1}{4k^2}\left|\sum_{\ell=0}^{\infty}(2\ell+1)\exp i(\delta_\ell^g + \delta_\ell^u)\sin(\delta_\ell^g - \delta_\ell^u)P_\ell(\cos\theta)\right|^2 \tag{96}$$

while, for the integral cross sections we obtain

$$\sigma_{el} = \frac{\pi}{k^2}\sum_{\ell=0}^{\infty}(2\ell+1)(\sin^2\delta_\ell^g + \sin^2\delta_\ell^u + 2\sin\delta_\ell^g\sin\delta_\ell^u\cos(\delta_\ell^g - \delta_\ell^u)) \tag{97}$$

$$\sigma_{ct} = \frac{\pi}{k^2}\sum_{\ell=0}^{\infty}(2\ell+1)\sin^2(\delta_\ell^g - \delta_\ell^u) \tag{98}$$

$$\sigma_{mt} = \frac{\pi}{k^2}\sum_{\ell=0}^{\infty}(\ell+1)(\sin^2\Delta_\ell^g + \sin^2\Delta_\ell^u + \sin\delta_{\ell+1}^g\sin\delta_\ell^u\cos\Delta_\ell^{gu} + \sin\delta_{\ell+1}^u\sin\delta_\ell^g\cos\Delta_\ell^{ug}) \tag{99}$$

$$\begin{aligned}\sigma_{vi} &= \frac{\pi}{k^2}\sum_{\ell=0}^{\infty}\frac{(\ell+1)(\ell+2)}{2\ell+3} \\ &\quad (\sin^2\Gamma_\ell^g + \sin^2\Gamma_\ell^u + \sin\delta_{\ell+2}^g\sin\delta_\ell^u\cos\Gamma_\ell^{gu} + \sin\delta_{\ell+2}^u\sin\delta_\ell^g\cos\Gamma_\ell^{ug})\end{aligned} \tag{100}$$

where $\Delta_\ell^a = \delta_{\ell+1}^a - \delta_\ell^a$, $\Delta_\ell^{ab} = \delta_{\ell+1}^a - \delta_\ell^b$, $\Gamma_\ell^a = \delta_{\ell+2}^a - \delta_\ell^b$, $\Gamma_\ell^{ab} = \delta_{\ell+2}^a - \delta_\ell^b$ and a and b stand for either u or g. These formulas are used in our calculations for hydrogen-ion–hydrogen-atom scattering with isotopically different nuclei.

Even at collision energies as low as 0.1 eV we find no difference in the differential cross sections for these $A^+ + B$ and $B^+ + A$ systems, where A and B ($A \neq B$) are any of the hydrogen isotope variations. This is due to the fact that the collision energy is significantly larger than the charge transfer threshold energy. Thus, we present the results only for $D^+ + H$, $T^+ + H$, and $D^+ + T$. The counterpart systems, $H^+ + D$, $H^+ + T$, and $T^+ + D$, can be considered as yielding identical results to these in the present energy range. Our calculations fully confirm such an assumption.

I.6 Calculation of the phase shifts

The elastic S-matrix element for the ℓ-th partial wave, S_ℓ, in the absence of inelastic channels, is uniquely connected with the relevant phase shift by the relation $S_\ell = \exp i2\delta_\ell$. As discussed above, in all cases considered, the radial functions (from which the asymptotic values of the S-matrix are extracted) satisfy uncoupled equations. For example, in case of H + H scattering the singlet and triplet states are uncoupled, while for $H^+ + H$ the gerade and ungerade states are uncoupled. Of course, each of the gerade states may be coupled with the excited gerade states, or each triplet may be coupled with excited triplet states. However, these couplings are readily neglected, since at low energies (0.1-100 eV) these are either below the threshold for the reaction or only slightly above, where the transition probability is very small. Similarly, in scattering of protons on He, only the He singlet ground state needs to be considered.

To solve the radial equations of nuclear motion, such as Eq. (2) or Eq. (63), we need the adiabatic potential energy surfaces governing the two colliding objects (found for a series of fixed separations R of the nuclei). This requires the solution of the diatomic eigenvalue problem. As demonstrated in the previous section it suffices in the energy range considered to use the diabatic potentials that do not depend on the nuclear masses but rather on the charges. Thus it is enough to calculate them for the $H^+ + H$ and H + H systems.

Calculation of the gerade and ungerade potential surfaces ($1s\sigma$ and $2p\sigma$ in the united atom limit molecular notation) can be calculated with arbitrary accuracy owing to the fact that one-electron–two-center problem is separable in prolate elliptic coordinates. These variables and their first derivatives were calculated with a step of 0.0002 a.u. up to $R \leq 1$ and a step of 0.001 up to $R \leq 50$ to obtain a smooth linear fit at the required R's with high accuracy for the calculation of the phase shifts. At even larger R an asymptotic expansion up to eleventh order in $1/R$ is used in analytic form [22]. Concerning the H + H system, we have used the best available ground state potentials (both singlet and triplet) provided by private communication from Jamieson [14] based on his extensive compilation and fit of the calculations of Kolos and Wolniewicz [23], slightly modified to remove a discontinuity present in the derivative of the potential.

The radial equations for the elastic amplitudes of the gerade and ungerade states of

$A^+ + B$ systems (A and B are any of the hydrogen isotopes) as well as those of the singlet and triplet states of the neutral $A + B$ systems were solved using the algorithm proposed by Johnson [24] for solution of the stationary Schrödinger equation using the logarithmic derivatives for each partial wave, with $R_{\text{max}} = 200$ a.u. in the former and R_{max}=30 a.u. in the latter case, and with R_{min}=0.01 a.u. in both cases. The step in R used on the numerical mesh was 0.0001 a.u. The convergence of the elastic S-matrix elements S_ℓ in partial waves was established for each energy by requiring that $\text{Re}\{S_\ell\} \geq 0.99999$ for at least ten consecutive partial waves. The values of ℓ_{max} for a sampling of energies spanning the full range under consideration for some of the ion-atom and atom-atom systems are shown in Table IV. We note that a significantly larger number of partial waves is needed for convergence of ion-atom amplitudes in comparison to those for atom-atom amplitudes. This is a consequence of the larger range of the effective potentials in the former case in comparison to those for neutral atoms.

System	H^+ + H	D^+ + H	T^+ + T	H + H	D + H	T + T
E(eV)	ℓ_{max}	ℓ_{max}	ℓ_{max}	ℓ_{max}	ℓ_{max}	ℓ_{max}
0.1	253	306	522	57	66	102
1	540	657	1120	130	152	241
5	924	1121	1917	240	283	452
10	1162	1409	2412	314	371	595
100	2501	2920	3960	795	938	1502

Table IV. Number of partial waves needed for convergence of the elastic amplitudes in representative ion- and atom-hydrogen collisions.

Once the elastic S-matrix elements S_ℓ were found, the phase shifts for each partial wave were calculated as

$$\delta_\ell = \text{mod}\left(\frac{1}{2}\text{arctg}\left(\frac{\text{Im}\{S_\ell\}}{\text{Re}\{S_\ell\}}\right), 2\pi\right). \tag{101}$$

The phase shifts were also calculated for all 31 collision energies in the range of 0.1 to 100 eV, and for all systems, using the semi-classical expression for the phase shifts

$$\delta_\ell^j = \int_{r_0}^{\infty} \left[k^2 - 2\mu(V_j(R) - \varepsilon_j) - \frac{(\ell + \frac{1}{2})^2}{R^2}\right]^{\frac{1}{2}} dR - \int_{r_0'}^{\infty} \left[k^2 - \frac{(\ell + \frac{1}{2})^2}{R^2}\right]^{\frac{1}{2}} dR \tag{102}$$

where r_0 and r_0' are the zeros (turning points) of the first and second integrand, respectively, and j stands for either the gerade or ungerade state in the ion-atom case, and for either the singlet or triplet state in the atom-atom case. The integration was performed for values of R as large as needed to achieve the convergence of δ_ℓ to within 0.0001. The convergence in ℓ was checked with a similar accuracy requirement of $\delta_\ell \leq 0.0001$. The number of partial waves needed to achieve these convergences is very similar to $\ell_{\max}$ in the fully quantal treatment presented in Table IV. Furthermore, in the energy range considered, the phase shifts calculated with the converged fully quantal and semi-classical procedures are almost indistinguishable, as are the relevant cross sections calculated from them (see Figure 2).

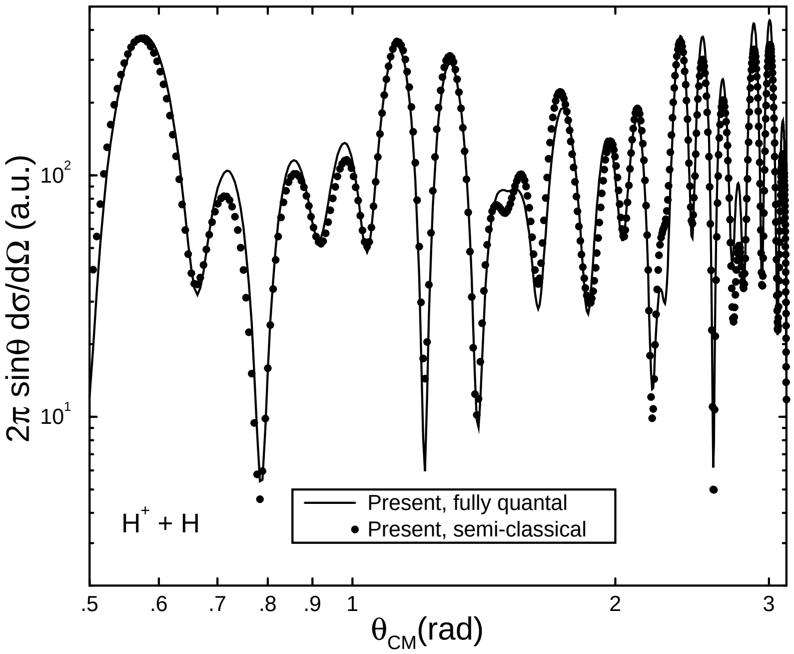

Figure 2: Comparison of the present fully quantal and semi-classical results for the 0.1 eV H^+ + H elastic differential cross section.

Figures 3 and 4 show a comparison of the elastic amplitudes calculated in the two approaches for some of the partial waves and energies for the H^+ + H collision system. For these cases we also show a comparison with the elastic amplitudes calculated by Hunter and Kuriyan [17]. This is, of course, reflected in the excellent agreement of the differential cross sections calculated by the two methods (fully quantal and semi-classical) and by Hunter and Kuriyan as shown in Figures 5-7.

For hydrogen-ion–helium elastic scattering there is a simplification compared to the hydrogen-ion–hydrogen-atom or hydrogen-atom–hydrogen-atom collisions discussed above, namely that only the ground state potential curve relevant for the elastic scattering is important. This potential curve was found utilizing a mixed hydrogen-helium Gaussian basis of 34 functions in the Restricted-Hartree-Fock–Full-Configuration-Interaction (RHF-CI) procedure in GAMESS (General Atomic and Molecular Electronic Structure System) [25], in steps of R of 0.02 a.u. for R as large as 20 a.u. For larger values of R, the common polarization potential of He was used. The convergence criteria used in the calculation of the phase shifts were very similar to those used in treating the H^+ + H.

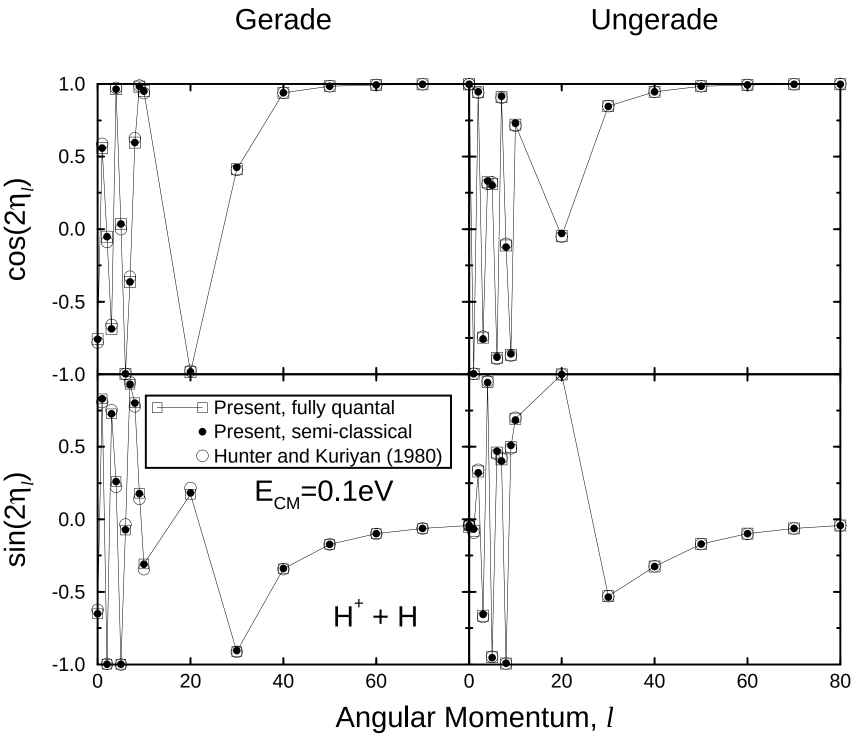

Figure 3: Real and imaginary parts of the elastic scattering amplitude for 0.1 eV H^+ + H collisions.

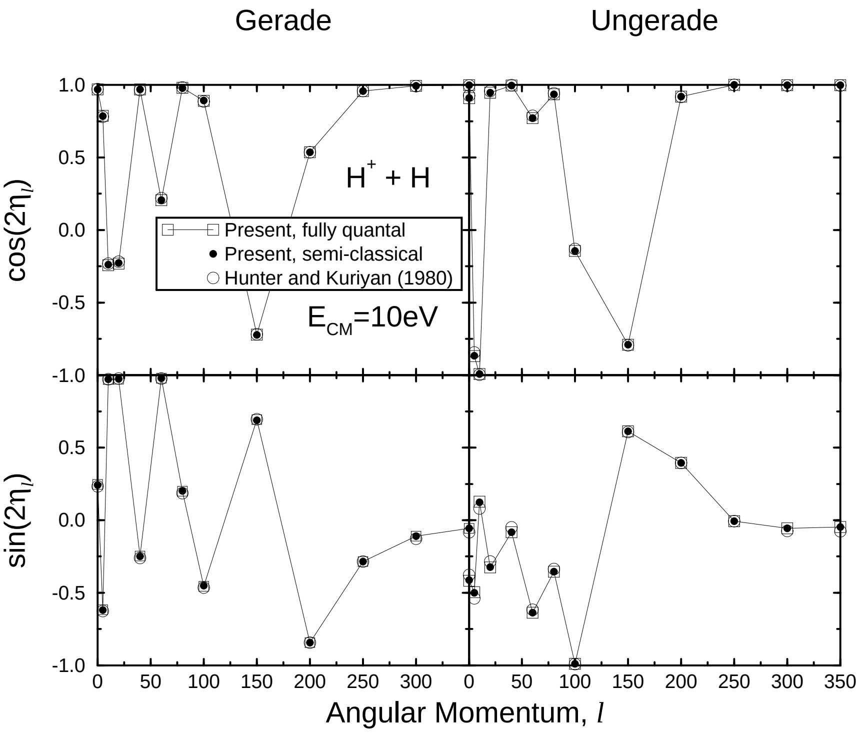

Figure 4: Real and imaginary parts of the elastic scattering amplitude for 10 eV H^+ + H collisions.

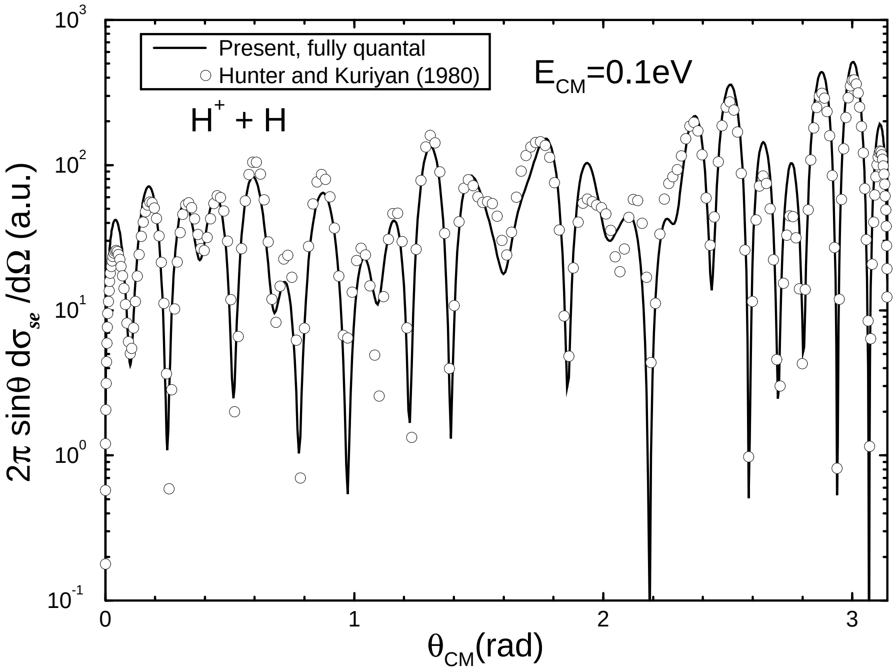

Figure 5: Example of the present spin exchange differential cross section compared with the results of Hunter and Kuriyan [17].

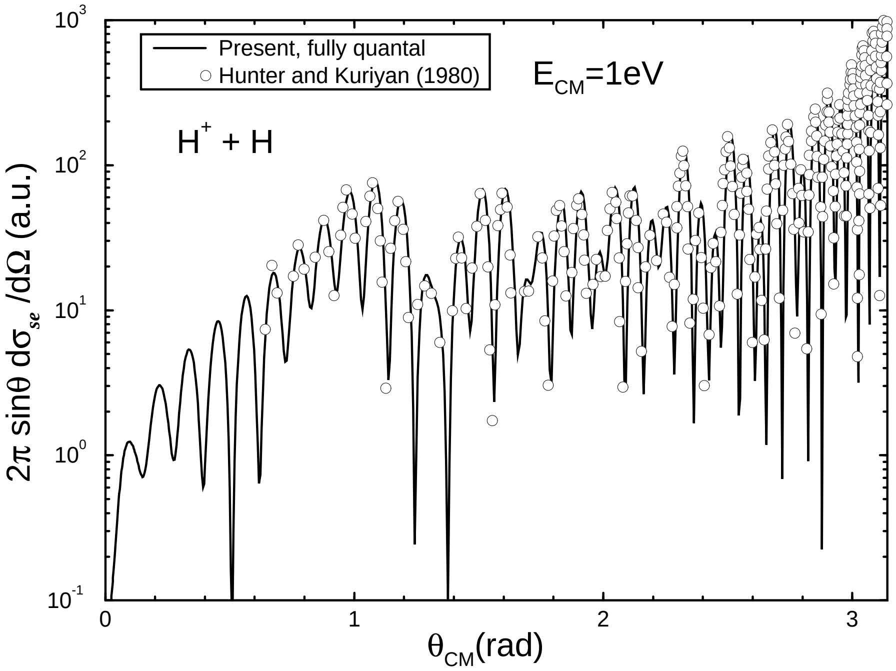

Figure 6: Same as Figure 5 but at $E_{CM} = 1$ eV.

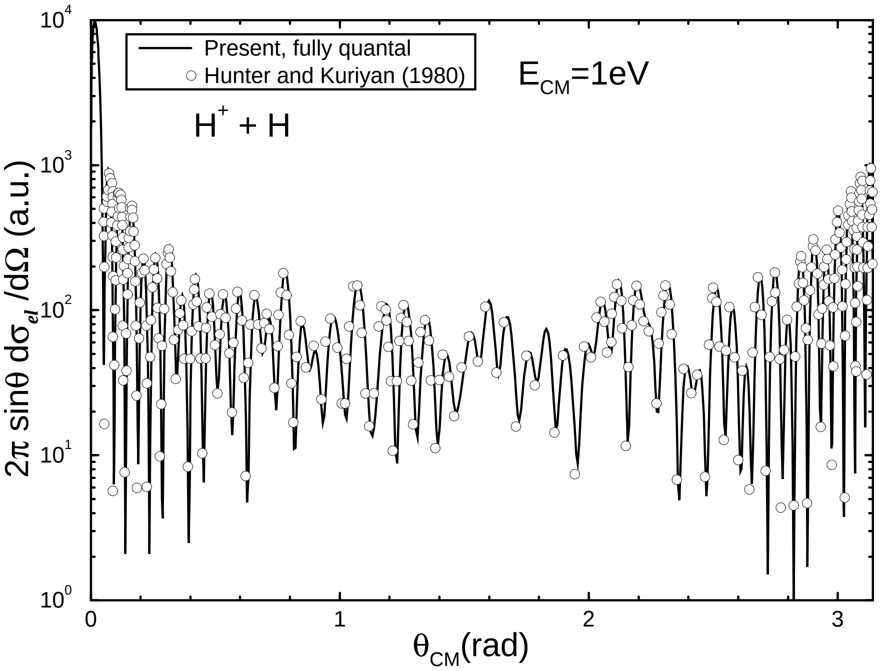

Figure 7: Same as Figure 5 but for the elastic differential cross section at 1 eV collision energy.

I.7 Ion-molecule and atom-molecule collisions

In this work we have also calculated the elastic differential cross sections for scattering of protons, deuterons and tritons from H_2, D_2, T_2, HD, HT, and DT molecules on the ground electronic and vibrational ($\nu = 0$) state and computed the integral cross sections (elastic, momentum transfer, viscosity). Inelastic (direct) vibrational transitions on the ground electronic surface were included in the calculation. Inelastic processes that involve a change of electronic molecular state were neglected on account of the low collision energy.

The number of degrees of freedom in the scattering from molecules is significantly increased in comparison to those present in ion-atom collisions. *Ab initio* numerical solution of the collision problem, with simultaneous inclusion of all degrees of freedom, is an extremely difficult computational task. Specifically, here we consider collisions of the type

$$\begin{aligned} A^+ + BC(\nu_i = 0) &\rightarrow A^+ + BC(\nu_f) \\ A + BC(\nu_i = 0) &\rightarrow A + BC(\nu_f). \end{aligned} \tag{103}$$

Although these are among the simplest of all ion/atom-molecule collisions (involving only two and three electrons, respectively), there exist no comprehensive data for these processes in the energy range below 100 eV.

The choice of approximations that can be reasonably applied to make computations for the processes in Eq. (103) tractable depends on the process to be considered as well as on the collision energy range. For example, in the range above a few hundred eV, the projectile is so fast that both the internuclear diatomic coordinate and its direction in space may be considered as frozen during the collision. This significantly simplifies the treatment of the collision dynamics of the electronic transitions, resulting in methods similar to those employed to treat ion-atom collisions.

In contrast, consideration of the energy range below about 100 eV, down to the order of 1 eV, requires simultaneous coupling of the electronic and vibrational motions. In particular, the excitation energy of the first vibrational state of H_2 is ~ 0.5 eV corresponding to a characteristic vibration time exceeding 50 a.u. which is comparable to the collision time. In contrast, the collision time is still short enough on the scale of molecular rotations (excitation energy $<$0.01 eV, i.e. the characteristic time ~ 300 a.u.), to enable one to treat the direction of the diatomic internuclear axis as fixed. This is often called the Infinite Order Sudden Approximation (IOSA) [26, 27, 28, 29]. The pertinent angle, γ, is defined as the angle between the reaction coordinate R (from the center of mass of the diatom to the projectile nucleus) with the diatomic internuclear axis. But since the adiabatic triatomic molecular surfaces, on which the collision dynamic evolves at these energies, is not isotropic with respect to γ, especially at small internuclear distances, one needs to calculate the observables for different angles γ and then average over them for the full solid angle. For a particular initial and final vibrational state this is equivalent to the summation over all final excited rotational states and the average over initial rotational states. This is the approach that we adopt in this work and which we describe in some detail.

The total Hamiltonian of the problem can be written in terms of the nuclear kinetic energy operator T_N and electronic energy operator $\mathcal{H}_e$

$$\mathcal{H} = T_N + \mathcal{H}_e \tag{104}$$

Using the Born-Oppenheimer prescription for separation of the fast electronic and slow nuclear motions, one expands the wavefunction in terms of a complete set of eigenfunctions $\Phi_k^e(\vec{r}, \{\vec{R}_N\})$ of the electronic Hamiltonian for fixed $\{\vec{R}_N\}$ as

$$\Psi = \sum_k f_k(\{R_N\}) \Phi_k^e(\vec{r}, \{\vec{R}_N\}) \tag{105}$$

where $\vec{r}$ and $\{\vec{R}_N\}$ are the sets of electronic and nuclear coordinates, respectively, and summation also implies integration over electronic continuum. Substituting Eq. (105) into the Schrödinger equation for the problem yields a set of coupled partial integro-differential equations for the "nuclear" amplitudes f_k

$$\sum_k H_{jk} f_k + [T_N + E_j(\{\vec{R}_N\}) - E] f_j = 0 \tag{106}$$

where E_j are eigenenergies of the electronic Hamiltonian, E is the total (conserved) energy of the colliding system and H_{jk} are matrix elements of the dynamic (nonadiabatic) interaction having the structure

$$H_{jk} \sim \left\langle \Phi_j \left| \nabla_N^2 \right| \Phi_k \right\rangle + \left\langle \Phi_j | \vec{\nabla}_N | \Phi_k \right\rangle \cdot \vec{\nabla}_N. \tag{107}$$

For an ion (or atom) scattering from a diatomic molecule the set of nuclear coordinates may be chosen in terms of the diatomic internuclear separation ρ, the internuclear separation of the ion (or atom) and the diatomic center of the mass, $\vec{R}$, and the angle γ between $\vec{R}$ and $\vec{\rho}$. For a fixed γ (IOSA) T_N simplifies significantly to yield the form [29]

$$T_N = -\frac{1}{2M}\frac{\partial^2}{\partial R^2} - \frac{1}{2\mu}\frac{\partial^2}{\partial \rho^2} + \frac{1}{2M}\frac{\ell(\ell+1)}{R^2}. \tag{108}$$

where M and μ are the reduced masses of the three-atom and diatomic molecule, respectively, and ℓ is the angular quantum number of the projectile motion.

In order to solve the problem defined above we expand the nuclear wavefunctions f_k for each electronic state k in the full set of vibronic wavefunctions $\lambda_\nu^{(k)}(\rho)$, (with $\varepsilon_\nu^{(k)}$ the corresponding eigenvalue), i.e.

$$(-\frac{1}{2\mu}\frac{\partial^2}{\partial \rho^2} + E_k(R \to \infty, \rho))\lambda_\nu^{(k)}(\rho) = \varepsilon_\nu^{(k)} \lambda_\nu^{(k)}(\rho). \tag{109}$$

We note that $E_k(R, \rho, \gamma)$ for finite R does not depend on γ when the projectile is far enough from the diatom, that is, the adiabatic potential is isotropic in that limit. The absence of a diatomic centrifugal energy term is one of the peculiarities of the IOSA. Therefore, with the ansatz

$$f_k = \sum_\nu a_\nu^{(k)}(R, \gamma, \ell) \lambda_\nu^{(k)}(\rho) \tag{110}$$

and using Eq. (108) and Eq. (106) yields

$$[-\frac{1}{2M}\frac{\partial^2}{\partial R^2} + \frac{1}{2M}\frac{\ell(\ell+1)}{R^2} - (E - \varepsilon_\nu^{(j)})] a_\nu^{(j)} + \sum_\mu W_{\nu\mu}^{(j)}(R, \gamma) a_\mu^{(j)} + \sum_{\mu,k} H_{jk}^{(\nu,\mu)}(R, \gamma) a_\mu^{(k)} = 0 \tag{111}$$

where

$$W_{\nu\mu}^{(j)}(R) =< \nu | \sum_\mu E_j(R, \rho, \gamma) - E_j(R \to \infty, \rho) | \mu > \tag{112}$$

and

$$H_{jk}^{(\nu,\mu)}(R,\gamma) =< \nu|H_{jk}(R,\gamma,\rho)|\mu > \tag{113}$$

for all electronic states j, and all vibrational states $\nu^{(j)}$. This system of ordinary differential equations is extremely difficult to solve, not so much because of its size, but rather due to the difficulties in accurately determining all of its matrix elements. Besides, it has to be solved for each orientation angle γ, since the cross sections are to be averaged over it.

Once the "vib-electronic" amplitudes are found by solving the system of differential equations, the differential cross section for a transition into vib-electronic state (ν,k) is [29]

$$\frac{d\sigma^{\nu,k}(E)}{d\Omega} = \frac{1}{8K^2}\sum_{\ell}\sum_{\ell'}(2\ell+1)(2\ell'+1)P_{\ell}(\cos(\theta))P_{\ell'}(\cos(\theta))\cdot$$
$$\int_0^{\pi} d\gamma \sin(\gamma)(\delta_{(\nu,k),(0,0)} - a_{\nu}^{(k)}(\infty,\gamma,\ell))(\delta_{(\nu,k),(0,0)} - a_{\nu}^{*(k)}(\infty,\gamma,\ell')) \tag{114}$$

where $\vec{K}$ is the initial projectile momentum, $\delta_{i,j}$ is the Kronecker symbol and the limit $R\to\infty$ is assumed. Finally, the total cross section is obtained by integration over the full scattering solid angle Ω, which yields

$$\sigma_{el}^{\nu,k}(E) = \frac{\pi}{2K^2}\sum_{\ell}(2\ell+1)\int_0^{\pi} d\gamma \sin(\gamma)\left|(\delta_{(\nu,k),(0,0)} - a_{\nu}^{(k)}(\infty,\gamma,\ell))\right|^2. \tag{115}$$

For the elastic channel ($\nu = 0, k = 0$) we also calculate the momentum transfer and viscosity cross sections, integrating numerically the differential cross sections over Ω, weighted with relevant θ-dependent functions (Eqs. (17-18)).

Specifically, we have solved the coupled Eqs. (111) for the ground electronic potential surface ($k = 0$) within a truncated set of vibrational states $0 \le v \le 9$, in the range of collision energies 0.1 eV $\le E_{CM} \le$ 100 eV, for the 10 values of $0 \le \gamma \le \pi/2$ (for $\pi/2 \le \gamma \le \pi$, the amplitudes are symmetric to those in the first quadrant of γ). The calculation is performed for 10 energies per decade, thus $E = 10^{0.1j-1}$, $j = 0, 20$, with only three values in the third decade ($j = 23, 27, 30$) due to the extreme computational intensity required and due to the relatively smooth behavior of the integral cross sections in this last energy decade. The Eqs. (111) were solved using Johnson's algorithm [24] of logarithmic derivatives for each angular quantum number ℓ until convergence in ℓ is achieved for the elastic amplitude.

The convergence check in number of partial waves $\ell_{\max}$ considered two principal criteria. All inelastic (vibrationally excited) channels were included until the elastic channel probability stably reached a value of 0.99999 (if it repeated 10 times in succession). This defined $\ell_{\max}^{inel}$. Still, except for the highest energies treated, this was far below the convergence in ℓ needed for the elastic channel: the elastic amplitude $a_0^{(0)}(\ell)$ oscillates as $\exp(i2\delta_{\ell})$ for a range of large values of ℓ until it reaches our adopted convergence criteria ($\ell_{\max}^{el}$, $\mathrm{Re}\{a_0^{(0)}(\ell)\} \ge 0.9999$, repeated 10 times in succession). The values of $\ell_{\max}^{el}$

depend on collision energy and on the reduced mass of the system. We show the typical variations of these quantities in Table V for the mass extremes of the ion-molecule and atom-molecule systems considered here. We also note that there is a weak dependence of $\ell_{\rm max}$ on molecular orientation (γ).

System	$H^+ + H_2$		$T^+ + H_2$		$H + H_2$		$T + T_2$	
E(eV)	$\ell^{inel}_{\rm max}$	$\ell^{el}_{\rm max}$	$\ell^{inel}_{\rm max}$	$\ell^{el}_{\rm max}$	$\ell^{inel}_{\rm max}$	$\ell^{el}_{\rm max}$	$\ell^{inel}_{\rm max}$	$\ell^{el}_{\rm max}$
0.1		56		90		42		68
1	41	153	80	257	17	98	38	183
5	152	326	277	561	144	191	255	358
10	251	455	443	787	209	216	367	472
100	1189	1314	2168	2406	649	649	1132	1132

Table V. Number of partial waves needed for convergence of inelastic and elastic amplitudes in representative ion– and atom–hydrogen-molecule collisions.

Three additional numerical convergence parameters are important in the calculation. These are the minimum and maximum values of the reaction coordinate R, and the step size of the numerical mesh. In all cases $R_{\rm min} = 0.05$ a.u., while $R_{\rm max} = 40$ and 15 a.u. for the ion-molecule and atom-molecule cases, respectively. The step size was varied between 0.0001 and 0.001 a.u., depending on the energy and the reduced mass of the system considered.

Significant attention was paid to obtain reliable potential surfaces $E_j(R, \rho, \gamma)$. For the atom-molecule systems, only the ground (lowest in energy) potential surface was needed, which is not the case for the ion-molecule systems. In the latter, there is a strong avoided crossing between the two lowest potential surfaces at $\rho \simeq 2.6 a.u.$, for all $R >\sim 4.5$ a.u. This is a consequence of the fact that when $\rho > 2.6$ the $H^+ + H_2$ surface is above the charge transfer surface $H + H_2^+$ when $R \to \infty$. When $R \to \infty$ the $H^+ + H_2$ surface becomes a function of only the diatomic coordinate ρ, i.e. $(H^+ + H_2)(R \to \infty, \rho, \gamma) \longrightarrow H_2(\rho)$. On the other hand, $(H + H_2^+)(R \to \infty, \rho, \gamma) \longrightarrow H(1s) + H_2^+(\rho)$. The two ρ-dependent triatomic curves cross at $\rho \approx 2.6$ a.u. Thus if the neutral molecule is in a high enough ($\nu \geq 4$) vibrational state, then upon the approach of the projectile H^+ to the H_2 target, a diabatic transition is made to the lower adiabatic surface. To account for the effect of this curve "crossing," we performed the calculation with the adiabatic surfaces transformed to the diabatic representation with the correct boundary conditions [29].

We have calculated the adiabatic surfaces for the ground state and first excited state of H_3^+ using a 54-state Gaussian basis in the Unrestricted-Hartree-Fock–Full-Configuration-Interaction (UHF-CI) approach using GAMESS [25]. The calculation was performed on a numerical mesh with 0.1 a.u. step in ρ between 0.1 and 6 a.u. and in R between 0 and 15 a.u., and for diatomic orientation angles γ = 0, 10, 20, 30, 40, 50, 60, 70, 80, 90°. The adiabatic potential surfaces of H_3^+ are used for any isotope combination in H_3^+. At even larger R we approximated the potential with dipole and polarization corrections. The surfaces were compared with the calculations of Ichihara [30] (who used a larger basis but in a narrower range of coordinates), and found agreement to within 1.5% for the ground state (lower) surface. The adiabatic-diabatic transformation was performed using the nonadiabatic radial matrix elements determined by the Diatom-In-Molecule (DIM) method (see e.g. [29]). This approach is quite accurate for values of R larger than 2 a.u. (where the "seam" of avoided crossings occurs). Only the diabatic surface which corresponds to H^+ + H_2 at $R \to \infty$ (elastic channel) was then taken into account in the calculation of the diabatic matrix elements between vibrational states, Eq. (113), which then were used to define the system of vibrationally coupled equations, Eq. (111).

The vibrational wavefunctions of all vibrational states were found by numerical solution of the radial Schrödinger equation, Eq. (109), for vibrational quantum numbers $0 \leq \nu \leq 9$, for all relevant molecules (H_2, HD, D_2, HT, DT, and T_2). Although we included as many as nine excited vibrational states in order to compute the elastic cross section correctly, and since for $\nu \geq 4$ excited states of the ground electronic surface are in some instances quasiresonant (and in most cases, exothermic) with some of the vibrational states of H_2^+, our differential cross sections for vibrational excitation for $\nu \geq 4$ might not be very accurate at the higher collision energies. Nevertheless, the elastic (ground) vibrational state is relaxed with the presence of these excited states enough to produce accurate elastic cross sections, which are the principle subject of this work.

This problem of charge transfer is not present in the collisions of the molecule with neutral projectiles although other serious problems emerge in these cases due to the high degree of symmetry present in the H + H_2 system. This is reflected in difficulties in calculating even the ground adiabatic potential surface accurately as well as in a strong particle interchange channel present in the dynamic regime. We used the same basis as in the H^+ + H_2 case to calculate the ground potential surface for $R, \rho \leq 1$ a.u., for various γ using the UHF-CI method. This is then smoothly continued to the excellent analytical surface fit of Boothroyd [31], for $R \leq 10$ a.u., and continued for large R with the analytic asymptotic potential of the van der Waals type [32, 33].

In both ion-molecule and atom-molecule cases, the R-dependent matrix elements, Eq. (113), were fitted using cubic splines for each fixed value of γ, and in that form used in the process of solving Eqs. (111).

I.8 Methods of fitting of the differential and total cross sections

I.8.1 Differential cross sections

To provide a means for plasma modelers to conveniently utilize the huge database of information produced in this work all integral and differential cross sections have been fitted to analytic forms with relatively few parameters. In particular, for all scattering systems and all energies considered, the differential cross sections were calculated at 768 nonuniformly distributed scattering angles θ, in the range $(0, \pi)$, chosen to facilitate the accurate calculation of integrals of the differential cross sections using Gauss-Legendre quadrature, as well as to represent the details of the many angle dependent oscillations of the differential cross sections. The fitting of these as a function of θ with a minimal number of fitting parameters is a difficult task due to the presence of often strong θ-dependent oscillations. These difficulties are particularly pronounced for ion-atom cases. Thus, we have not used the 768 angles directly in the fitting procedure, but rather averaged over the oscillations in each of 48 flexibly chosen nonequal ranges of angles dividing the $0 - \pi$ interval, and then performed the fitting utilizing the resulting points.

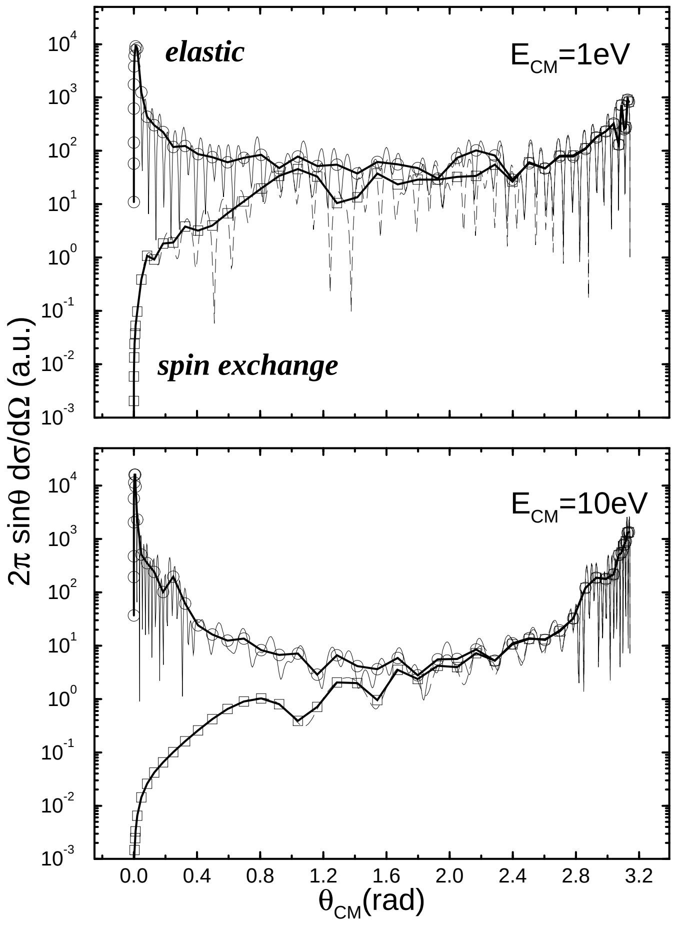

Figure 8: Example of the complete (thin lines) $H^+ + H$ differential cross sections and the averaged (heavy lines and symbols) results used for fitting.

Figure 8 shows examples of such averaged curves in the case of $H^+ + H$, for collision energies of 1 and 10 eV. The asymmetry in the oscillations causes an averaged curve to pass through the upper parts of each oscillation. The fitting through the 48-point curves is performed in two steps:

1. Using a rational-Chebyshev fit [34], the analytical representation is obtained in the

form

$$g(\theta) = 2\pi \sin\theta \frac{d\sigma}{d\Omega} \approx \exp\left(\frac{\sum_{i=0}^{M} a_i z^{i-1}}{1+\sum_{j=1}^{K} b_j z^j}\right), z = \log\theta. \tag{116}$$

2. $g(\theta)$ is further fitted to the form

$$g'(\theta) = (A + B(1-\cos\theta) + C\sin^2\theta)g(\theta) \tag{117}$$

in order to achieve the requirements that the integral elastic, momentum transfer, and viscosity cross sections obtained from the fit $g'(\theta)$ is equal to the relevant actual integral cross sections, obtained from the original differential cross section.

Warning: In principle, the parameters A, B and C can be calculated exactly to satisfy the above requirements, since the three conditions constitute a linear system of equations in the unknowns. In practice this could not be realized always, as can be seen in the figures in Parts B and C. At high energies ($E_{CM} > 2$ eV), due to the many orders of magnitude over which the differential cross sections vary, the fitted differential cross sections would become negative or would have an unreasonable dip or dips at large values of θ. In these cases, the parameters A, B and C were varied from their computed values to keep the fitted cross sections in good (visual) agreement with the original ones. The integral elastic cross section is relatively insensitive to these difficulties since it is dominated by forward scattering for which the fit was always more accurate. For those collision systems and energies in which the fitted momentum transfer or viscosity cross sections deviate by more than 20 percent from the original cross sections, a warning is printed in the tables of fitting coefficients. In some cases, owing to the sensitivity of these cross sections to the large angle behavior, the transport cross sections obtained by integration over scattering angle of the fitted elastic differential cross section can deviate by as much as a factor of five or ten from the original value.

I.8.2 Integral cross sections

The integral cross sections (elastic, momentum transfer, viscosity, and charge transfer, or, in the case of neutral atoms, spin exchange) were fitted, using the rational Chebyshev fit, to the form

$$\sigma_{el,mt,vi,ct(se)} = \frac{\sum_{i=0}^{M} a_i z^{i-1}}{1+\sum_{j=1}^{K} b_j z^j}, \;\; z = \log\theta. \tag{118}$$

Although many of these fits extend beyond the range of energies 0.1-100 eV in a reasonable fashion, we recommend that such an extension be checked for each particular system and cross section.

I.9 Discussion of the accuracy of the results

The factors listed below influence the accuracy of the results obtained. In only a few cases can all these factors be fully assessed. For the other cases we describe the level of accuracy either qualitatively or estimate the upper bounds of the errors made.

(1) *Accuracy of the adiabatic potential energy curves describing the ion-atom and atom-atom interactions and the adiabatic potential energy surfaces for the ion-molecule and atom-molecule collisions.*

In hydrogen-ion–atom collisions, the one-electron, two-center adiabatic Hamiltonian is separable and computer codes exist for finding the potential energy curves with essentially arbitrary accuracy (in the present work to eight significant digits). Taking into account the fidelity of the cubic spline fitting procedure used to calculate values needed to solve the dynamical (collision) problems, we estimate the accuracy of the potential curves to be about five significant digits. Values were calculated with a step size in interparticle separation of 0.0002 a.u. for $R \leq 1$ and 0.001 for $R \leq 50$.

For hydrogen-ions colliding with He (nonseparable, two-electron, two-center case) the potential curves were determined by the Hartree-Fock–Full-Configuration-Interaction (HF-CI) numerical method of computational chemistry, with a finite expansion basis set. Since only the ground state curve was needed, the variational convergence obtained indicated an accuracy better than 0.1% in the range of interparticle distances required. Due to the time consuming nature of this procedure, the calculation was performed with a step of 0.02 a.u. The estimated error obtained in these potential curves is less than 0.3%.

For molecular targets, these computational difficulties are further exacerbated due to the need for a HF-CI solution of a three-center, two- or three-electron problem in three dimensions. Thus, the calculations were limited to spatial steps along each interparticle direction of 0.1 a.u. and 10° in diatomic angle. Although the estimated accuracy of the calculated points is better than 0.5%, the fitting procedures used to produce a finely spaced mesh increased the potential surface's uncertainty up to 1%. In addition, for H + H_2, i.e. the calculation of adiabatic surfaces for H_3, additional difficulties arise due the symmetry of the problem, especially at larger internuclear distances. For this case, we adopt the analytical fit made by Boothroyd [31] for the H_3 surface, augmenting it with our HF-CI results at internuclear distances smaller than 1 a.u. We estimate that this procedure does not introduce errors in matrix elements larger than 5%.

(2) *Accuracy of the method chosen to compute the elastic scattering phase shifts (semi-classical versus fully quantal methods).*

Both semi-classical and quantal approaches were utilized in computing the elastic scattering phase shifts for the ion-atom and atom-atom collision systems, in order to test the limits of applicability of the semi-classical method. For $E_{CM} > 1$ eV, the semi-classical results are practically identical to the fully quantal results. Below this value, some of the small oscillations of the total cross sections are shifted from the positions determined using the fully quantal approach. These differences do not exceed 5% near E_{CM}=0.1 eV, and do not exceed 0.1% at 1 eV. Owing to the multi-channel aspects of the ion-molecule and atom-molecule collisions considered, only the fully quantal method was utilized to treat those systems.

(3) *Accuracy of the simplifying assumptions such as truncation of the basis sets, i.e. role of the inelastic processes which were not taken into account.*

It is difficult to precisely constrain these sources of errors without comparing to more elaborate and computationally expensive calculations which actually include the inelastic processes. Such calculations are of current research interest. The smallest values of the differential cross sections, located at larger angles (i.e. near $\theta_{CM} = \pi/2$ or π) are particularly sensitive to the inclusion of these channels. Therefore, these effects influence especially the momentum transfer and viscosity cross sections rather than the total elastic cross section which is predominantly determined by forward scattering. A number of precautions were therefore taken.

First of all, by limiting the range of collision energies to a maximum value of 100 eV, most inelastic channel cross sections are much smaller than those for elastic scattering. At low collision energy the inelastic probabilities exponentially increase from zero with increasing energy as $1/v$, where v is the relative collision velocity, which greatly suppresses these processes in the presently considered energy range. The exception is the case where symmetric inelastic processes occur (e.g. symmetric charge transfer: $H^+ + H \longrightarrow H + H^+$), for which cases we explicitly and fully take them into account.

In ion- and atom-molecule systems inelastic vibrational excitations within the ground electronic surface can be significant even for $E_{CM} < 100$ eV. We included these excitations explicitly in our calculations, up to the vibrational state $\nu = 9$, starting from the ground vibrational state ($\nu = 0$). These were enough to obtain full convergence of the elastic ($\nu = 0$) amplitudes to six significant figures. Still, two effects, not included explicitly in the calculation deserve attention.

First, we used the IOSA, which, as described above, means that we freeze the rotational excitations, averaging probabilities over the ensemble of possible molecular orientation angles. Since a typical rotational excitation energy for the hydrogen molecule does not exceed 0.01 eV, we limit our calculations to energies above 0.1 eV, thus meeting qualitatively the conditions for application of the IOSA. Our results for each ν represent the cross sections summed over all final rotational excitations. Although the calculations are explicitly performed for the ground rotational state, they represent (within the IOSA prescriptions) the cross sections averaged over the populations of the initial rotational states.

Second, in the ion-molecule case, the charge exchange $H + H_2^+$ surface experiences a close avoided crossing with the ground $H^+ + H_2$ surface for vibrational, diatomic coordinates greater than 2.6 a.u. for all reaction coordinates R greater than approximately 4.5 a.u. As a consequence, the vibrationally excited states $\nu \geq 4$ are strongly coupled with the charge exchange channels. We do not explicitly take the charge exchange into account (which may mean that our cross sections for the highly excited vibrational states are not accurate). However, the large number of the vibrational states included in the calculation is enough to describe the depletion of the population from the elastic channel, especially at low energies, regardless of the final state of these populations. In addition, the calculation is done on the diabatic surface constructed from both ground and charge exchange surfaces, thus indirectly taking into account the propagation of the wavefunction onto the excited potential surface in a part of the collision. Under these circumstances, we do not consider neglect of the charge exchange as a significant source of uncertainties for the $\nu = 0$ elastic channel.

(4) *Accuracy of the numerical procedure in calculations of the elastic probabilities (this includes also the large but finite distance where initial and boundary conditions are set, the size of the step in the numerical integration of the Schrödinger equation, and the convergence in the number of partial waves).*

These sources of uncertainties are the easiest to control in our calculations. For each collision energy, convergence was obtained in the elastic channel probability to at least 7 significant digits by systematically increasing the number of partial waves included. The typical size of spatial mesh used in the solver for the system of coupled partial differential equations was in the range of 10^{-3}–10^{-4} a.u., depending on the convergence behavior of the differential cross section (for a particular scattering angle and collision energy) resulting in convergence to 4 significant digits. The size of the numerical box was increased until convergence in the differential cross section was reached to 5 significant digits.

Thus, we estimate that the sources of the uncertainties in the numerical procedure do not exceed 0.1% for all scattering angles, and all collision energies involved. Additional insight in the accuracy of the approaches applied here can be obtained from the comparison with the available theoretical results of other workers as described below in section I.10.

I.10 Comparison with the literature data

A surprisingly small number of elastic cross section data are found in the literature, particularly in the range of energies 0.1-100 eV. As expected, the most detailed work has been done for the H^++ H system, and we compare here our results for this system with available integral and differential cross sections. We also compare our results with the more sparsely available data for the H^+ + He, H + H, H^+ + H_2 and H + H_2 systems. Except for H^+ + D collisions no data are available for comparison with the isotopically modified systems.

I.10.1 H^+ + H

Integral Cross Sections Figure 9 shows a comparison of our fully quantal and semi-classical results with the heretofore most reliable low energy elastic and symmetric charge transfer data of Hodges and Breig [35] (HB) and of Hunter and Kuriyan [20]. The former have also considered the momentum transfer cross section below 10 eV of collision energy. The agreement of all of these data with our own is generally excellent for the whole range of energies considered.

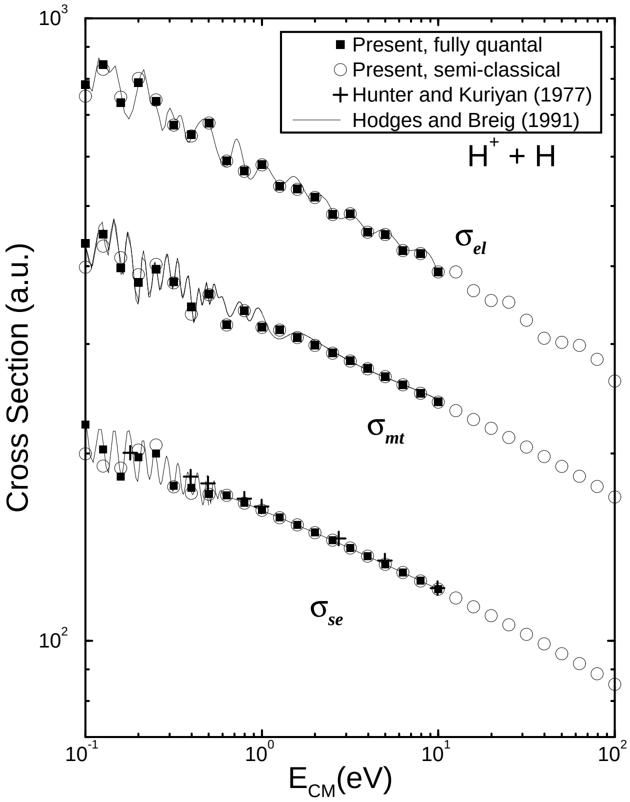

Figure 9: Present H^+ + H integral cross sections and those from other works.

With regard to the comparison of the semi-classical and quantal integral elastic cross sections, the former is significantly shifted ($< 6\%$) from the latter only at the lowest energies (0.1 eV), as expected. Already at 0.5 eV the two sets of results agree to within less than 0.1%. On the other hand, agreement of our quantal results with those of Hunter and Kuriyan is better than 0.1% for all energies in the range 0.1-10 eV, while our disagreement with the data of Hodges and Breig of 2% at 0.1 eV, decreases to below 0.1% at energies > 0.5 eV.

Considering the momentum transfer cross sections, the agreement of our quantal data with those of Hodges and Breig is better than 0.1% at 0.1 eV, but varies irregularly toward higher energies. For example, they disagree by 2.8% at 0.5 eV and 1.5% at 1 eV. We attribute the disagreement to the imprecision of our digitizing procedure used to obtain the data from Hodges and Breig's published diagrams which may be expected to introduce on the order of 2-3% uncertainty into the comparison. Our semi-classical data deviate from the quantal ones by about 8% at 0.1 eV, but this improves to below 0.1% at energies ≥ 0.5 eV. The dispersion of the symmetric charge transfer data shown by the four sets of integral cross sections is larger than that for the elastic channel at the lowest energies. Specifically, our semi-classical data deviate by about 10% from fully quantal calculations at 0.1 eV. This difference drops to below 0.05% at 0.5 eV. The Hodges and Breig charge transfer cross section differs by about 6% from our quantal calculation, and this difference drops with energy ($< 3\%$ at 0.5 eV, and $< 1.5\%$ for 1 eV). Similarly, the Hunter and Kuriyan data differ from ours by 4% at 0.1 eV, which drops to less than 1.2% at 0.5 eV. The HK data apparently differ even more from the HB results since their deviations are in opposite directions from our data. Still, we stress that in this case both sets of referenced data were obtained by digitizing the published data, which can introduce an error of a few percent. There are no quantum mechanical viscosity cross section data for this system in the literature.

Differential Cross Sections The only comprehensive set of differential cross section data for the low energy range in the literature were published by Hunter and Kuriyan [17]. The deviation of their elastic differential cross section from our fully quantal calculation at 0.1 eV is within the errors of digitization. The deviation of our semi-classical data from the quantum mechanical one is bigger, especially at larger angles, which is consistent with the conclusions drawn regarding the integral cross sections. It is interesting to note that already at 0.1 eV, the semi-classical data reflect in full the correct structure of the differential data (positions of the peaks), underestimating the peak values by only a few percent (Figure 2).

At a collision energy of 1 eV, there is no deviation between our quantal and semi-classical data, noticeable in the differential cross section, while any visible difference between ours and the data of Hunter and Kuriyan can be attributed to the digitization errors (Figure 7). A similar comparison for 10 eV, with the data of Hodges and Breig is given in Figure 10. Figures 5 and 6 have shown the comparison of our data with those of Hunter and Kuriyan for symmetric charge transfer at 0.1 and 1 eV, respectively, with conclusions similar to those given for Figures 2 and 7.

Elastic and Charge Transfer Amplitudes Hunter and Kuriyan made an extensive tabulation of the phase shifts which they obtained from their fully quantal calculations of elastic and charge transfer cross sections [17, 36]. These data are particularly convenient for comparison not only because of their fundamental nature but also because digitization errors are absent. We have compared the real and imaginary parts of the amplitudes (Figures 3 and 4) rather than the phase shifts, because the latter are not uniquely defined (up to mod(2π)). The comparison has been given for representative partial waves ℓ, from 0 to ℓ_{max}, for 0.1 (Figure 3) and 10 eV collision energy (Figure 4), for both scattering

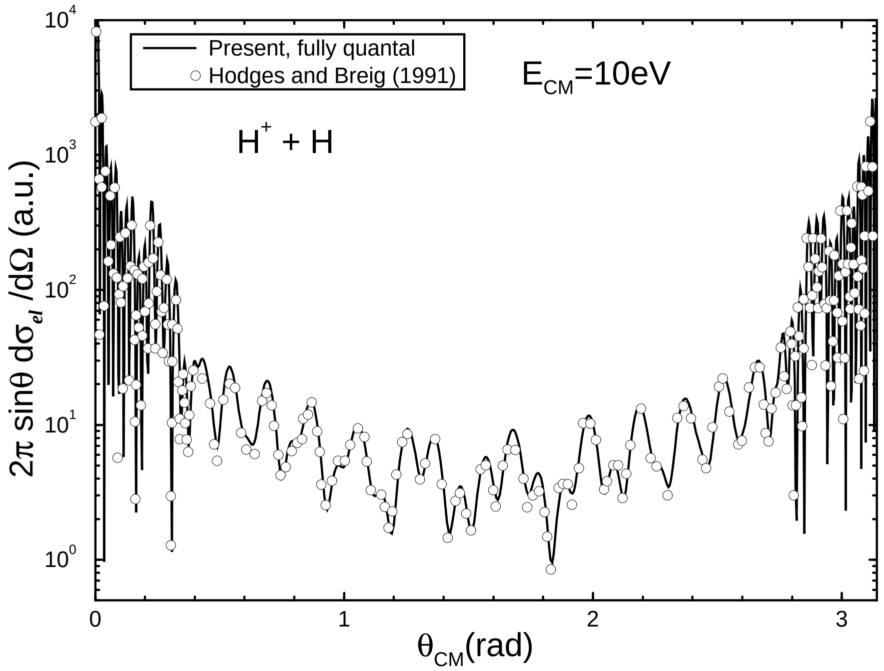

Figure 10: Example of the present elastic differential cross section compared with the results of Hodges and Breig [35].

on gerade and ungerade ground states of H_2^+. A characteristic of the data for the gerade state for 0.1 eV is that for the lowest values of ℓ better agreement is achieved between our quantal and semi-classical data than with the Hunter and Kuriyan data. Our quantal results and the HK data completely converge to each other as ℓ increases, which is the case also with our semi-classical data. For 10 eV, our quantal and classical amplitudes completely agree, as well as with the HK data in the case of scattering on the gerade potential. For ungerade scattering, the HK amplitudes occasionally deviate from ours by up to 8%. We attribute this deviation to the imprecision of the potential used by HK as discussed below.

Assessment of the Quality of the Data The calculation of Hodges and Breig essentially repeats the calculation of Hunter and Kuriyan [36], using their tabulated adiabatic potentials (67 values in the interval of R between 1/64 and 50 a.u.), and uses the same procedure for integration of the radial Schrödinger equation (Numerov method). The values of the potentials needed were then found by cubic spline interpolation. For R greater than 50 a.u., a polarization potential ($1/R^4$) was used to find the values for both gerade and ungerade potentials. At large R, Hunter and Kuriyan used an analytic approximation to the solution of the radial equation, while Hodges and Breig solved it all numerically. Extensive checks of the convergence were performed by HB, leading to somewhat different values of ℓ_{max}, as well as a slight disagreement of the two sets (HK and HB) of the elastic and charge transfer cross sections.

In this work, we calculated the gerade and ungerade potentials with 8-digit accuracy at 10^5 points from $R = 0.0002$ to 50 a.u., thus reducing the error in interpolating the potentials at the points required by the numerical solver. For larger distances, we used the asymptotic expansion for the adiabatic potentials up to 11^{th} order, rather than only up to 4^{th} order. Our numerical procedure was based on Johnson's algorithm with logarithmic derivatives, which achieved a better accuracy and a better numerical stability than the Numerov method. Finally, our convergence criteria were more stringent than those in the works of both Hodges and Breig and Hunter and Kuriyan. Specifically in our calculation we required a 2-3 times greater number of partial waves (see the Table IV) than they used. For example, for 0.1 eV we used 253 partial waves, while HB used 120 and HK used 147. At 5 eV we used 924, while HB used 340 and HK 300 partial waves. For 10 eV HB used only 420 partial waves while our convergence criteria required 1162. These increased numbers of partial waves and more accurate long range potentials resulted in increased accuracy in the differential cross sections especially for small scattering angles. An estimate of the maximum relative error of our quantal results for the differential cross sections for elastic scattering and charge transfer in H^+ + H collisions gives the value of 10^{-7}, which is the best value achieved so far. Nevertheless, this is not necessarily a physical result accurate to 7 digits. Neglect of the nonresonant, inelastic channels may significantly reduce this accuracy, especially at higher energies, where these channels open.

Comparison with Classical Cross Sections Two factors may significantly influence the reliability of the elastic cross sections obtained by classical calculations. 1) Classically, the colliding particles are distinguishable, even if they are identical. This is not correct at low collision energies and can only be resolved by an adequate quantum mechanical treatment. 2) The elastic cross section cannot be properly defined within classical mechanics, unless the interaction potential is of finite range. That is not the case here, and thus the classical integral elastic cross section is infinite. There are possible cures for this situation, and one possibility is the introduction of a cutoff in the classical deflection function. Still, a high degree of arbitrariness in the choice of cutoff may introduce significant errors in the results. Unlike the elastic cross section, both momentum transfer and viscosity cross sections are finite even classically, if the interaction potential decreases at large distances faster than the Coulomb one. This is the case for the present systems, and one can expect reasonable results even classically. Of course, classical distinguishability may be inappropriate at lower energies even in the momentum transfer and viscosity cross sections. In Figure 11 we compare our semi-classical results for the integral elastic, momentum transfer, and viscosity cross sections with the classical results of Bachmann and Reiter [2].

Our present calculation includes identity of the nuclei for the H^+ + H case and thus

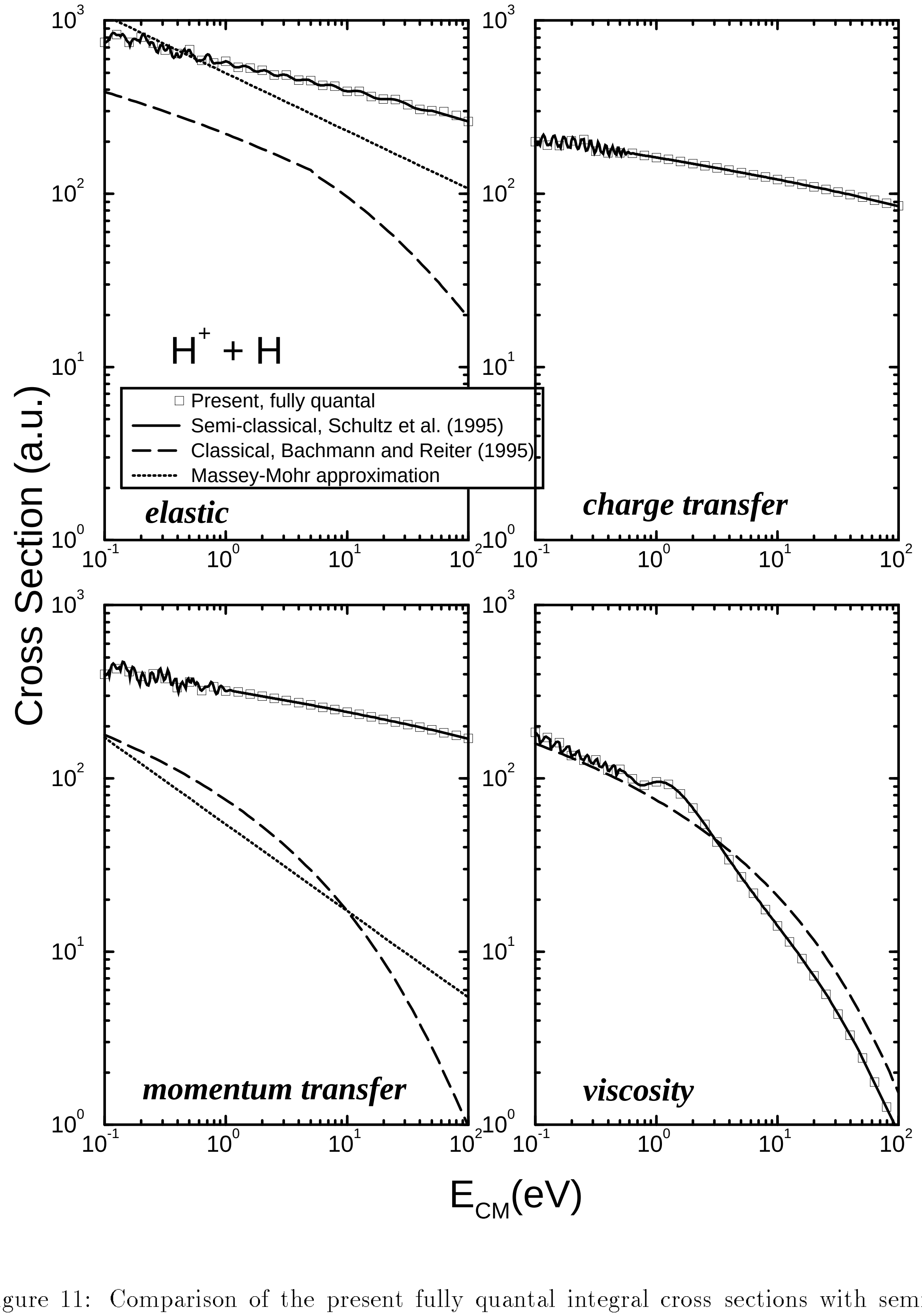

Figure 11: Comparison of the present fully quantal integral cross sections with semi-classical and classical approximations for $H^+ + H$ collision.

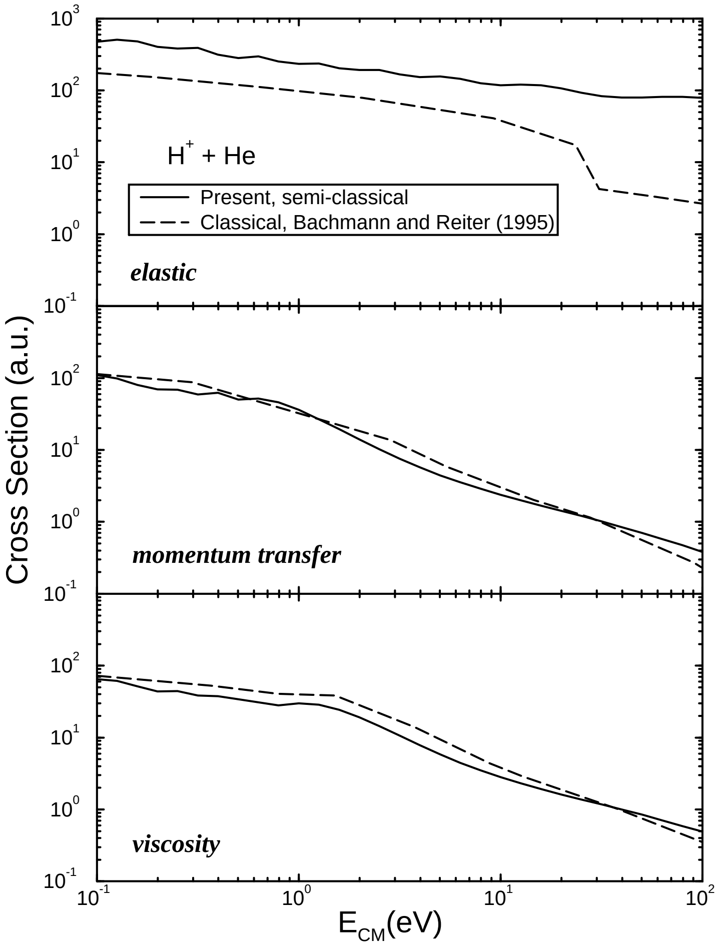

Figure 12: Same as Figure 11 except for H^+ + He.

indistinguishability of the protons coming from the elastic scattering and from charge transfer. As a consequence, the quantum mechanical momentum transfer cross section is significantly larger than the classical one. The momentum transfer cross section is mostly influenced by elastic scattering in the backward direction. This scattering is significantly smaller in the case of distinguishable particles than in the opposite case, since backward scattering is mixed with the charge transferred protons. This explains why our result has such a significantly different momentum transfer cross section from the classical one. (As can be seen in Figure 12, where our results for H^+ + He are compared with the classical result, there is reasonable agreement between the semi-classical and classical data.)

Considering the elastic (H^+ + H) cross section, the difference between our quantal calculations and the classical results of Bachmann and Reiter [2] cannot be attributed only to the classical particle distinguishability. The difference is also a function of the choice of the cutoff deflection function. The viscosity cross section, being influenced mostly by the value of the elastic differential cross section for angles near $\pi/2$, agrees reasonably well with our calculations. We also show in Figure 11 the analytical result of the semi-classical Massey-Mohr approximation (see e.g. [4]) with distinguishable particles.

Isotope Effects: H^+ + D and D^+ + H Finally in this subsection, we compare our results for $H^+ + D$ (and identically $D^+ +$ H in our calculation in the energy range considered) with those of Hunter and Kuriyan [36]. HK determined the cross section by solving molecular-orbital coupled equations for the almost resonant (at large R) $1s\sigma$ and $2p\sigma$ states, while we considered them as satisfying the gerade-ungerade symmetry, with appropriate adiabatic corrections to the potential curves, due to the isotope effect (as discussed in detail in Section I.5.4). The HK results exhibit differences from ours for energies below 0.5 eV, especially for the elastic cross section. Since the threshold for charge transfer in $H^+ + D$ collisions is at much lower energies ($E_{CM}^{threshold} = 0.0037$ eV) the differences with the HK results might be somewhat exaggerated by neglecting the radial coupling of the two surfaces. Nevertheless, the overall agreement of our results with the HK calculations is good (Figure 1). We note that our semi-classical calculation starts to differ slightly from the fully quantal results below 0.2 eV.

I.10.2 $H^+ + H_2$

Integral Cross Sections In Figure 13 we compare the present integral cross section data with those of Phelps [37] and of Baer *et al.* [38]. Phelps derived a recommended curve for momentum transfer in the range of CM energies between 0.067 eV and 6.67 keV. The only data contributing to that recommendation that were obtained from experiments (on ion mobility) are for $E_{CM} < 2.3$ eV. These data were then interpolated up to the cross sections of Smith *et al.* [39], obtained for energies above 330 eV. As discussed by Phelps, the resulting curve is about an order of magnitude above the quantum mechanical calculations of Giese and Gentry [32] for energies of a few tens of eV. As can be seen in Figure 13, in the range of the experimental data the Phelps curve is in excellent agreement with our fully quantal calculations. At the lowest energies, below 0.2 eV, this curve slightly diverges from our result. This happens also for the high energy wing where the Phelps' interpolation is also an order of magnitude above our momentum transfer cross section which agrees well with the Giese and Gentry results.

Another indication that the Phelps momentum transfer cross section is overestimated in the 10-100 eV region is the behavior of the charge transfer cross section calculated by Baer [38]. He calculated this cross sections at 20 eV by solving the Schrödinger equation numerically within the IOSA with full inclusion of vibrational motion on both the H_2 and H_2^+ states. The major approximation of Baer is the DIM approximation for both ground and excited potential surfaces of H_3^+, as well as for the nonadiabatic couplings. Still comparison of his differential cross sections for vibrational excitation and for vibrationally resolved charge transfer with the experimental results indicates that the DIM approximation at 20 eV collision energy describes correctly the important parts of the potential surfaces and interactions. Our comparison of the integral elastic cross section with that of Baer shows reasonable agreement.

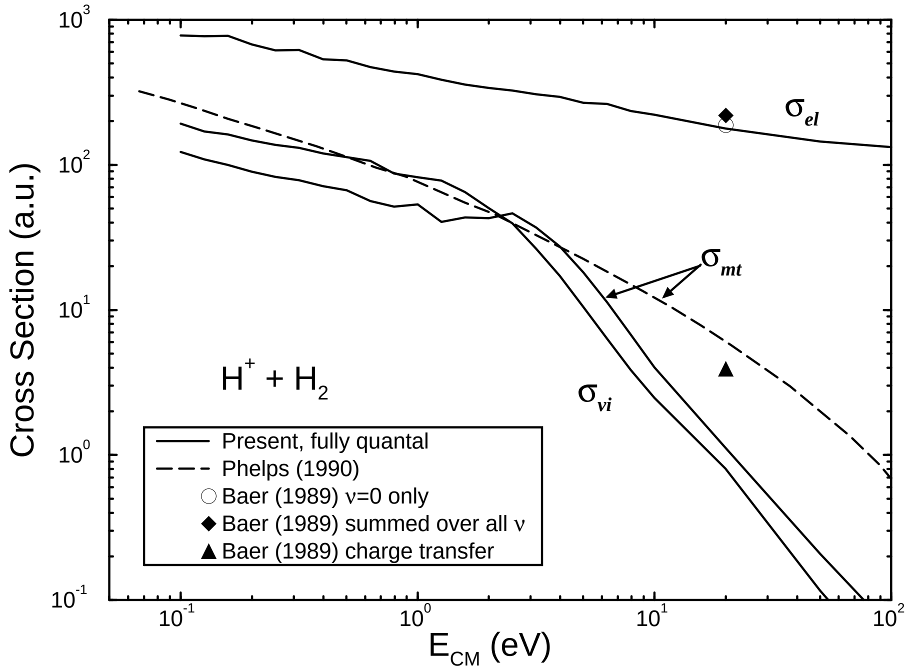

Figure 13: Comparison of the present results for the integral elastic, momentum transfer, and viscosity cross sections for $H^+ + H_2$ with results of other fully quantal calculations (Baer *et al.* [38]) and semi-empirical recommendations (Phelps [37]).

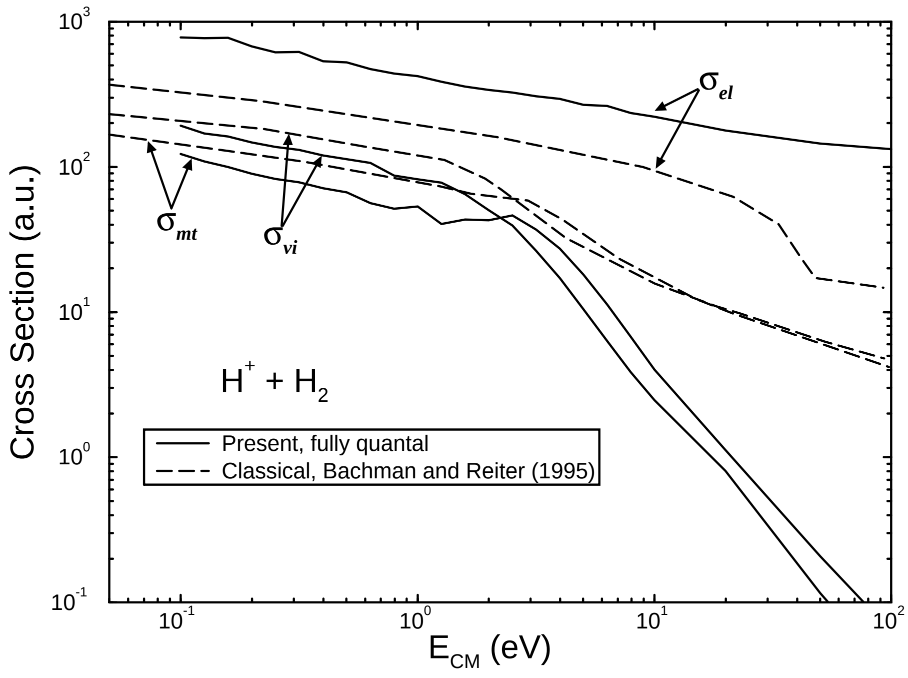

Figure 14: Same as Figure 13 except comparing with classical calculations.

As seen with the other asymmetric collision systems with an elastic differential cross section strongly peaked in the forward direction, the momentum transfer cross section is always, in the range of energies considered here, significantly smaller than the charge transfer cross section. The reason for the sudden drop of the momentum transfer in our results is the strong presence of vibrational excitations in the energy range above 10 eV. At 100's of eV, vibrations of the molecule become frozen during the collision and the scattering resembles that of the ion-atom case. In defining the momentum transfer cross section, if one does not explicitly include the vibrational excited states but rather sums over all vibrational states, this results in an increase of the elastic cross section. Thus, we predict that in the gap between the actual data used by Phelps (between 2.3 and 330 eV) there is a deep minimum in the momentum transfer cross section, caused by the regime of strong and resolvable vibrational excitations. The fact that we have not taken into account the vibrational states of the charge transfer channel does not influence the conclusion. This would effectively increase the number of excited vibrational states and thus make the minimum even deeper.

Figure 14 displays a comparison of our elastic data with the classical ones of Bachmann and Reiter [2]. The classical elastic cross section is underestimated due to the specific choice of the cutoff parameter while momentum transfer and viscosity cross sections show reasonable agreement with our results up to 10 eV. Beyond this energy, they stay too high, similar to the Phelps result. The classical calculation does not take into account any vibrational structure. We stress that our cross sections are truly elastic (within the IOSA), that is, that they describe elastic scattering on the ground vibrational state (and the ground rotational state which in the IOSA amounts to the same thing as an average over the possible initial rotational levels).

Differential Cross Sections In Figure 15 we compare our elastic differential cross section at 5 eV with the one obtained by Schinke and McGuire [40] at 4.67 eV. Schinke used a time-dependent impact parameter form of the sudden approximation for rotation. This approximation is based on the assumption that at sufficiently high collision energy the angular momenta of the projectile and of the diatomic molecule decouple, thus allowing the reduction of the problem to that of coupled equations in space for the rotational states of different vibrational manifolds. As an additional approximation these authors used the fitted potential surface of Giese and Gentry [32].

The level of agreement of our fully quantal differential cross section in the range of angles around the rainbow with the Schinke and McGuire result (digitized from their published data) for the ground vibrational state manifold, summed over all rotational cross sections in the manifold, is remarkable. A similar semi-classical approach was applied in another work by Schinke *et al.* [33] for a collision energy of 10 eV, in this case, using a significantly improved potential surface found by accurate *ab initio* molecular eigenvalue calculations. In Figure 16 we compare the present elastic differential cross section at 10

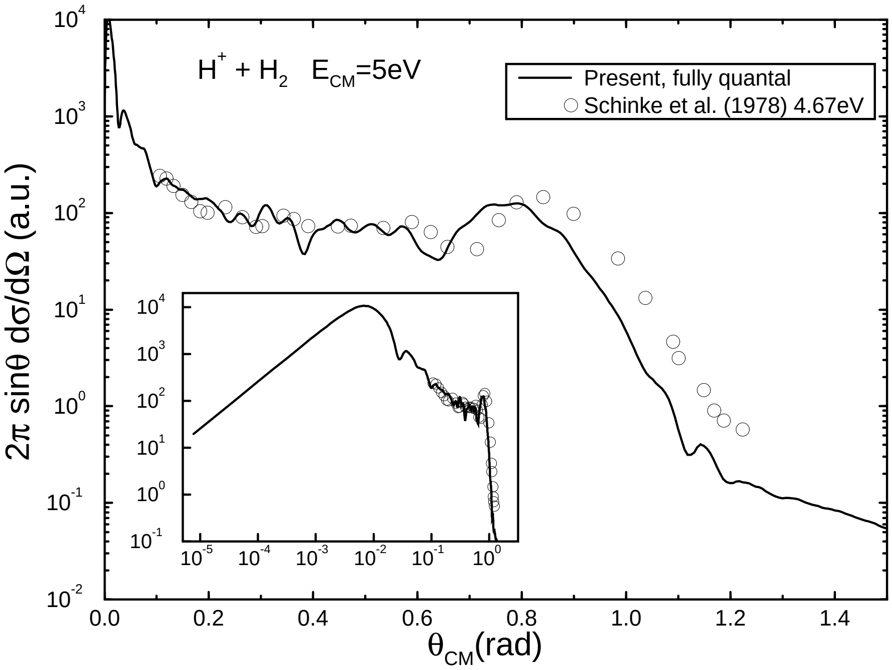

Figure 15: Comparison of the present elastic differential cross section for 5 eV $H^+ + H_2$ with other calculations.

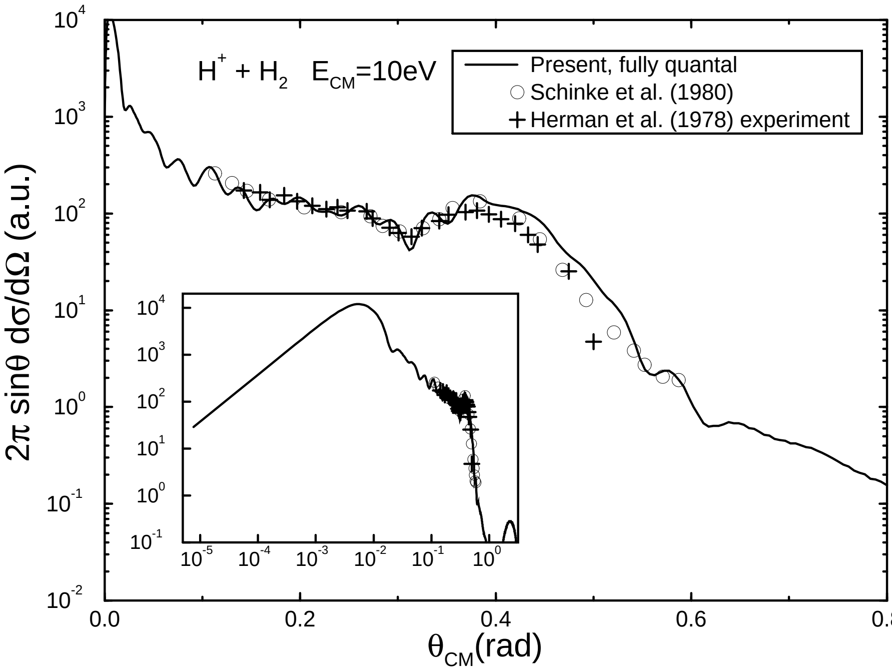

Figure 16: Comparison of the present elastic differential cross section for 10 eV $H^+ + H_2$ with other calculations and with experimental measurements.

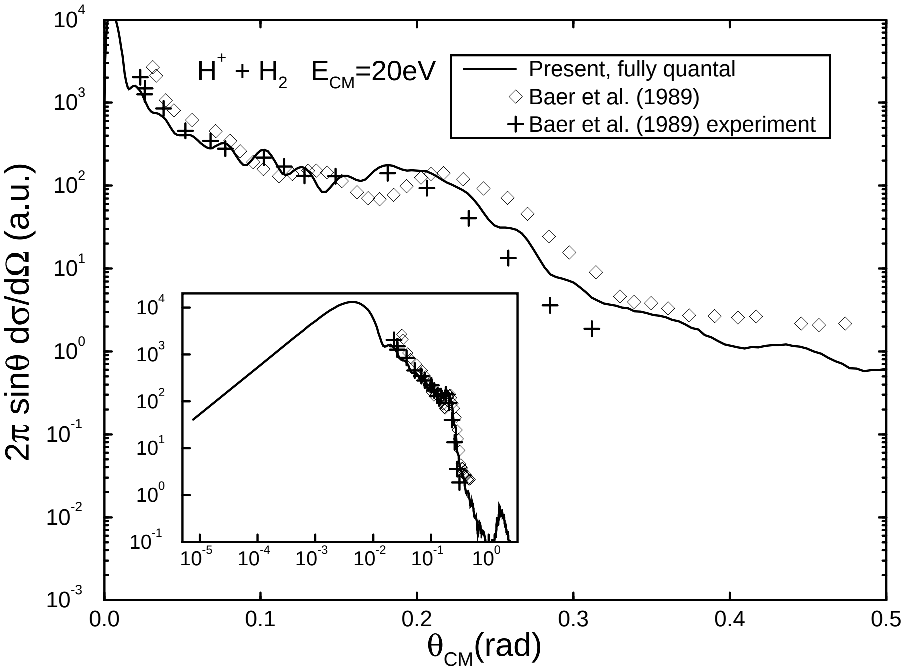

Figure 17: Same as Figure 16 but at E_{CM} = 20 eV.

eV with the calculations by Schinke *et al.*, as well as with the experimental results of Herman *et al.* [41]. The agreement of the three sets of data is practically perfect in all details.

In Figure 17 we compare our data for the differential cross section at 20 eV to those calculated by Baer [38] as well as to experimental result of Niedner *et al.* [42]. In spite of the use of the DIM potential surface, Baer's results agree well with both the experiment and our calculations. Some deviations toward small scattering angles can be explained by the insufficient number of angular momenta Baer used in his calculation (about 250 compared to about 600 we found to be needed for the convergence of the elastic amplitudes). The indications of deviations at larger scattering angles might be attributed to inaccuracy of the DIM potentials at small internuclear distances.

I.10.3 H^+ + He

Surprisingly, there is only one comprehensive study of elastic scattering of protons by He that we could use for comparison with our results in the range of energies considered here. This is the classical calculations of Bachmann and Reiter [2]. Again, as in the case of H^+ + H, the classical calculation of the elastic cross section, being dependent on a somewhat arbitrary cutoff parameter (deflection angle), underestimates our calculation by a factor of 2 to 3 (Figure 12). On the other hand, the classical calculations of momentum transfer and viscosity cross sections converge even without introducing external parameters because of the de-emphasis of the divergent behavior of the differential cross section for small angles, and thus the classical results are in reasonable agreement with ours (Figure 12).

I.10.4 H + H

We note that little attention has so far been given to the study of elastic collisions between neutral hydrogen atoms in the presently considered energy. For example, the range of energies between 0.1 and 100 eV is somewhat above that of interest for many astrophysical applications and below the range of energies where inelastic processes compete with the elastic ones. In addition, experiments seeking to observe the scattering of neutral hydrogen atoms are very difficult, and thus the data available are sparse even at higher or lower energies.

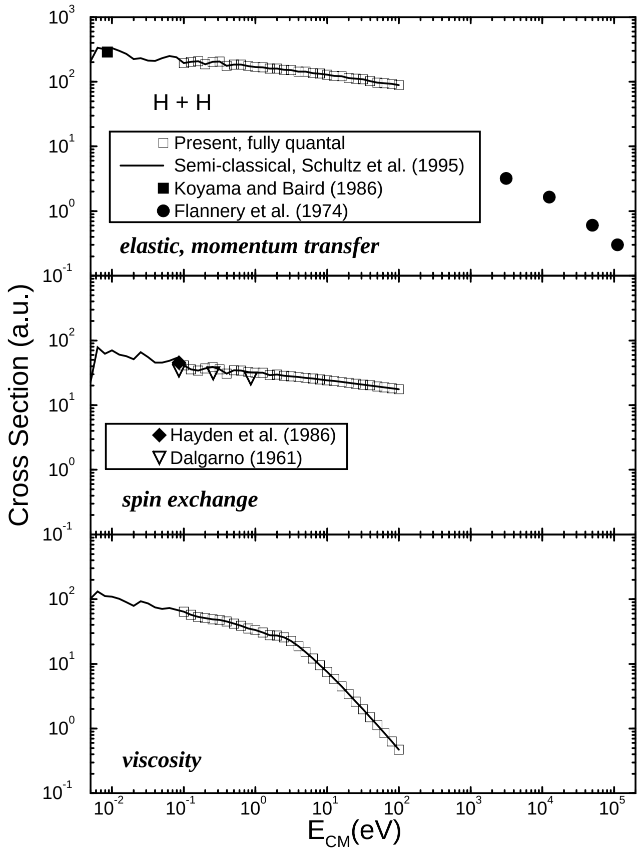

Figure 18: Comparison of the present results with other available data for H + H elastic and transport cross sections.

As a consequence, we can compare our data with only few calculations, and these are mostly oriented to the astrophysically interesting spin exchange process. Figure 18 shows our elastic data compared with one point of Koyama and Baird [43]. Since this point is at low energy (1000 K), far from our energy range, we use the previous semi-classical calculation of Schultz *et al.* [4] to extend our curve toward lower energies. At keV energies we display the results obtained by Flannery *et al.* [44], indicating that at higher energies, where inelastic processes start to play a significant role, the elastic cross section might experience a significant drop. Concerning the spin exchange cross section, our results are in reasonable agreement with those of Dalgarno [45] and of Hayden *et al.* [46], as well as in excellent agreement with the previous semi-classical calculations of Schultz *et al.* [4], as shown in Figure 18.

I.10.5 H + H_2

There are only very few data available for the elastic cross sections for neutral atoms colliding with a neutral molecule. For H + H_2 in the energy range considered here, the available data are those of Phelps for the momentum transfer cross section. We show in Figure 19 a comparison of our fully quantal IOSA calculations with the estimate made by Phelps [37]. As in the case of H^+ + H_2 scattering the agreement is within 30% at the lower energies, until at higher energies vibrational excitations become intensive, resulting in a sudden drop in our elastic cross section.

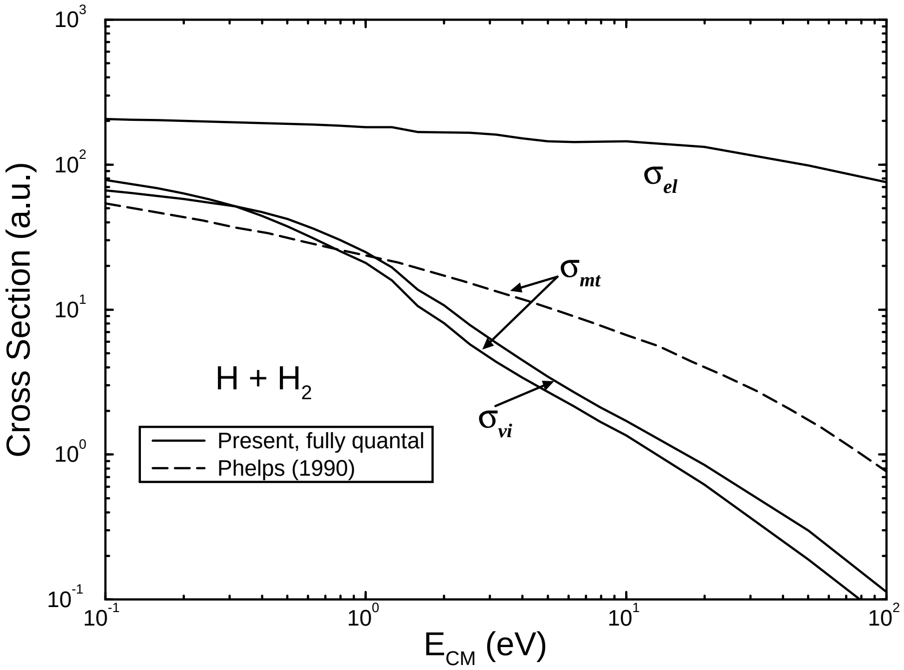

Figure 19: Comparison of the present results for H + H_2 with those of Phelps [37].

I.11 Scaling relations among isotopic variations

For the ion-atom and atom-atom systems considered here, we performed semi-classical calculations of the elastic phase shifts [4] in addition to fully quantal calculations, in the range of center of mass collision energies between 0.1 and 100 eV. This energy range is well within the region of validity of the semi-classical approach for all of the ion-atom and atom-atom collision systems. In addition we have demonstrated by our comparisons between the semi-classical and fully quantal results for the phase shifts and differential cross sections that this applicability is realized in practice. Thus, from the semi-classical point of view, the defining quantities for the elastic cross sections and its higher integral moments are the phase shifts, η_ℓ. For small angle scattering on the short range potentials these scale with relative collision velocity [8]. This is the most general scaling relation for the integral elastic cross sections that we have found regarding all the systems considered, even when molecular targets are involved. Other details of the scaling depend on particulars of the collision system. We have been able to find this kind of scaling only for the integral cross sections. Indeed, no scaling was discovered for the differential cross sections appropriate for the whole range of scattering angles.

Due to their potential value for use in reducing the number of different cross section fit parameters needed in modeling, we present in the following subsections the scaling relations for the various integral cross sections.

I.11.1 H$^+$ + H

We recall that the cross sections for symmetric systems ($A^+ + A$, A=H,D,T) were calculated taking into account the indistinguishability of nuclei. Thus, at higher energies the "elastic" cross section in this case tends to the total scattering cross sections (i.e. adding to the pure elastic cross section the spin exchange cross section, ignoring all other inelastic processes). The spin exchange cross section tends at higher energies (above 1 eV) to the charge transfer cross section and we denote this process generally as "*ct*."

We find that for the symmetric cases the elastic scattering and spin exchange cross sections scale as

$$\sigma_{el}^{A^++A}\left(\frac{\mu_{A_2^+}}{\mu_{H_2^+}}E_{CM}\right) = \sigma_{el}^{H^++H}(E_{CM}) \tag{119}$$

$$\sigma_{ct}^{A^++A}\left(\frac{\mu_{A_2^+}}{\mu_{H_2^+}}E_{CM}\right) = \sigma_{ct}^{H^++H}(E_{CM}) \tag{120}$$

where $\mu_{A_2^+} = (M_A^+ M_A)/(M_A^+ + M_A)$ is the reduced mass of $A^+ + A$. For an asymmetric case, the dependence on collision energy for both the charge transfer and elastic cross sections is the same as in the symmetric case, but the elastic cross section must be multiplied by $\sqrt{2}$ in order to match approximately the H$^+$ + H result, i.e.

$$\sqrt{2}\sigma_{el}^{A^++B}\left(\frac{\mu_{AB^+}}{\mu_{H_2^+}}E_{CM}\right) = \sigma_{el}^{H^++H}(E_{CM}) \tag{121}$$

$$\sigma_{ct}^{A^+ + B}\left(\frac{\mu_{AB^+}}{\mu_{H_2^+}} E_{CM}\right) \quad = \quad \sigma_{ct}^{H^+ + H}(E_{CM}) \tag{122}$$

where $\mu_{AB^+} = (M_A^+ M_B)/(M_A^+ + M_B)$ is the reduced mass of $A^+ + B$, $B =$ H, D, T.

The symmetric system cross sections are bigger by $\sqrt{2}$ because of the backward peak in the differential cross sections that is due to the indistinguishability of the elastically scattered and charge transferred nuclei. The backward peak in the elastic differential cross section is approximately equal to the charge transfer. Assuming that at the higher energies considered here particles can be distinguished as in the asymmetric cases, one obtains

$$\sigma_{ct}^{A^+ + A}(E_{CM}) = (\sqrt{2} - 1)\sigma_{el}^{A^+ + A}(E_{CM}) \tag{123}$$

These scalings are presented in Figure 20.

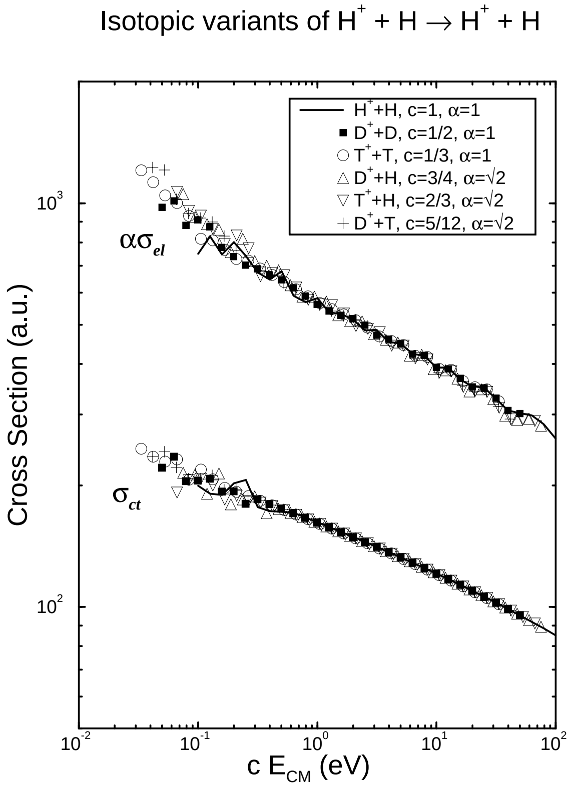

Figure 20: Isotope scaling for H^+ + H elastic and charge transfer (and spin exchange) cross sections.

Scaling of the momentum transfer cross sections similarly must be considered separately for the symmetric and asymmetric cases. This is again due to the pronounced backward peak in the “elastic” cross section for a symmetric case arising from the inclusion of spin exchange which is absent in the asymmetric case. The largest contribution to the momentum transfer comes from backward angles, as discussed before, and thus, the momentum transfer is significantly larger for the symmetric cases.

The scaling of the momentum transfer cross section for $A^+ + A$ collisions relative to those for the H$^+$ + H case is accomplished through only a shift in energy, i.e.

$$\sigma_{mt}^{A^+ + A}\left(\frac{\mu_{A_2^+}}{\mu_{H_2^+}} E_{CM}\right) = \sigma_{mt}^{H^+ + H}(E_{CM}). \tag{124}$$

All of the momentum transfer cross sections are almost identical in the asymmetric cases involving hydrogen-ion–hydrogen scattering with the condition of distinguishability of nuclei (as clearly exists with different isotope combinations). Thus, the momentum transfer cross section is isotopically invariant, i.e.

$$\sigma_{mt}^{A^+ + B}(E_{CM}) = \sigma_{mt}^{C^+ + D}(E_{CM}) \tag{125}$$

where $A, B, C,$ and D are any (different) combinations of H, D, and T. This is illustrated in Figure 21.

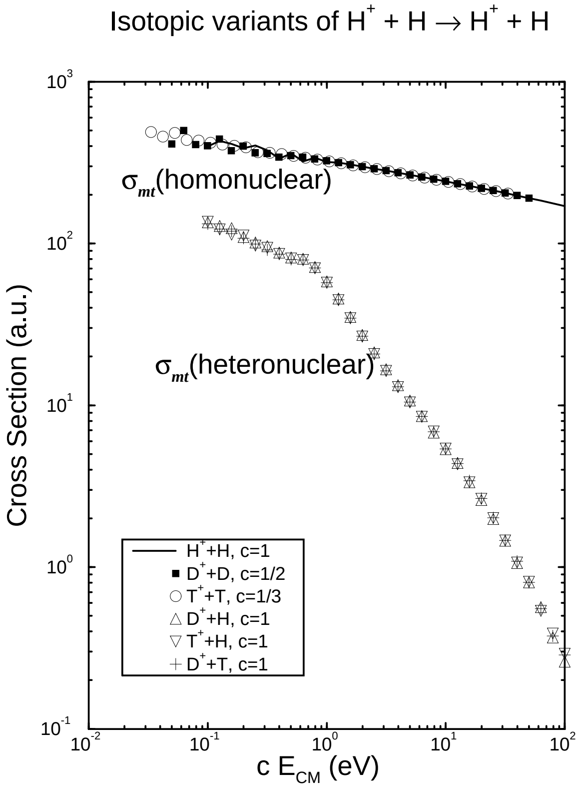

Figure 21: Scaling relations illustrated for isotopic variants of H$^+$ + H regarding the momentum transfer cross section.

The viscosity cross section for symmetric systems turns out to be independent of the reduced mass and no scaling factors are needed. It is also true separately for the asymmetric systems. In addition, the latter completely coincide with the former if multiplied with a factor of 2, which is again a consequence of definition of the elastic cross section for distinguishable versus indistinguishable particles. Thus

$$\sigma_{vi}^{A^{+}+A}(E_{CM}) = \sigma_{vi}^{H^{+}+H}(E_{CM}) \tag{126}$$
$$2\sigma_{vi}^{A^{+}+B}(E_{CM}) = \sigma_{vi}^{H^{+}+H}(E_{CM}). \tag{127}$$

The origin of factor of 2 may also be seen by recalling the discussion given above (section I.5) regarding the factor 2 difference between the differential cross section derived with either the assumption of distinguishable or indistinguishable particles at $\theta = \frac{\pi}{2}$. Since the viscosity cross section mostly picks up the region of the elastic differential cross section about this angle, the factor of 2 is directly manifested. The scaling of the viscosity cross sections is illustrated in Figure 22.

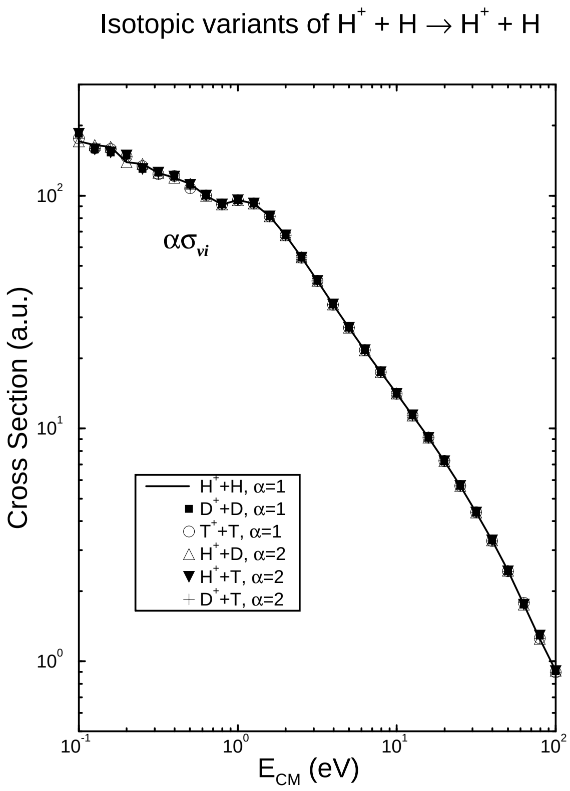

Figure 22: Scaling of the isotopic variants of $H^+ + H$ regarding the viscosity cross section.

In Figure 23 we show the compliance of our results with the well known relation

$$\sigma_{mt} \approx 2\sigma_{se} \tag{128}$$

valid for the symmetric systems, in the energy range considered. The agreement is complete for energies above 1 eV. Although Figure 23 shows only the $H^+ + H$ case, it is clear from Figure 20 that the relation is also valid for $D^+ + D$ and $T^+ + T$.

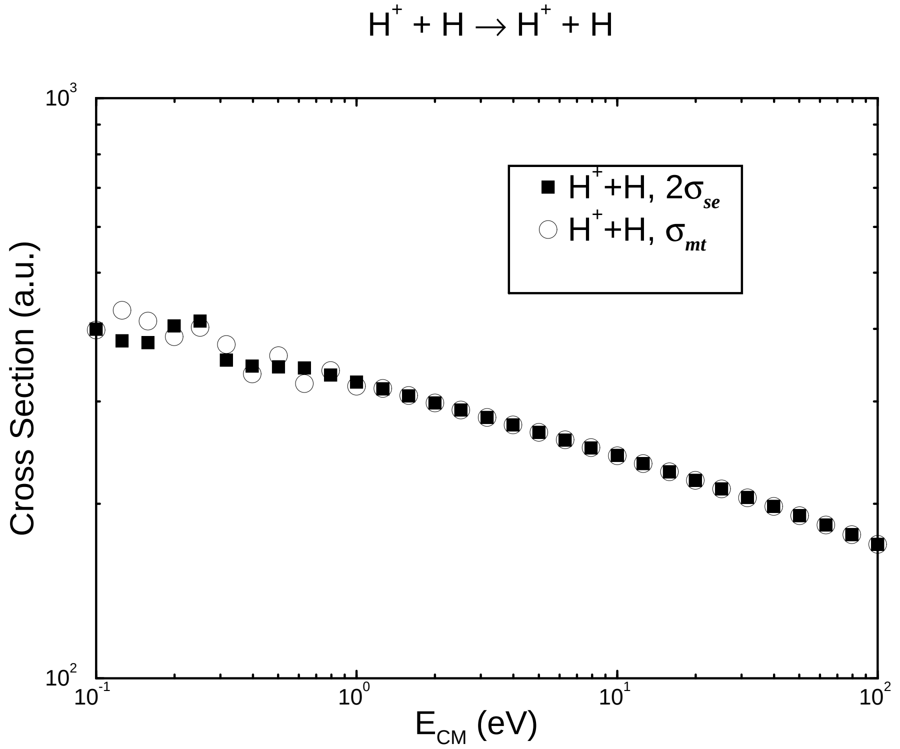

Figure 23: Illustration of the well known relation between the elastic and spin exchange cross section for $H^+ + H$.

I.11.2 $H^+ + H_2$

The collisions of hydrogen ions with hydrogen molecules have been treated as collisions of distinguishable particles and thus one should not expect any difference between the systems except to account for differences in masses and vibrational couplings. In spite of the different vibrational channels of excitation, and in spite of the averaging over molecular orientations, the elastic cross sections do not depend much on the reduced mass and the details of molecular target as long as the projectile is kept the same. This is especially valid at energies above 0.3 eV. Figure 24 illustrates this for protons colliding with the six different isotopic variants of the hydrogen molecule.

The same is approximately true for the momentum transfer and viscosity cross sections, especially for energies below 3 eV, as illustrated in Figure 24. Thus, one can write

$$\begin{aligned}
\sigma_{el}^{A^+ + CD}(E_{CM}) &= \sigma_{el}^{A^+ + C'D'}(E_{CM}) \\
\sigma_{mt}^{A^+ + CD}(E_{CM}) &= \sigma_{mt}^{A^+ + C'D'}(E_{CM}) \\
\sigma_{vi}^{A^+ + CD}(E_{CM}) &= \sigma_{vi}^{A^+ + C'D'}(E_{CM}) \qquad (129)
\end{aligned}$$

If one varies the projectile for the same molecular target, neither the momentum transfer nor the viscosity cross section changes significantly for energies below 2 eV. For

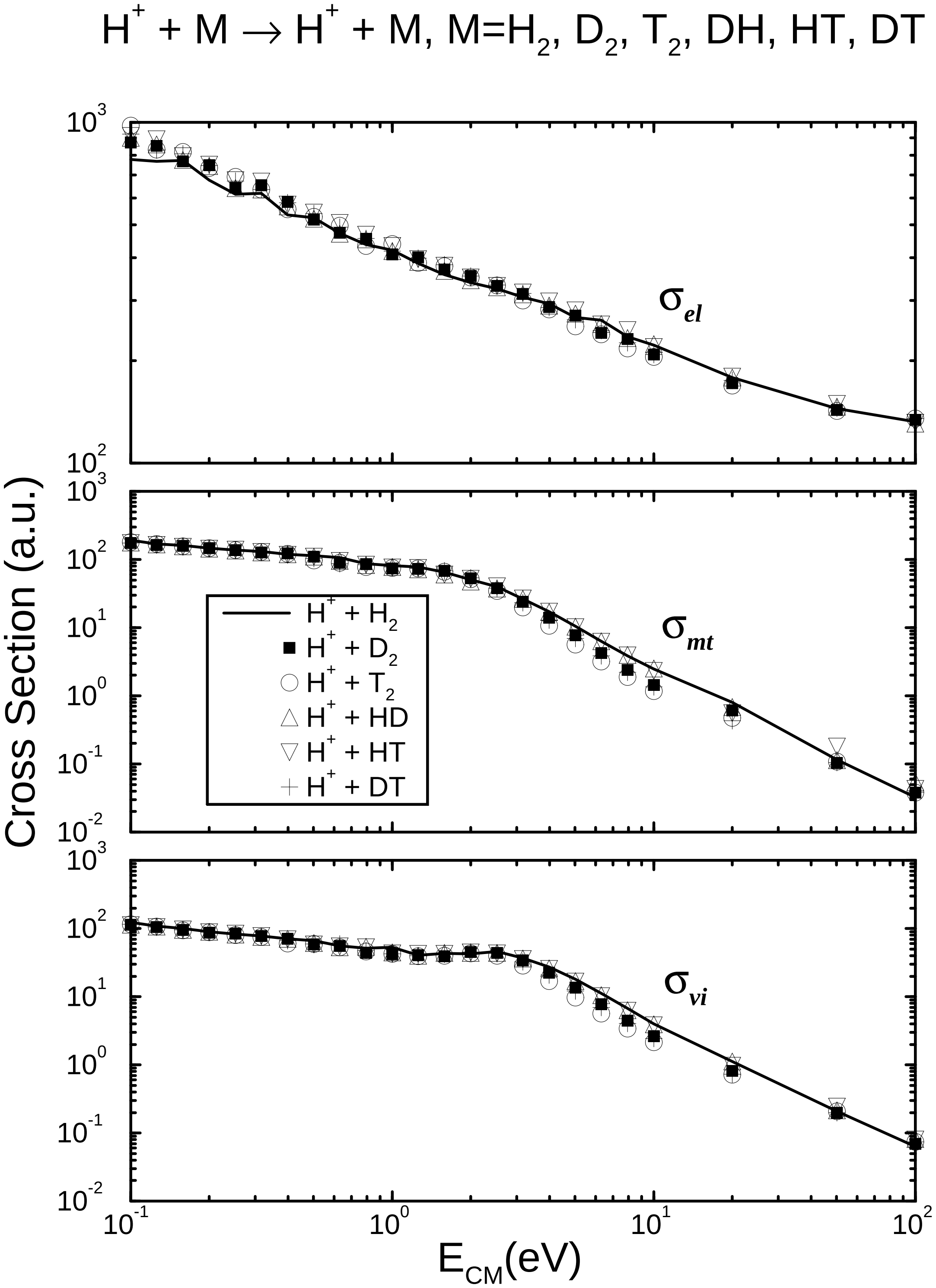

Figure 24: Comparison of the elastic and transport cross sections for protons colliding with the isotopic variants of H_2.

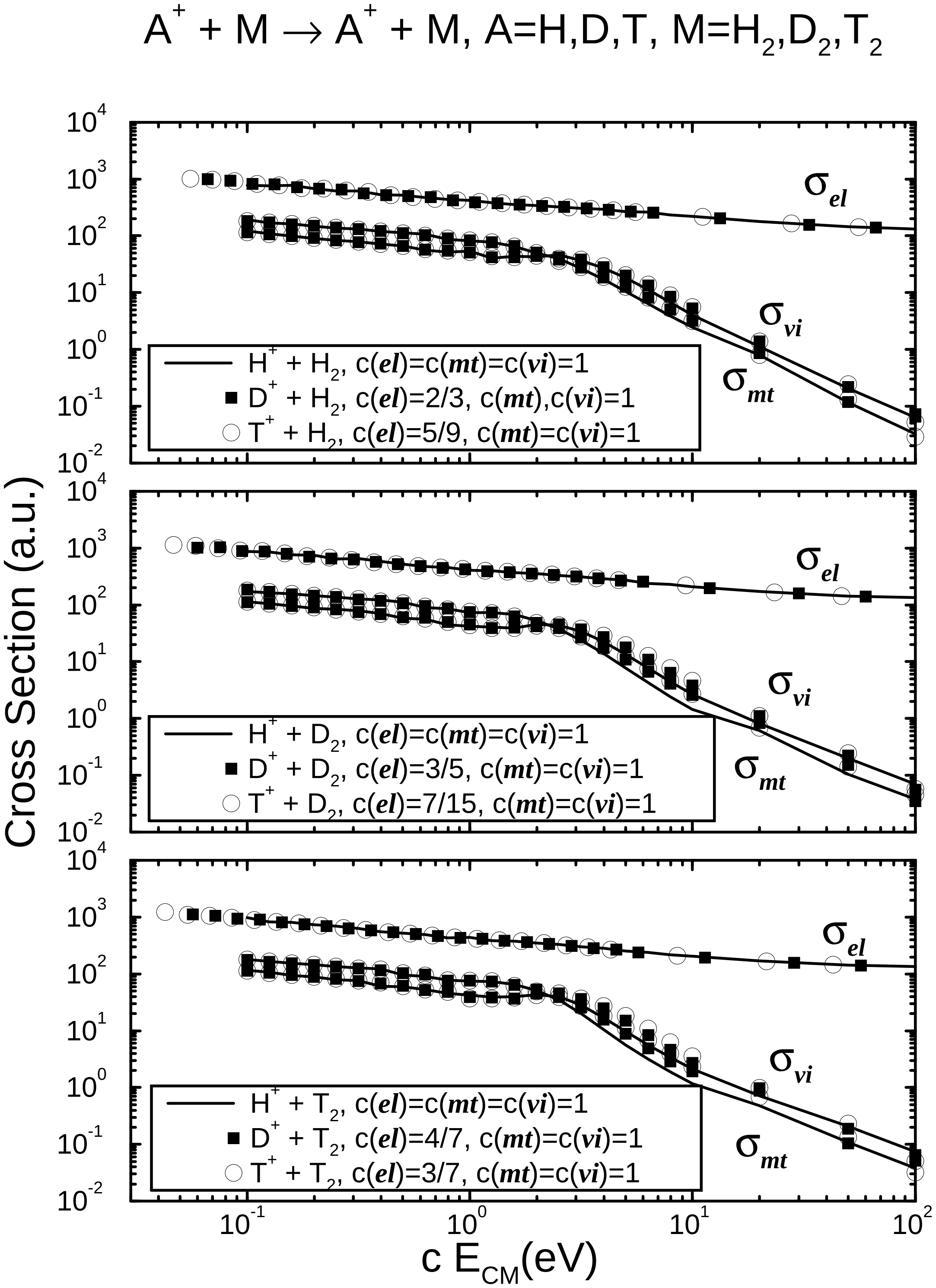

Figure 25: Comparison of the elastic and transport cross sections for isotopic variants of H^+ colliding with H_2, D_2, and T_2.

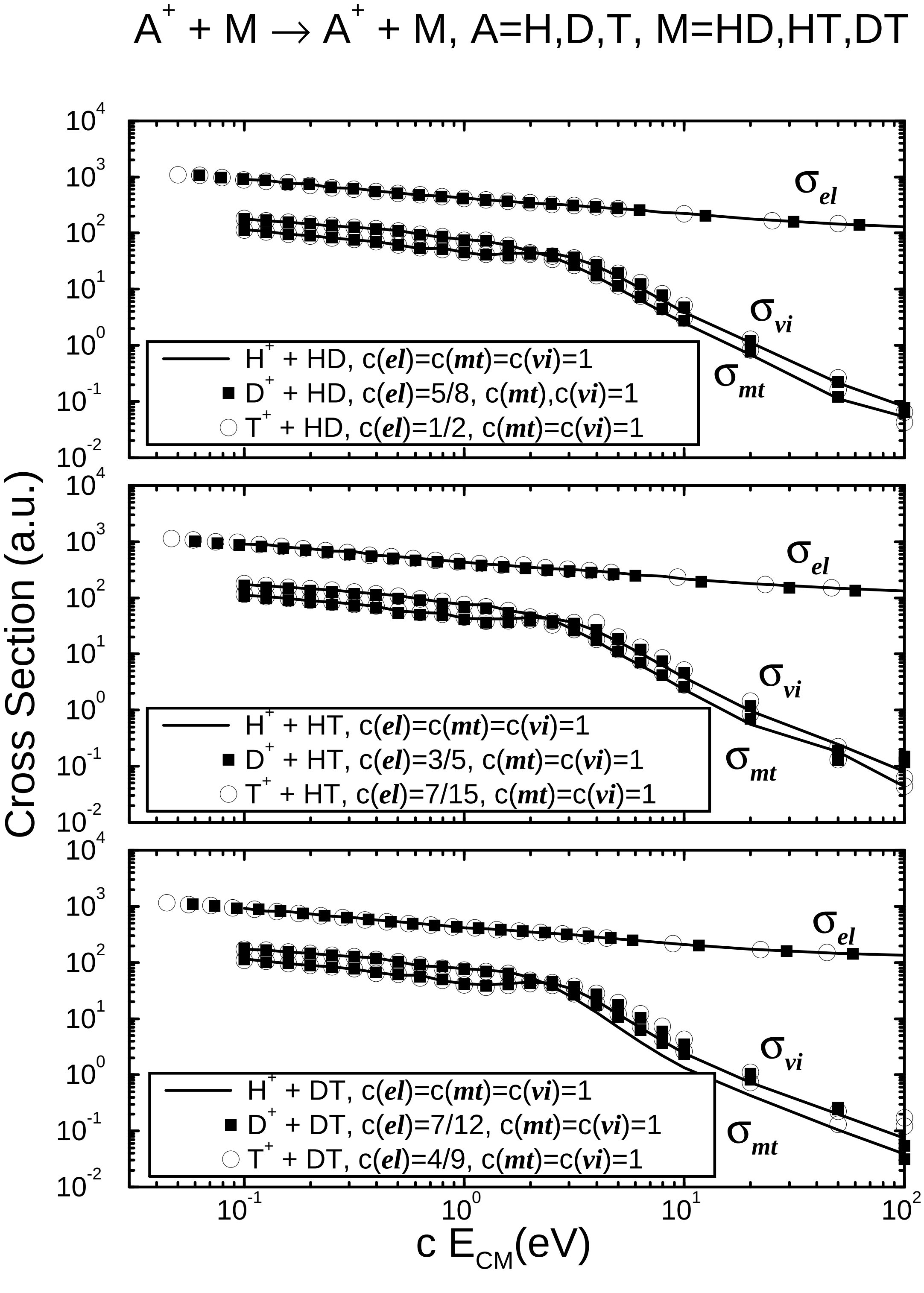

Figure 26: Comparison of the elastic and transport cross sections for isotopic variants of H^+ colliding with HD, HT, and DT.

higher energies the agreement somewhat deteriorates. The elastic cross sections for these systems, on the other hand, match quite well if one scales the energy with the reduced mass, as in the ion-atom case. Thus

$$\begin{aligned}
\sigma_{el}^{A^{+}+CD}(\frac{\mu_{ACD}}{\mu_{H_3^+}}E_{CM}) &= \sigma_{el}^{H^{+}+C'D'}(E_{CM}) \\
\sigma_{mt}^{A^{+}+CD}(E_{CM}) &= \sigma_{mt}^{H^{+}+C'D'}(E_{CM}) \\
\sigma_{vi}^{A^{+}+CD}(E_{CM}) &= \sigma_{vi}^{H^{+}+C'D'}(E_{CM})
\end{aligned} \tag{130}$$

where $\mu_{ACD} = (M_A M_{CD}^{+})/(M_A + M_{CD}^{+})$. These scaling relations are illustrated in Figures 25 and 26.

I.11.3 H$^+$ + He

The elastic cross sections for H$^+$, D$^+$, T$^+$ + He are found to scale as

$$\sigma_{el}^{A^{+}+He}(\frac{\mu_{AHe^{+}}}{\mu_{HHe^{+}}}E_{CM}) = \sigma_{el}^{H^{+}+He}(E_{CM}) \tag{131}$$

where $\mu_{AHe^{+}} = \frac{M_{A^{+}}M_{He}}{M_{A^{+}}+M_{He}}$. The momentum transfer and viscosity cross sections almost coincide for all three systems in the energy range considered, i.e.

$$\sigma_{mt,vi}^{A^{+}+He}(E_{CM}) = \sigma_{mt,vi}^{H^{+}+He}(E_{CM}) \tag{132}$$

indicating a weak dependence of differential cross sections on reduced mass at larger scattering angles where the predominant role played by the differing details of the potential occurs. These relations are illustrated in Figure 27.

I.11.4 H + H

We recall that the cross sections for the symmetric systems $A+A$, ($A =$ H, D, T) were calculated with taking into account the indistinguishability of the nuclei, as discussed Section I.5.2, but then divided by 2, which, due to the full symmetry of the system, accounts for the correct classical limit. Thus, at higher energies, when interference of the different channels averages out, the "elastic" cross section in this case tends to the sum of the scattering cross section on the singlet and triplet states, separately, as is the case at all energies for the asymmetric, distinguishable particle cases. This is reflected by the data shown in Figure 28, where, upon scaling of the collision energy with the mass, all elastic cross sections, symmetric and asymmetric, approximately coincide, especially at energies higher than 1 eV. The total spin exchange cross sections, besides scaling of the collision energy with the mass, requires additionally the division of the cross section by approximately $\alpha = 1 + \sqrt{3}$, for the asymmetric cases. Thus,

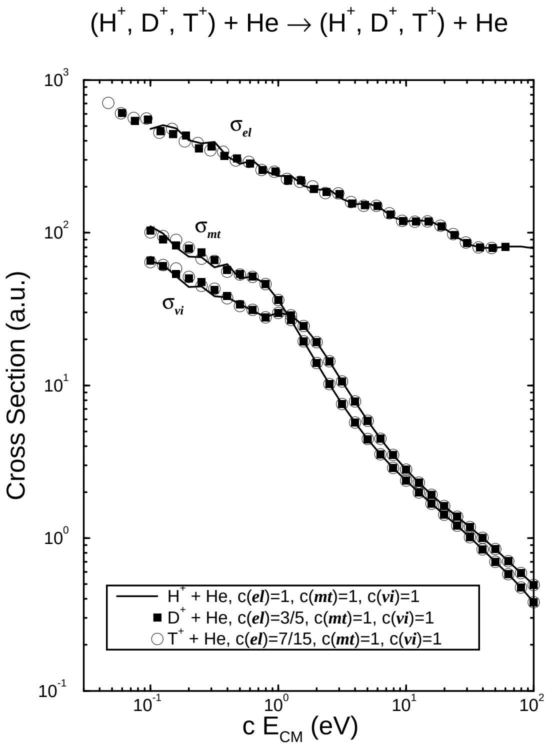

Figure 27: The elastic and transport cross sections for isotopic variants of H^+ + He.

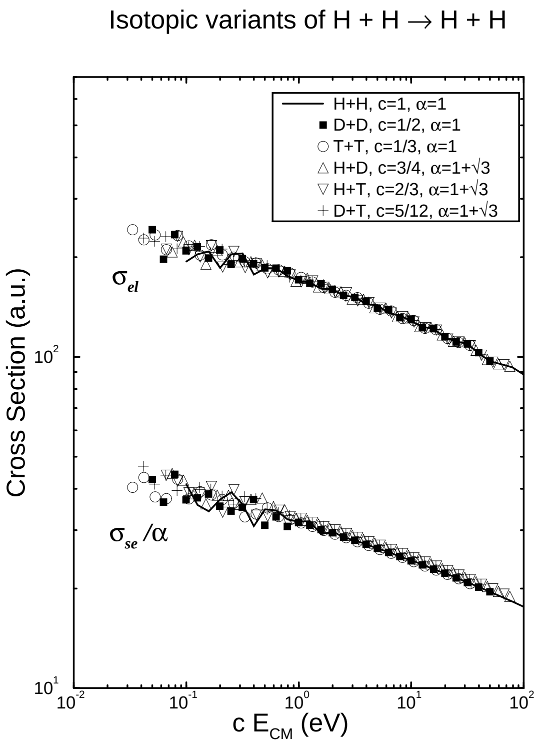

Figure 28: The elastic and transport cross sections for isotopic variant of H + H.

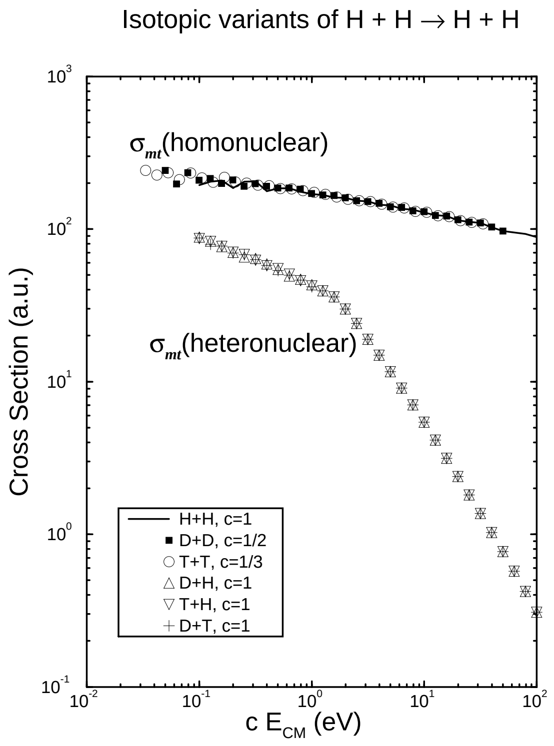

Figure 29: Scaling of the momentum transfer cross section for isotopic variants of H + H.

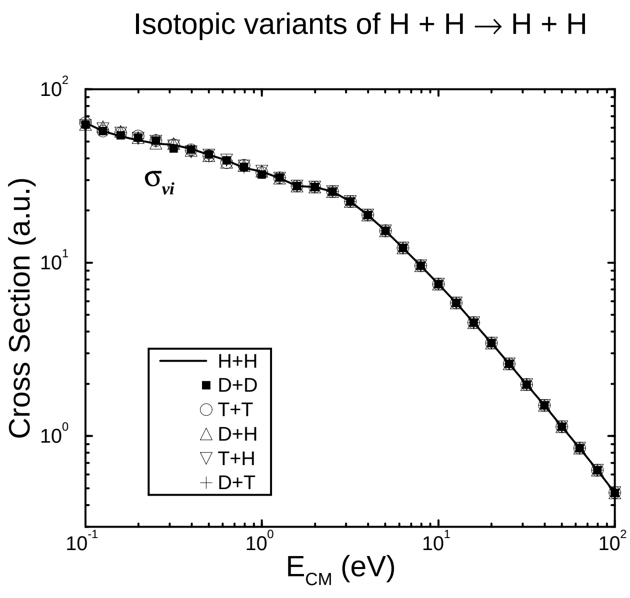

Figure 30: The viscosity cross section for isotopic variants of H + H.

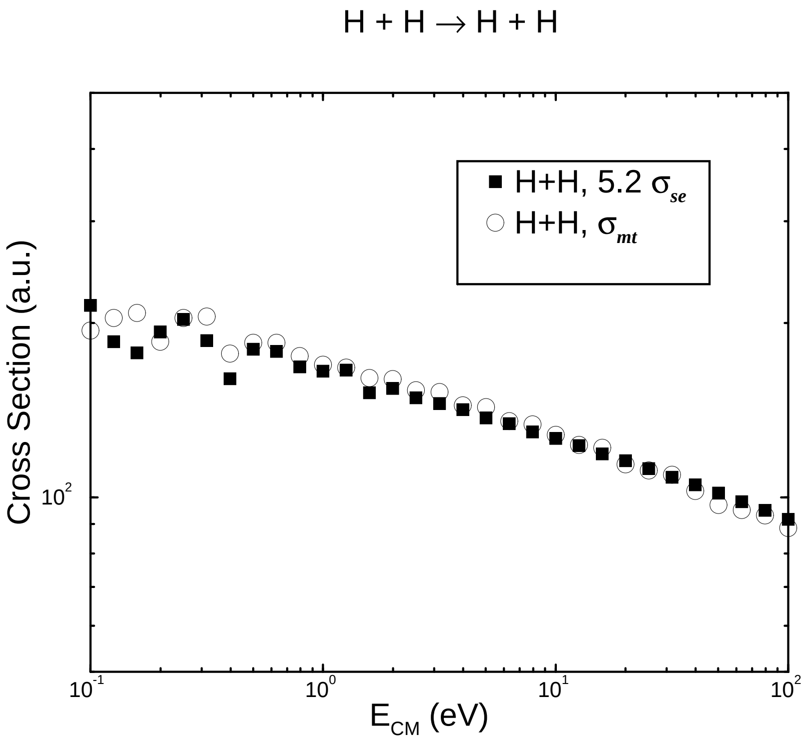

Figure 31: Scaling relation between the H + H spin exchange and momentum transfer cross sections.

$$\sigma_{el}^{A+B}(\frac{\mu_{AB}}{\mu_{H_2}}E_{CM}) = \sigma_{el}^{H+H}(E_{CM}) \tag{133}$$

$$\sigma_{se}^{A+B}(\frac{\mu_{AB}}{\mu_{H_2}}E_{CM}) = \frac{1}{\alpha}\sigma_{se}^{H+H}(E_{CM}) \tag{134}$$

where μ_{AB} is the reduced mass of $A + B$.

Scaling of the momentum transfer cross sections needs to be considered separately for the symmetric and asymmetric cases. This is due to the pronounced backward peak in the "elastic" cross section for the symmetric cases, absent in the asymmetric cases. The largest contribution to the momentum transfer cross section comes from the backward angles, as follows from its definition (i.e. the factor $(1 - \cos\theta)$) and thus, the momentum transfer cross section is significantly larger for the symmetric case.

The scaling of the momentum transfer for the symmetric $A + A$ scattering (identical to the elastic cross section) only necessitates an energy shift, i.e.

$$\sigma_{mt}^{A+A}(\frac{\mu_{AB}}{\mu_{H_2}}E_{CM}) = \sigma_{mt}^{H+H}(E_{CM}). \tag{135}$$

All of the momentum transfer cross sections are almost identical in the asymmetric cases as was demonstrated for hydrogen-ion–hydrogen scattering with the condition of distinguishability of nuclei (i.e. different isotopic combinations). Thus, the momentum transfer cross section is isotopically invariant, i.e.

$$\sigma_{mt}^{A+B}(E_{CM}) = \sigma_{mt}^{C+D}(E_{CM}) \tag{136}$$

where A, B, C, D are any (different) combinations of H, D, and T. These scaling relations are illustrated in Figure 29.

The viscosity cross section for both symmetric and asymmetric systems is independent of the reduced mass and no additional scaling is needed, as shown in Figure 30. Thus

$$\sigma_{vi}^{A+B}(E_k) = \sigma_{vi}^{H+H}(E_k). \tag{137}$$

Unlike the H^+ +H case, where the momentum transfer cross section is approximately a factor of 2 larger than the charge transfer cross section, here the momentum transfer cross section for H + H case is more than five times larger than the spin exchange cross section, i.e.

$$\sigma_{mt} \approx 5.2\sigma_{se} \tag{138}$$

which we find to be valid for all symmetric isotopic variants of the H + H system, in the energy range considered (Figure 31).

I.11.5 H + H_2

The collision of a hydrogen atom with a hydrogen molecule is treated as the collision of distinguishable particles and thus we do not expect any difference between the systems, except to account for difference in masses and vibrational couplings. In spite of the different vibrational channels of excitation, and in spite of averaging over the molecular orientations, the elastic cross sections do not strongly depend on the reduced mass or on the details of the molecular target as long as the projectile is kept the same, as is the case for scattering of isotopic variants of hydrogen ions on hydrogen molecules. Figure 19 illustrates this for hydrogen colliding with six different isotopic variants of molecular hydrogen. The same relationship is approximately valid for the momentum transfer and viscosity cross sections, but in these cases, it is in fact better for low collision energies, as is the case for hydrogen-ion–molecule scattering. This is illustrated in Figures 32 and 33. Thus, one can write

$$\begin{aligned}
\sigma_{el}^{A+CD}(E_{CM}) &= \sigma_{el}^{A+C'D'}(E_{CM}) \\
\sigma_{mt}^{A+CD}(E_{CM}) &= \sigma_{mt}^{A+C'D'}(E_{CM}) \\
\sigma_{vi}^{A+CD}(E_{CM}) &= \sigma_{vi}^{A+C'D'}(E_{CM}).
\end{aligned} \tag{139}$$

If one varies the projectile for the same molecular target, neither the momentum transfer or viscosity cross sections changes significantly. For higher energies this agreement does not deteriorate, as is the case for hydrogen-ion–molecule scattering. The elastic cross

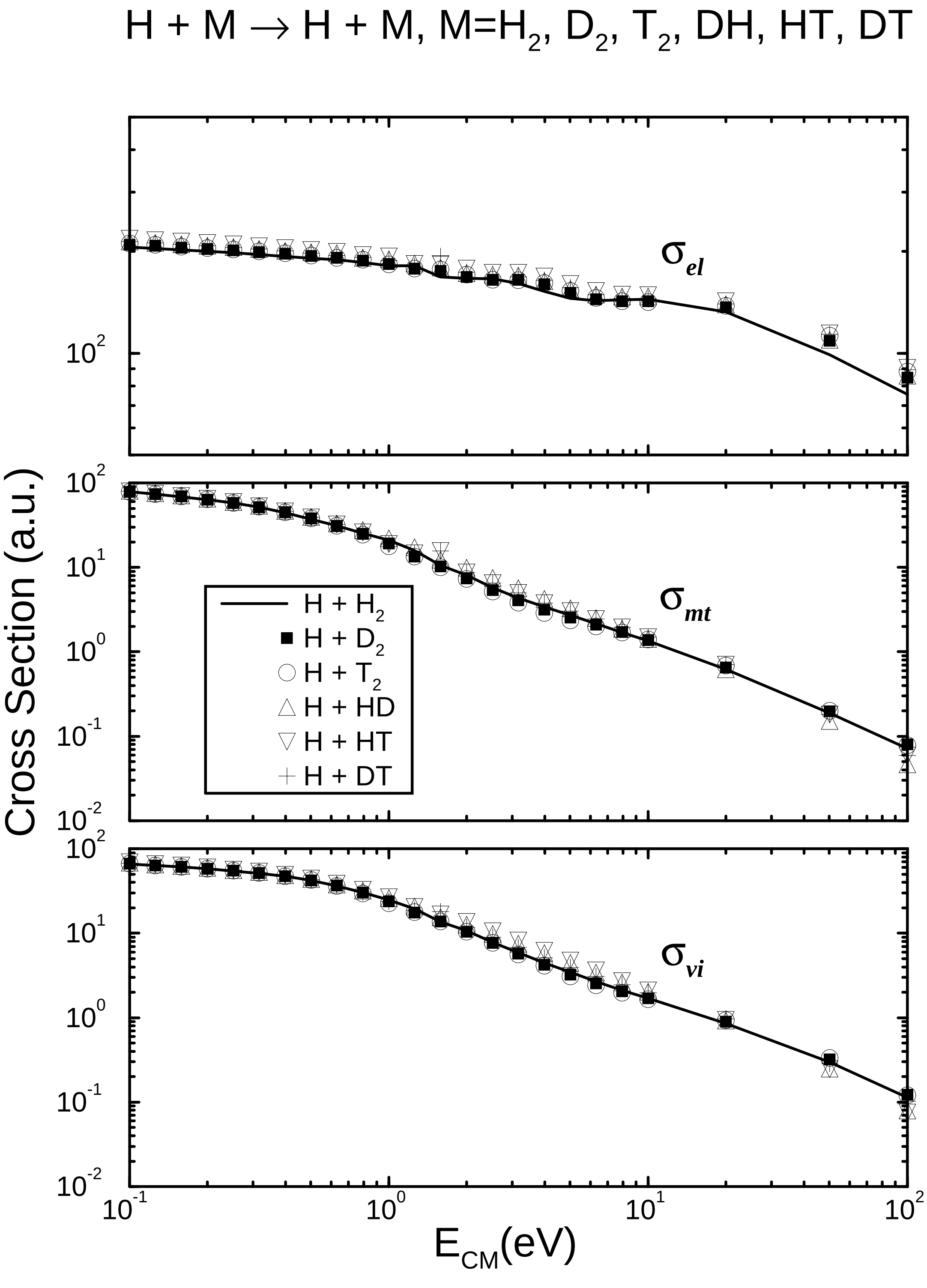

Figure 32: The elastic and transport cross sections for H colliding with the isotopic variants of H_2.

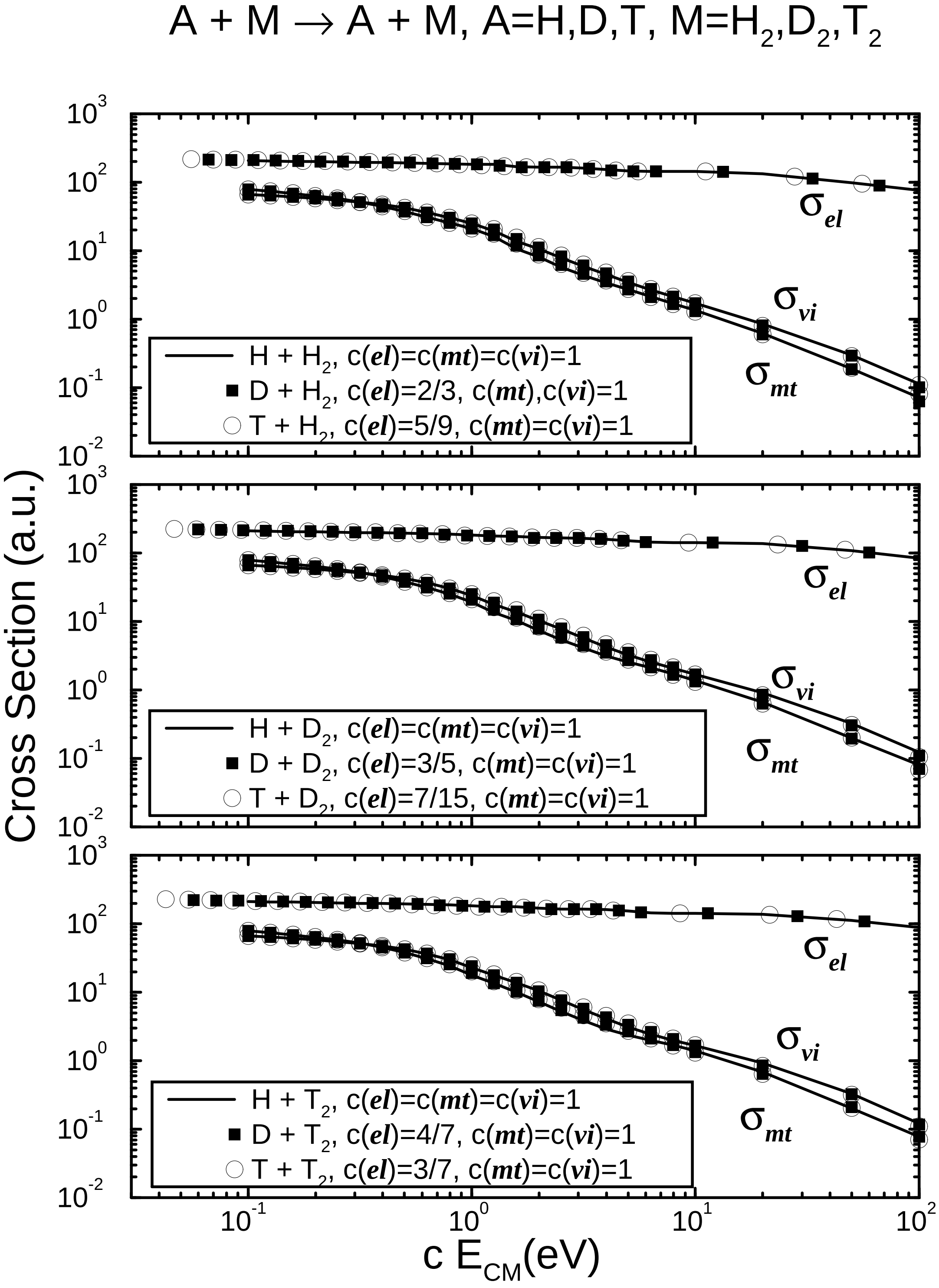

Figure 33: Scaling of the elastic and transport cross sections for isotopes of H colliding with H_2, D_2, and T_2.

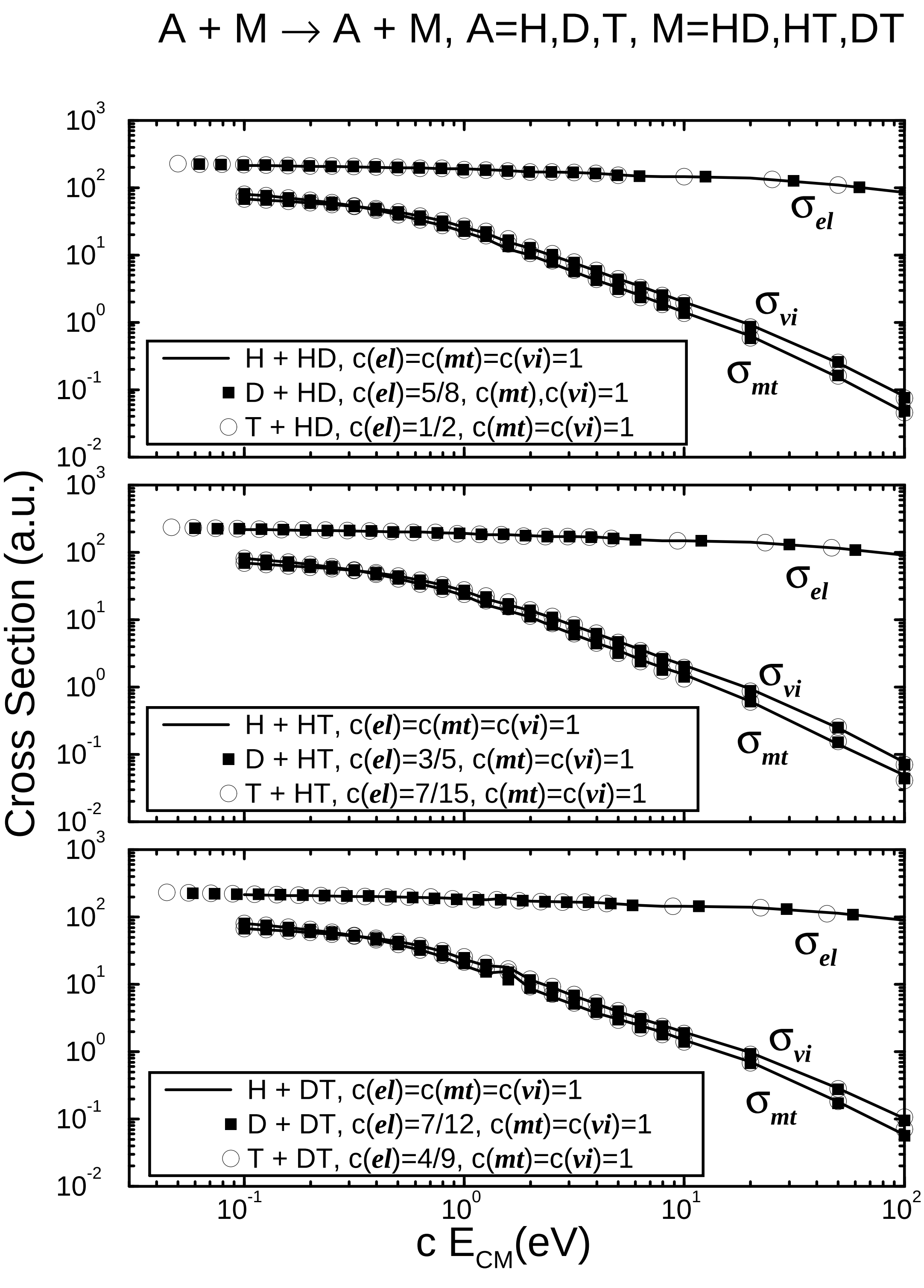

Figure 34: Scaling of the elastic and transport cross sections for isotopes of H colliding with HD, HT, and DT.

sections, on the other hand match quite well if one scales the energy with the reduced mass, as in the hydrogen-ion–atom and hydrogen-ion–molecule cases. Thus

$$\begin{aligned}
\sigma_{el}^{A+CD}(\frac{\mu_{ACD}}{\mu_{H_3}}E_{CM}) &= \sigma_{el}^{H+C'D'}(E_{CM}) \\
\sigma_{mt}^{A+CD}(E_{CM}) &= \sigma_{mt}^{H+C'D'}(E_{CM}) \\
\sigma_{vi}^{A+CD}(E_{CM}) &= \sigma_{vi}^{H+C'D'}(E_{CM}). \qquad (140)
\end{aligned}$$

These relations are illustrated for all isotopic variants of the hydrogen molecule in Figures 32-34.

I.11.6 Comparisons among the various systems

Comparison of the elastic cross sections for six cases typical of those discussed above is shown in Figure 35 (i.e. for H^+ or H as the projectile and the targets are varied).

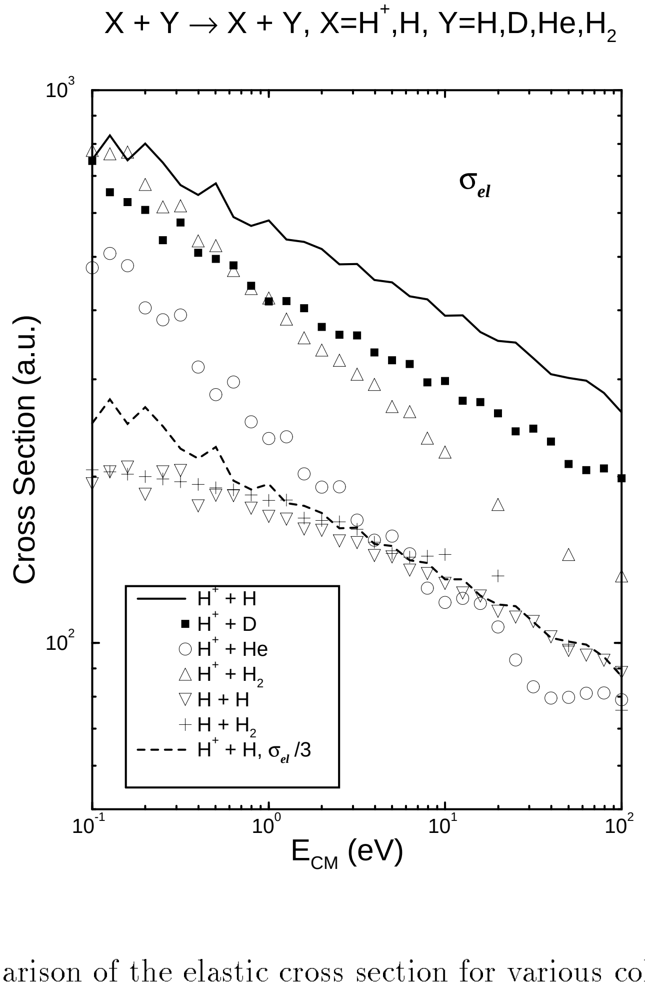

Figure 35: Comparison of the elastic cross section for various collision systems.

Pronounced oscillations in the cross sections exist for all cases at energies below 1 eV. The cross sections for hydrogen-ion projectiles (with both atomic- and molecular-hydrogen targets) fall within a range of 50% of one another and almost coincide at 0.1

eV. The cross sections for molecular targets decrease faster toward higher energies because of the increasing involvement of the inelastic vibrational excitations, while for H^+ + H and H^+ + D the cross sections differ at higher energies by almost a constant factor, originating from the different definitions of the elastic cross sections (for indistinguishable and distinguishable nuclei). Elastic scattering from He is different from that for H, due to the absence of the gerade-ungerade symmetry. On the other hand, the elastic cross section for scattering of a hydrogen atom from both atomic and molecular hydrogen is almost coincident, particularly at energies below 10 eV. The cross section for proton scattering from hydrogen is about three times larger than the corresponding one for a hydrogen projectile, the latter already containing division by a factor of 2.

The behavior of the momentum transfer cross sections with hydrogen-ion and hydrogen-atom projectiles is summarized in Figure 36. The cross section for proton scattering from hydrogen is about a factor of 2 greater than that for H + H. The asymmetric cases have a smaller dispersion than they display for the elastic cross section. The viscosity cross sections (Figure 37) have an even smaller dispersion than the momentum transfer cross sections, particularly at low energies. Again, the H^+ + H viscosity cross section is about a factor of 2 larger than that for H + H.

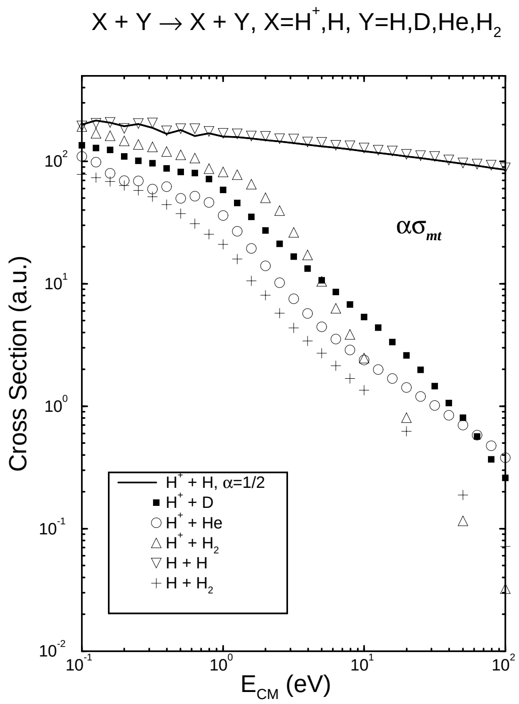

Figure 36: Same as Figure 35 except for the momentum transfer cross section.

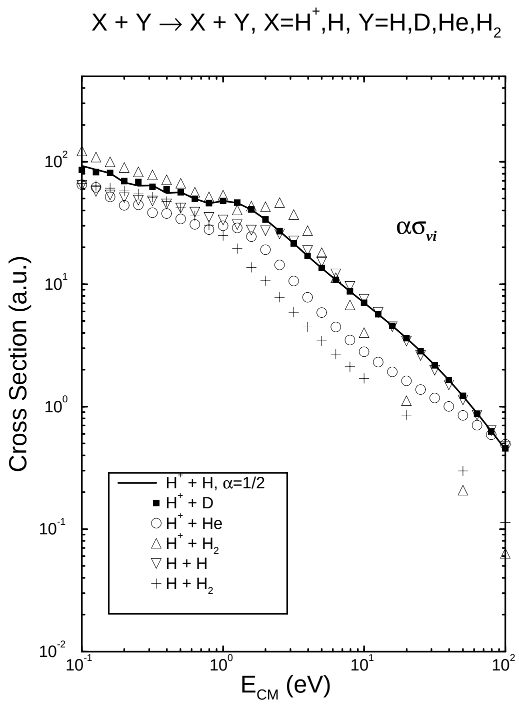

Figure 37: Same as Figure 35 except for the viscosity cross section.

References

[1] R.K. Janev, editor, *Atomic and Molecular Processes in Fusion Edge Plasmas* (Plenum, New York, 1995).

[2] P. Bachmann and D. Reiter, Contr. Plasma Phys. **35**, 45 (1995).

[3] P. Bachmann and H.J. Belitz, Max Planck Institut für Plasmaphysik Report IPP 8/2 (1993).

[4] D.R. Schultz, S.Yu. Ovchinnikov, and S.V. Passovets, *Atomic and Molecular Processes in Fusion Edge Plasmas*, R.K. Janev, editor (Plenum, New York, 1995), p. 279.

[5] L.D. Landau and E.M. Lifshitz, *Quantum Mechanics - Nonrelativistic Theory* (Pergamon Press, New York, 1965).

[6] A.S. Davidov, *Quantum Mechanics* (Pergamon Press, New York, 1965).

[7] B.H. Bransden and M.R.C. McDowell, *Charge Exchange and the Theory of Ion-Atom Collisions* (Clarendon Press, Oxford, 1992).

[8] M.R.C. McDowell and J.P. Coleman, *Introduction to the Theory of Ion-Atom Collisions* (North-Holland, London, 1970).

[9] B.H. Bransden and C.J. Joachain, *Physics of Atoms and Molecules* (Longman, London, 1983).

[10] C.J. Joachain, *Quantum Collision Theory* (North-Holland, Amsterdam, 1983).

[11] E.W. McDaniel, *Collision Phenomena in Ionized Gases* (John Wiley & Sons, New York, 1964); *Atomic Collisions: Heavy Particle Projectiles* (John Wiley & Sons, New York, 1993).

[12] J.O. Hirschfelder, C.F. Curtiss, and B.B. Bird, *Molecular Theory of Gases and Liquids* (John Wiley& Sons, New York, 1964).

[13] M. Abramowitz and I.S. Stegun, *Handbook of Mathematical functions* (Dover., New York, 1972).

[14] M.J. Jamieson, A. Dalgarno, and J.N. Yukich, Phys. Rev. A **46**, 6956 (1992).

[15] A.C. Allison and F.J. Smith, Atomic Data **3**, 317 (1971).

[16] F. Masnou-Seeuvs and A. Salin, J. Phys. B **2**, 1274 (1969).

[17] G. Hunter and M. Kuriyan, Atom. Data Nuc. Data Tables **25**, 287 (1980).

[18] F.J. Smith, Proc. Phys. Soc. **92**, 866 (1966); Proc. Space Sci. **14**, 929 (1966).

[19] E.A. Solov'ev, Sov. Phys. Usp. **32**, 228 (1989).

[20] G. Hunter and M. Kuriyan, Proc. Roy. Soc. London A **358**, 321 (1977).

[21] J.H. Macek and K.A. Jerjian, Phys. Rev. A **33**, 233 (1986).

[22] R.J. Damburg and R.Kh. Propin, J. Phys. B **1**, 681 (1968).

[23] L. Wolniewicz, J. Chem. Phys. **99**, 1851 (1995) and references therein.

[24] B. Johnson, J. Comp. Phys. **13**, 445 (1973).

[25] M.W. Schmidt, K.K. Baldridge, J.A. Boatz, S.T. Elbert, M.S. Gordon, J.H. Jensen, S. Koseki, N. Matsunaga, K.A. Nguyen, S.J. Su, T.L. Windus, M. Dupuis, and J.A. Montgomery, J. Comput. Chem. **14**, 1347 (1993).

[26] L. Monchick and E.A. Mason, J. Chem. Phys. **35**, 1676 (1961).

[27] D.J. Kouri, in *Atom Molecule Collision Theory*, R.B. Bernstein, editor (Plenum Press, New York, 1979).

[28] M. Baer and H. Nakamura, J. Chem. Phys. **66**, 1363 (1987).

[29] M. Baer, G. Niedner, and J.P. Toennies, J. Chem. Phys. **88**, 1461 (1988); M. Baer, *State-Selected and State-to-State Ion-Molecule Reaction Dynamics, Part 2: Theory*, M. Baer and C.-Y. Ng, editors, in *Advances in Chemical Physics* **LXXXII**.

[30] A. Ichihara and K. Yokoyama, J. Chem. Phys. **103**, 2109 (1995).

[31] A.I. Boothroyd, W.J. Keogh, P.G. Martin, and M.R. Peterson, J. Chem. Phys. **95**, 4343 (1991).

[32] C.F. Giese and W.R. Gentry, Phys. Rev. A **10**, 2156 (1974).

[33] R. Schinke, M. Dupuis, and A. Lester, Jr., J. Chem. Phys. **72**, 3909 (1980).

[34] W.H. Press, B.P. Flannery, S.A. Teukolsky, and W.T. Vetterling, *Numerical Recipes in Fortran* (Cambridge University Press, Cambridge, 1992).

[35] R.R. Hodges, Jr. and E.L. Breig, J. Geoph. Res. **96**, 7697 (1991).

[36] G. Hunter and M. Kuriyan, Proc. Roy. Soc. London **353**, 575 (1977).

[37] A.V. Phelps, J. Phys. Chem. Ref. Data **19**, 653 (1990).

[38] M. Baer, G. Niedner-Schatteburg, and J.P. Toennies, J. Chem. Phys. **91**, 4169 (1989).

[39] K.A. Smith, L.K. Johnson, R.S. Gao, and R.F. Stebbings, in *Abstracts of Contributed Papers for the International Conference on the Physics of Electronic and Atomic Collisions*, edited by J. Geddes, H.B. Gilbody, A.E. Kingston, C.J. Latimer, and H.R.J. Walters (North-Holland, Amsterdam, 1987), p. 681.

[40] R. Schinke and P. McGuire, Chem. Phys. **31**, 391 (1978).

[41] V. Herman, H. Schmidt, and F. Linder, J. Phys. B **11**, 493 (1978).

[42] G. Neidner, N. Noll, and J.P. Toennies, J. Chem. Phys. **87**, 2685 (1987).

[43] N. Koyama and J.C. Baird, J. Chem. Soc. Japan **55**, 801 (1986).

[44] M.R. Flannery and K.J. McCann, Phys. Rev. A **9**, 1947 (1974).

[45] A. Dalgarno, Proc. Roy. Soc. London **262**, 132 (1961).

[46] M.E. Hayden, M.D. Hurlimann, and W.N. Hardy, Phys. Rev. A **53**, 1589 (1996).

List of abbreviations

a.u.	atomic unit, e.g. atomic unit of energy, 27.2116 eV
$anti$	antisymmetric
B	Boltzmann
CM	Center of Mass
ct	charge transfer
DIM	Diatom-In-Molecule
el	elastic
g	gerade
GAMESS	General Atomic and Molecular Electronic Structure System [25]
HB	Hodges and Breig
HF-CI	Hartree-Fock–Full-Configuration-Interaction
HK	Hunter and Kuriyan
IOSA	Infinite Order Sudden Approximation
mt	momentum transfer
RHF-CI	Restricted-Hartree-Fock–Full-Configuration-Interaction
s	spin or singlet, depending on context
se	spin exchange
sym	symmetric
t	triplet
u	ungerade
UHF-CI	Unrestricted-Hartree-Fock–Full-Configuration-Interaction
vi	viscosity
WWW	World Wide Web